UNIVERSITY OF CALIFORNIA SAN DIEGO

Quantifying Cellular Adhesion Strength of Tumor Cells as a Metric for Migratory and Metastatic Potential

A dissertation submitted in partial satisfaction of the requirements for the degree
Doctor of Philosophy

in

Biomedical Sciences

by

Afsheen Banisadr

Committee in charge:

Professor Adam Engler, Co-Chair
Professor Frank Furnari, Co-Chair
Professor Alexandra Newton
Professor Dwayne Stupack
Professor Jing Yang

2020

The Dissertation of Afsheen Banisadr is approved, and it is acceptable in quality and form for publication on microfilm and electronically:

_____

_____

_____

_____
Co-Chair

_____
Co- Chair

University of California San Diego

2020

DEDICATION

To my family, past, present, and future:

Your love, care, and support inspire me and give me the strength to achieve the impossible.

I am forever grateful.

EPIGRAPH

"It is not the critic who counts; not the man who points out how the strong man stumbles, or where the doer of deeds could have done them better. The credit belongs to the man who is actually in the arena, whose face is marred by dust and sweat and blood; who strives valiantly; who errs, who comes short again and again, because there is no effort without error and shortcoming; but who does actually strive to do the deeds; who knows great enthusiasms, the great devotions; who spends himself in a worthy cause; who at the best knows in the end the triumph of high achievement, and who at the worst, if he fails, at least fails while daring greatly, so that his place shall never be with those cold and timid souls who neither know victory nor defeat."

–Theodore Roosevelt Jr.

TABLE OF CONTENTS

LIST OF FIGURES AND TABLES

ACKNOWLEDGEMENTS

First, I would like to thank Professors Adam Engler and Frank Furnari for all of their mentorship and guidance throughout my scientific journey. You both saw my potential, and chose to make an investment in cultivating my scientific and professional career. You were the mentors that I not only wanted, but that I needed. Your efforts molded me into the scientist I am today, and I am forever thankful for your invaluable support, care, and friendship throughout my doctorate. I would like to also thank my committee: Professors Alexandra Newton, Dwayne Stupack, and Jing Yang for your guidance and mentorship throughout my journey. All three of you have been a championing force during my doctorate, and I am grateful for all of your time and energy. Thank you to the National Science Foundation Graduate Research Fellowship Program for their support, which allowed me to focus on my research and immerse myself in my science.

I would like to thank all of the member of both the Engler and Furnari labs, especially Ciro, Nate, Jesse, Alex, Jorge. Your guidance and friendship made my time in lab as fun and exciting as it was educational and productive. You all taught me that when you enjoy what you do, it seems less like work. A special thank you to all of the undergraduate students whom I mentored over the years, particularly Mariam Eick, Mana Abbasinik, and Tristian Saucedo. The three of you taught me the value of imagination, the power of effort, and you brought a light of happiness to my time in lab.

Thank you to the biomedical sciences program, for making my time in graduate school joyous. From the students who made the program fun and supportive, to the care and kindness of Leanne and Pat, and the leadership of the professors such as Debbie, Arshad and Kevin who

took the time to guide me through my journey. Thanks to all of your efforts I always felt as though I was part of a happy graduate school family. Professors Hamid Ghandehari and Adam Gormley, you helped me to develop my passion for research in my undergraduate career. You both taught me that science can not only be intellectually stimulating, but when you do it with your friends it can be exciting and fun. Dr. Harshini Mukundan your guidance and support during my time at Los Alamos National Lab was instrumental in my development as a researcher, and foundational to the scientist I have developed into.

I am very fortunate that throughout my entire career I have had the support of my friends from high school, and who still serve an inspiration and support for all of my endeavors. Arick, Calvin, Colin, Paolo, Kelsey, Julie, Niko, Heather, Martina, Kevin, Janis, and Blake it is thanks to you all that I have my confidence, and my drive. Though I was never the smartest of the group you all encouraged my hard work, and supported me from an early age. Your journeys through life inspired me to follow my dreams of a PhD, and your love has carried me through my rough times. I am forever grateful for all of your friendships and feel truly blessed to be surrounded by such kind and inspiring people to this day.

The victories and tribulations of graduate school forged bonds with those around your which can only be paralleled by family. The friendships that I have made during my graduate education are ones that I will hold onto for the rest of my life. Michael, Sarah, Nathan, Rachel Nick, James, Tim, Nikos, Ian, Alex, David, Vanessa, Harry, Terry, Hannah, Yon, Vanessa, Doug, Nessa, Mike, Aaron, Ryan, and countless others, I could not have made it through without you. You all have been here with me to celebrate my accomplishments and commiserate with me in my times of need. You expanded my world both scientifically and personally, you pushed me to

have confidence in myself and supported me when I fell. My life has been made richer in every aspect by having you with me.

From the beginning of my career, I have always had a support network who have cared for me as if I were their own. Having a refuge where you are comfortable and happy give you strength in times of difficulty. Throughout my time at the University of Utah Terri, Cory, Phyllis, and Patti your love gave me the comfort and self-assurance to reach for my goals. Time with you was always a sanctuary of happiness. Family is not always the people you are born to, but the people you whom you chose to be around. To my chosen family the Painters, thank you for everything you have done for me. Grace, Dan, Bobbi, Ashley, Zach, and Ian, you have always welcomed me with open arms, celebrated my achievements, and treated me as family. I have treasured all of the time we have spent together, and am grateful all of you support and love. I am fortunate to be part of your lives and am thankful that you are such a large part of mine. Family is also the people who choose to be around you, and when that person is truly kind and caring your world becomes all the better for it. I am fortunate that the person whom has chosen to be a part of my family, my brother's wife Alexa, is one of the kindest people I have ever known. Alexa, over the past 4 years you have encouraged me as a friend and supported for me like a sibling. I am thankful to you, not only for the kindness and advice that you have given me, but the life that you and Bahram have built together through love and hard work. You are an amazing person and I feel blessed that you are in my life.

Throughout my life's journey, no matter the circumstances, my family has always been there to support and guide me. From a young age my grandparents encouraged my inquisitive nature. From my grandfather's Sadri and Nosrat to my grandmother's Eshrat and Mehri, my

grandparents have spent their lives inspiring and teaching me the. To my uncles Farokh, Jahan, and Amir thank you for all of the laughs, adventures, and strength. To my aunts Ziba, Pari, and Roshi thank you for all of the warmth, kindness, and love. To all of my cousins David, Bahareh, Rod, Ava, Adam, Shadi, Arash, Sacha, and Shauna you all are the source of my excitement and happiness.

My parents laid the foundation for my success was long before I started my doctorate. My earliest memories in life are of love and encouragement from my mother Homa Nassiri and my father Farhad Banisadr. Mom and Dad, you are the ones who taught me to dream and cultivated my enthusiasm to pursue those dreams. You never limited me in my pursuits, only encouraged my efforts, strengthened my resolve my enthusiasm and provided me with the tools to be successful. Your lives have also served as a constant model for me to strive toward. The strength you showed in order to escape from the only lives you had known in order to build a better future is truly inspiring. The sacrifices you made to provide Bahram and I with the best chance of success has motivated me throughout my life. Your word of motivation taught me to dream and your cheers of enthusiasm inspired me to pursue those goals. You gave me the confidence to challenge myself in life, and the resilience to persist through difficulties. You both are truly the best people I know, and I am forever in your debt for all that you have done. I owe everything to you.

The bond between siblings is one that cannot be paralleled. Bahram, though you are my younger brother, you have always served as a mentor in my life. As a true mentor, you have always led by example, demonstrating that through dedication, hard work, and tenacity you can always achieve your goals. You have inspired me with your courage. Though you may have fears

in life, you never let them hold you back. I am emboldened by your determination, no matter the challenge, you never let anything stand in your way. I am heartened by your devotion, the love you show for your friends, and family is paralleled only by Alexa, and is truly moving. You are an unstoppable force for good and you inspire me every day with your words, actions and thoughts. I am forever grateful to

Most importantly, to the love of my life Chelsea. Throughout my entire journey in higher education and as a scientist, you have been the most caring, supportive and loving partner I could hope for. I still remember the moment we met as if it were yesterday, and every time I do it fills me with joy. We have been in each other's partners for nearly a decade, but whether it is planning a surprise adventure or it is you still manage to take my breath away in the most delightful ways. I take inspirations from your kindness and love. You care for others, no matter the pressures you face, and picking me up when I am not strong enough to carry myself. I am in awe of your bravery, no matter the challenge in front of you, you do not let fear prevent you from action. Whenever we have faced an obstacle, you have helped to illuminate our path forward together. You are truly the light of my life. Lastly, I am thankful for our love. No matter the path ahead of us, our love has been unwavering, and it has made us stronger because of it. I am excited for our next step in life, and want this adventure to be even more exhilarating and joyous than the last. Chelsea, you are my world, and I cannot imagine my life without you.

Chapter 2, in full, is a reprint of the material as it appears in Fuhrmann, A., Banisadr, A., Beri, P., Tlsty, T.D., and Engler, A.J. "Metastatic State of Cancer Cells may be indicated by Adhesion Strength." *Biophys J*, 2017. 112(4): 736-745. The dissertation author was a co-author of this paper.

Chapter 3, in full, is a preprint of material submitted for publication in Banisadr, A., Eick, M., Beri, P., Parisian, A. D., Yeoman, B., Placone, J., Engler, A.J., Furnari, F. “EGFRvIII contributes to glioblastoma migration by cell intrinsic and cooperative mechanisms that reduce cell-matrix adhesion.” The dissertation author was the primary author of this paper.

VITA

2013 Bachelor of Science, University of Utah

2020 Doctor of Philosophy, University of California San Diego

PUBLICATIONS

Fuhrmann, A., **Banisadr, A.**, Beri, P., Tlsty, T. D., & Engler, A. J. (2017). "Metastatic State of Cancer Cells May Be Indicated by Adhesion Strength." *Biophysical Journal*, 112(4), 736-745.

Banisadr, A., Eick, M., Beri, P., Parisian, A. D., Yeoman, B., Placone, J., Engler, A.J., Furnari, F. (2020) "EGFRvIII contributes to glioblastoma migration by cell intrinsic and cooperative mechanisms that reduce cell-matrix adhesion." *In preparation for submission.*

ABSTRACT OF THE DISSERTATION

Quantifying Cellular Adhesion Strength of Tumor Cells as a Metric for Migratory and Metastatic Potential

by

Afsheen Banisadr

Doctor of Philosophy in Biomedical Sciences

University of California San Diego, 2020

Professor Adam J. Engler, Co-Chair

Professor Frank Furnari, Co-Chair

The ability of tumor cells to reestablish a niche and cause recurrence of the tumor, either within the primary tissue that the tumor initially formed or to a secondary site within the body, enhances tumor malignancy and causes patient morbidity and mortality. The propensity of tumor cells to migrate away from their primary site poses several challenges. First is the high variability in driver mutations between patients, as well as the variability in patient background genetics,

both of which can induce variability in tumor cell migratory and metastatic propensity. Second, is a lack of universal markers, either genetic or molecular, which can accurately predict tumor cell migratory and metastatic potential. Together these challenges prevent the stratification of different tumors and prevents the implementation of patient-specific interventions tailored to prevent tumor cell migration and metastasis.

An emerging field which is providing insight into the tumor metastatic process is biophysical analysis. However, the field is currently focused on analyzing the presence of circulating tumor cell through turbulent flow microfluidics as an indicator for metastasis, not predicting tumor metastatic potential from the primary site. Therefore, there is a need for a rapid and quantitative biophysical metric which can predict the migratory and metastatic potential of those primary tumors. This dissertation addresses the need to predict tumor migratory and metastatic potential by gaining an understanding of how those characteristics are linked to cell adhesion in glioblastoma and mammary tumors, respectively.

In order to determine the relationship between adhesion strength and cell migratory and metastatic potential first we characterized the adhesion strength of metastatic and non-metastatic mammary cancer cells. In order to evaluate cellular adhesion strength as well as understand the effects of the tumor microenvironment on cell biophysical characteristics, we built a spinning disk shear device. This device gave us the capability of interrogating cellular adhesion characteristics in a quantitative and high throughput manner, as well as being able to modulate extracellular divalent cation conditions Mg^{2+} and Ca^{2+} to mimic those found in patients. We found that in the absence of divalent cations those metastatic cells showed an overall decrease in the cellular adhesion strength as well as a broader range of adhesion characteristics

than those non-metastatic cell lines. Comparison of those metastatic cells to their non-metastatic counterparts demonstrated a decrease in the assembly state of focal adhesions in both number and size. Similarly, the exposure of those non-metastatic cells to cyclic RGD peptides also induced a decrease in focal adhesion assembly state as well as decreasing cellular adhesion strength and increasing cell migratory phenotype. Together, these data suggest that there is a correlation between decreased cellular adhesion strength, an increase in metastatic potential, and that this correlation is due to altered assembly state of focal adhesion structures.

Next, I wanted to understand if the correlation between decreased cellular adhesion strength and increased cell migratory phenotype extended beyond mammary tumors to glioblastoma (GBM). In order to investigate the effects of common GBM mutations on cellular adhesion strength, isogenic murine astrocytes were exposed to fluidic shear stress via spinning disk assay. Specifically, astrocytes with combinations of CDKN2A/B deletion (occurring in 61% of patients), Pten deletion (occurring in 41% of patients), or alteration of epidermal growth factor receptor (EGFR) (occurring in 57% of patients) were analyzed. This analysis showed that unlike mammary tumors, decreased astrocyte adhesion strength was dependent on the presence of divalent cations. Furthermore, I found that the decrease in adhesion strength was limited to those cells expressing EGFRvIII independent of other mutations, and correlated with increased migratory phenotype. Further analysis found that this change in EGFRvIII expressing cells biophysical phenotype is a result of a signaling-dependent decrease in integrin expression which results in alteration of focal adhesion assembly state. In order to investigate what EGFRvIII dependent signaling cascades modulate decreased adhesion strength, I utilized small-molecule inhibitors to target multiple pathway nodes such as: the EGFR receptor itself, MEK, SRC, and Stat3

in a systematic manner. I found that those cells treated with MEK inhibitor or EGFR inhibitor showed an increase in EGFRvIII cell adhesion strength, similar to non-EGFRvIII expressing cells. Lastly, it has been well documented that cell-cell communication allows those EGFRvIII cells to affect behavior of non-EGFRvIII cells within that tumor. In order to understand if EGFRvIII cells are capable of altering cell adhesion strength of other cells, I educated wtEGFR with EGFRvIII conditioned media prior to analyzing cellular adhesion strength. I found that those wtEGFR expressing cells altered their adhesion strength after education with vIII CM, and that this decrease in adhesion strength was dependent on the presence of the soluble factor TNF-α.

Throughout this dissertation I will demonstrate the value of utilizing fluidic shear as a methodology for analyzing cellular adhesion strength and its application for predicting tumor migratory and metastatic potential. Furthermore, I will also demonstrate how fluidic shear can be used to understand the genetic and molecular mechanisms that contribute to and enhance tumor cell malignancy.

Chapter 1.

Utilizing cell-ECM dynamics to model and measure epithelial cancers

1.1 Abstract

Detecting and predicting tumor cell migration and metastasis has been a focus of the tumor biology field for decades. This is because detection and prediction of tumor cell migratory and metastatic potential is fundamental in understanding and preventing tumor recurrence as well as related patient morbidity and mortality. Classically, analysis of tumor migratory characteristics and prediction of metastatic potential has been performed using a combination of histopathological analysis of the primary tumor and repeated follow-up imaging. With the expansion of genetic analysis and molecular testing, more quantitative prediction of those most common and malignant markers have been established. However, the large diversity in driver mutations, as well as patient background genetics, prevents prediction of tumor behavior through a universal biomarker. In this chapter we will discuss the benefits and shortcomings of these classic techniques, and will also look at how the field of tumor monitoring and predictive analysis has evolved. Specifically, we will focus on extracellular matrix modeling, microfluidics, biophysical analysis, and how these fields are being used independently, as well as in combination, to monitor and predict tumor cell migratory and metastatic potential.

1.2 Introduction

Tumor recurrence is the primary cause of patient morbidity and mortality[1,2]. The ability of tumor cells to establish secondary sites, either in the same tissue or in distal sites in the body, prevents the complete removal of those cells and eventually results in recurrence[3,4]. The process of secondary tumor formation is universal in solid tumors extending from epithelial tumors such as mammary tumors to astrocytic tumors such as glioblastoma (GBM)[3,4]. More explicitly, the process of tumor cell dissemination is a coordinated one wherein a tumor cell must detach itself from the bulk tumor, migrate away from the tumor and invade into healthy stroma by utilizing insoluble extracellular matrix proteins i.e. fibronectin[5–7] (Figure 1.1). The tumor cell can then establish residency in a secondary site with a favorable microenvironment in the surrounding proximal tissue stroma[3,4]. In the case of metastatic tumors, this means intravasating into the blood or lymph system, circulating around the body, extravasating from that system and invading into other tissues[8–10]. Migration is similar for invasive tumors but does not necessitate intravasation and extravasation (Figure 1.1).

Despite the process of cancer cell migration being ubiquitous to all solid tumors, no universal biomarker for predicting tumor cell migratory and metastatic potential has been found[11]. This lack of a universal maker is due to the vast amount of genetic and epigenetic heterogeneity in cancer. This is true not only between different types of tumors, but also between patients with the same type of cancer, as well as for individual cells within a single tumor[5,12,13]. This genetic and epigenetic heterogeneity results in a large variety of pathways being altered, and as a consequence, leaves no universal pathway or gene which can sufficiently act on its own to induce a migratory or invasive phenotype.

In order to address this lack of universal markers, stratify patient populations, and interrogate the mechanisms involved in tumor cell migration and metastasis, targeted analysis of migratory and metastatic cells has been performed. Specifically, the implementation of techniques such as microdissection, circulating tumor cell isolation, and single cell sequencing have helped to resolve some of the previously undiscovered mechanisms involved in tumor cell migration and metastasis[14–16]. For example, the application of assays such as laser capture microdissection (LCM) has been utilized in extracting and analyzing those GBM tumor cells which have migrated into healthy parenchyma[14,15]. Similarly, the isolation and characterization of circulating tumor cells from the blood or lymph is being performed in order to understand what genetic, molecular, and physical properties (such as size, or circularity) those metastatic cells exhibit in comparison to their non-metastatic counterparts[16,17]. Though these data has given some insights into the mechanisms involved tumor cell migration, and metastasis, they are limited in their resource pool due to the rarity of these data they are trying to collect, throughput of data, and most importantly cannot necessarily predict tumor behavior from a primary tumor site[15,18].

A new field of research that is emerging in order to characterize primary tumor cell characteristics, independent of genetic or molecular markers is the field of biophysical analysis. Specifically, analysis of primary tumor cell properties such as nuclear stiffness, cellular deformability, interrogation of tumor cell migration characteristics, and investigation of cellular adhesion strength, are being look at as metrics for tumor cell migratory and metastatic potential[19–25]. These biophysical analyses serve as a more encompassing metric for predicting, interrogating, and understanding those metrics responsible for migration. Furthermore, these

data may serve to stratify patient populations and eventually allow for the targeting of those characteristics to improve patient outcomes. One example of this biophysical analysis is the interrogation of nuclear envelope stiffness and rupture during cellular migration through the surrounding microenvironment[19,26]. These analyses have shed light on the importance of nuclear composition and physical characteristics, and how they can be utilized to characterize those more migratory and metastatic tumor cells. However, these analyses present their own limitations as far as throughput and downstream analysis.

In this chapter I will describe the strengths and weaknesses of using these various methodologies towards analyzing tumor cell migratory and metastatic potential. In addition, I will touch upon methodologies which show promise in improving our understanding of tumor biophysical characteristics, how that knowledge can be used to improve cancer therapeutics and eventually patient outcomes.

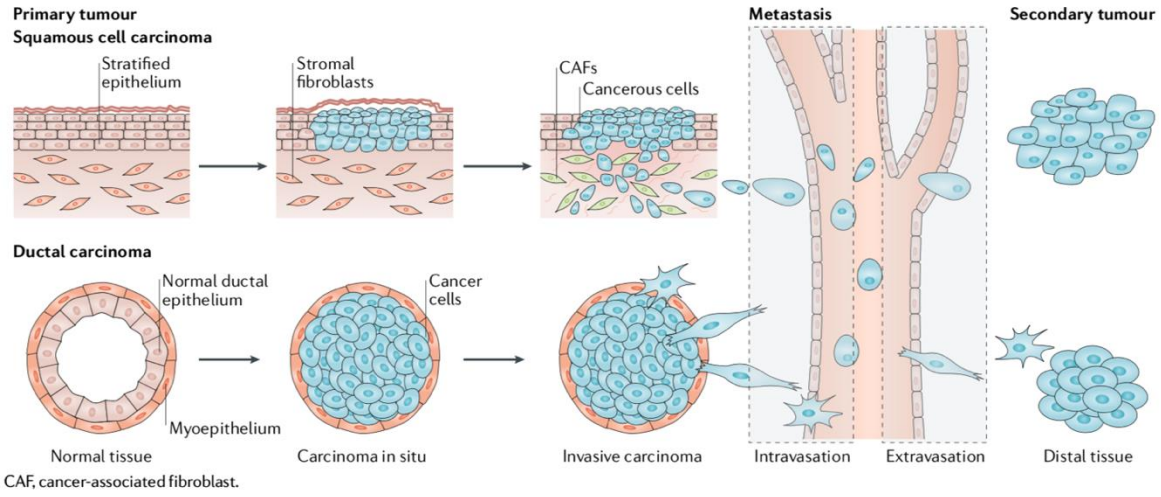

Figure is reproduced and modified with permission from ref.,[27]

Figure 1.1. The process of tumor development, migration and metastasis:

The mutation of a single cell leads to uncontrolled division, resulting in an excess of abnormal cells. As the mass grows, the cells can acquire additional mutations and remodel the surrounding tissue, forming a primary tumor. Tumors are heterogeneous and often lack the polarity and cellular organization of the original tissue. Epithelial-to-mesenchymal transition (EMT) is a cellular program that causes cells within a primary tumor to lose characteristic cell–cell adhesions, to break the basement membrane associated with an epithelial phenotype, to transition to a mesenchymal phenotype that lacks cell polarity and to upregulate and/or activate specific transcription factors, such as Twist family bHLH transcription factor 1 (TWIST1). The EMT program enables cells of the primary tumor to locally invade the surrounding stroma and is characterized by a shape change of the cells in the primary tumor. Intravasation is the migration of cancer cells from tumor-adjacent stroma into a blood or lymphatic vessel. This is a multistep process, during which metastatic tumor cells migrate through the extracellular matrix and between cells in the vessel as well as through the water-tight junctions between endothelial cells to reach the fluid in the lumen of the vessel. Extravasation is the exit of cancer cells from a blood or lymphatic vessel through the endothelial cell layer lining the vessel and into a secondary site distant from the primary tumor. This is also a multistep process, during which circulating tumor cells slow down and stop along the vessel wall through adhesion to endothelial cells. Cells break through the water-tight junctions between endothelial cells and the matrix within the vessel to invade new tissue. A malignant tumor that grows in a secondary organ from cells originating from a primary tumor.

1.3 Tumor Analyses

1.3.1 Conventional methodologies to investigate tumor migration and metastasis

Once diagnosed with a solid tumor, patients undergo very similar treatment and diagnostic modalities. Specifically, patients undergo some combination of surgical resection of the tumor, pathology analysis of the tumor and surrounding tissue, as well as radiation, chemotherapy and post-treatment imaging to monitor disease progression[28].

These classic approaches to analyzing, detecting, and predicting tumor characteristics has extended the time of disease-free recurrence and has improved patient outcome. For example, post therapeutic imaging modalities such as mammograms for breast cancer, flexible sigmoidoscopy for colorectal cancer[29] and chest radiography scans for lung cancer[30–32] are some of the oldest and most effective ways of detecting tumor recurrence. The efficacy of imaging as a method for detecting tumor recurrence and metastasis is due to several factors. First, is its non-invasive or minimally invasive rapid nature, which promotes patient compliance due to nominal impact on the body, and low false positive rate[33].These imaging modalities are swift and allow for a rapid prognosis and intervention of the patient[29–32]. It is important to note, however, that tumor imaging presents its own shortcomings as well. Specifically, imaging resolution and sensitivity of solid tumors, is limited to the macroscopic scale and is often times obscured in dense tissue[34,35]. Furthermore, although imaging allows for a rapid analysis of tumor presence, it is not able to predict tumor malignancy nor is it able to provide any characterization of tumor cell genetic, molecular or biophysical properties.

Immunohistopathological analyses are a second tumor analytical technique which has been used for decades to measure tumor properties[36–38]. Through pathology, doctors and patients are able to better understand the tumor physical characteristics such as disease stage, and molecular profiling /genetic testing of the tumor itself[36–38]. For example, pathology analysis had been instrumental in establishing the TNM staging system for describing disease progression, and pairing that analysis with appropriate therapeutics[39]. Specifically, the TNM system determines tumor progression through visual inspection of the tumor and surrounding stroma and analyzing size and extent of the primary tumor, the number of nearby lymph nodes that are positive for tumor residence, and analysis of metastasis[39]. Once disease stage is determined, molecular analysis of the resected tumor is performed to investigate for the presence of markers which may indicate either increased likelihood of tumor metastasis (loss of cell-cell receptor E-cadherin)[39,40] or may be used to implement targeted therapy (targeting of estrogen receptor positive cells by tamoxifen)[41–43].

Although there are several benefits of tumor pathology analysis, there are several shortcomings as well. First, tumor analysis by pathology requires highly skilled and trained individuals and whom are limited in the throughput with which they can analyze tumor characteristics[44–46]. In addition, tumor pathology analysis is subject to variability due to the physical considerations that must be taken into consideration during surgical resection of the tumor. For example, surgeons are limited in the amount of healthy tumor-adjacent tissue they can remove when resecting a GBM tumor[44–46]. This limitation not only introduces variability into pathology analysis, but may present only a partial picture of the migratory front of the tumor. Importantly, however, these assays are not predictive of tumor malignancy. More specifically,

although interrogation of common molecular markers helps to focus patient therapies, these analyses do not predict tumor migratory or metastatic potential[5,11–13,47–49]. This is because, although the tumor pathology has made considerable strides in identifying molecular markers of tumor migration and metastasis non have been ubiquitous through all tumor types[11]. Furthermore, though the tumor TNM staging system is helpful in scaling cancer progression, it is also not necessarily predictive of future tumor malignancy.

1.3.2 Modern genetic, molecular, and cellular analysis

Alongside, and in complement with pathology, genetic testing has proven to be extremely valuable in understanding tumor initiation, proliferation, and migration characteristics. This is because, at a fundamental level, cancer is a disease of genetic alteration whether it be mutation, loss of function, or over expression[50]. The advent of more accurate, rapid, and less expensive genetic testing of both the tumor and the patient samples has expanded our ability to more thoroughly understand tumor biology[51]. Specifically, sequencing has given us the ability to predict patient risk for tumor formation based on germline mutations, discover and analyze common and conserved driver mutations, predict of tumor malignancy based on recurring gene profiles, and target some of those common mutations[50,52,53]. These assays vary widely both in technique and the information they are able to discern, for example, analysis of chromatin availability[54] to binding of transcription factors[55] to quantification of gene expression. Furthermore, higher resolution techniques are continuing to be developed, in order to provide improved understanding of genomic information, and have reached the level of single-cell sequencing[54–58].

On example of genetic analysis is whole-genome sequencing (WGS). WGS has expanded our ability to determine and test for those common mutations which contribute to tumor formation, and malignancy[57,59,60]. Analysis of common underlying germline mutations has shed light on those mutations which may predispose patients toward higher tumor risk[61]. WGS works by isolating DNA from patient blood and tumor samples, through commercially available methods[62], enzymatically cleaved through restriction enzyme digestions, and amplified to ensure high signal purity during sequencing. The digested and amplified strands are then read through polymerization of the complimentary strand using fluorescently labeled nucleotides[63]. Together this knowledge has allowed for the implementation of more personalized therapies in preventing, detecting, and treating tumors. For example, the presence of BRCA germline mutations has been shown to drastically increase the risk of developing a mammary or ovarian tumors[50,64], and germline analysis of those patients. Likewise, genetic analysis of malignant melanomas tumors has found commonality in the BRAF[65] and MEK pathway mutations[66]. Small molecular inhibitors against these pathways have been developed, and show significant improvement in patient survival[67].

Though whole genome DNA sequencing has proven to be extremely helpful in enhancing our understanding of tumor formation, and malignancy, it does not give a full-spectrum analysis of genomic effects on tumor cell behavior. For example, until recently, genetic testing has been limited to bulk tumor samples, and not individual cells. The tumor and its environment, however, are very diverse and heterogeneous[68] comprised of many different cell types with a variety of genetic and epigenetic differences[48,56,69,70]. As a result, although bulk tumor sequencing is able to investigate genetic heterogeneity of tumors between patients (intertumoral), it is not able to

evaluate cell-to cell heterogeneity within a single tumor (intratumor)[13,49,71]. This means that the genetic signature of the small portion of the tumor cell populations which is highly migratory[8] and/or metastatic may be lost in comparison to the other tumor cells which are not[13,49,71]. Additionally, though DNA sequencing is able to determine the number of copies of a gene, it is not able to quantify expression of those genes in the way that RNA sequencing is able to[57].

In order to understand differences in gene expression and investigate intratumor heterogeneity, single-cell RNA sequencing (scRNA-seq) is now being performed on patient tumor samples[56]. The principles of scRNA-seq are similar to DNA sequencing, but necessitates additional steps in order to isolate individual cells. Specifically, once a tumor is resected, individual cells are isolated using either known cell-surface tumor markers (i.e. flow cytometry) or with marker-free methods (i.e. microfluidic chip)[13]. Both methodologies result in isolation of single-cells and allow for extraction of RNA, its conversion to cDNA, and genetic analysis[13]. These data are then compared to the other cells within the tumor, and across patients[72]. As previously mentioned, RNA-seq has several benefits over traditional bulk-tissue DNA sequencing such as ability to analyze gene expression levels, as well as stratification of heterogeneous cell populations in a tumor[5,13,73]. In addition, scRNA-seq allows for analysis of tumor cell "evolution" by investigating common mutations and reverse-engineering which cell populations contain original driver mutations and which cells combined those original drivers with other mutations[74,75]. This analysis is helpful in understanding central driver mutations of tumors, and the origins of tumor therapeutic resistance by identifying conserved and novel genetic alterations in primary and recurrent tumors respectively[48,76]. Moreover, the computational basis of scRNA-seq allows for

the combination of patient data in order to understand which genetic markers are most, common and stratify those groups which show the highest risk/lowest survival.

Though scRNA-seq provides some distinct advantages over traditional WGS, it also demonstrates some shortcomings[15]. First is the trade-off between throughput of single-cell separation and the need for tumor-specific markers. More explicitly, in order to perform scRNA-seq, cells have traditionally been isolated using FACS or antibody functionalized magnetic beads against tumor markers which have been previously characterized i.e. EpCAM[15,17,77]. Although these methodologies allow for the rapid and hi-throughput separation of tumor cells into single-cells suspension, they rely on known markers and show only a limited scope of the tumor cells from the bulk tumor. Conversely, separation of tumor cells in to single-cell suspensions independent of cell markers is much slower and lower throughput[15]. Marker-free separation utilizes either microfluidic separation or manual isolation and is limited in the number of cells (10k-100k cells) but is able to capture a more diverse array of cells compared to marker-based methods[15,78]. This trade-off between low throughput assays which characterize a wide array of cells or high throughput which are limited to known molecular markers prevents the application of scRNA-seq in predicting tumor migratory and metastatic potential.

Overall, tumor genetic analysis has made vast improvements in the field of tumor biology, not only in enlightening those common driver mutations, but improving understanding of tumor mutational evolution and heterogeneity[74,75]. Moreover, the cost, throughput and speed of these analyses is constantly improving allowing for more common implementation in helping to improve patient treatment and survival. However, its use as a methodology for predicting tumor

migratory and metastatic behavior is incomplete and must be complimented with other techniques.

1.3.3 Current techniques for analyzing invasive tumor cell population

In order to gain a more complete understanding of the mechanisms involved in tumor cell migration and metastasis, targeted genetic analysis of those migratory tumor cell populations is now being performed. To interrogate the differences of those migratory and the non-migratory cell populations (i.e. tumor bulk, and tumor periphery), cells are isolated using Laser Capture Microdissection (LCM)[18] and analyzed downstream for their genetic, epigenetic and molecular differences. LCM has emerged as a vital tool in extracting and analyzing those migratory tumor cells. LCM works by using high-power IR lasers to capture cells of interest or UV lasers to ablate all non-essential cells from the sample of interest (Fig 1.2)[79]. In addition, LCM is able to isolate cells from heterogeneous tissue section, cytological preparation, or live cell culture without the effect of contamination from other cell populations. When paired with high resolution genetic and molecular analysis such as scRNA-seq LCM has been able to illuminate those alterations that are involved in increasing cellular migratory phenotype[14].

LCM presents several benefits when compared to other methodologies such as bulk tumor genetic/molecular analysis, or even whole tumor single-cell sequencing. As previously mentioned, when paired with genetic analysis, such as scRNA-seq, LCM is able to directly analyze those cells which have disseminated away from the tumor site without obfuscation from other cell populations[14,80]. These data provide a clearer understanding of how changes in tumor cell genetic lineage or genetic heterogeneity may contribute to cell migratory phenotype. The ability to isolate whole cells allows for molecular analysis of those cells through high sensitivity methods

such as protein micro arrays[18]. Moreover, LCM is able to isolate those migratory cells from healthy parenchyma and directly measure their migratory characteristics as a metric for malignancy[14,81,82].

Though LCM has shown some distinct benefits in analyzing invasive tumor cells, there are, however, also several limitations associated with LCM. For example, the ability to isolate those migratory cells, and analyze their genetic or molecular markers is dependent upon a variety of technical variables. These variables include sample quality, methodology of preservation/ fixation, and the quality of sample extraction, and all of which contribute variability to the data that is collected[79]. In addition, although LCM allows for the interrogation of those tumor cells which have migrated into the healthy tissue stroma, the number and of cells which can be analyzed is limited by the margin of tissue during surgical resection (e.g. GBM)[46]. These data limitations not only obfuscate the data but give an incomplete picture of cell malignancy, but also limits the types of assays which can be performed (i.e. 1 cell for scRNA-seq vs ~5,000-30,000 cells for molecular profiling array)[18]. Most importantly, the time-intensive and the low-throughput nature of LCM limits its application in detecting and predicting tumor migratory and metastatic behavior.

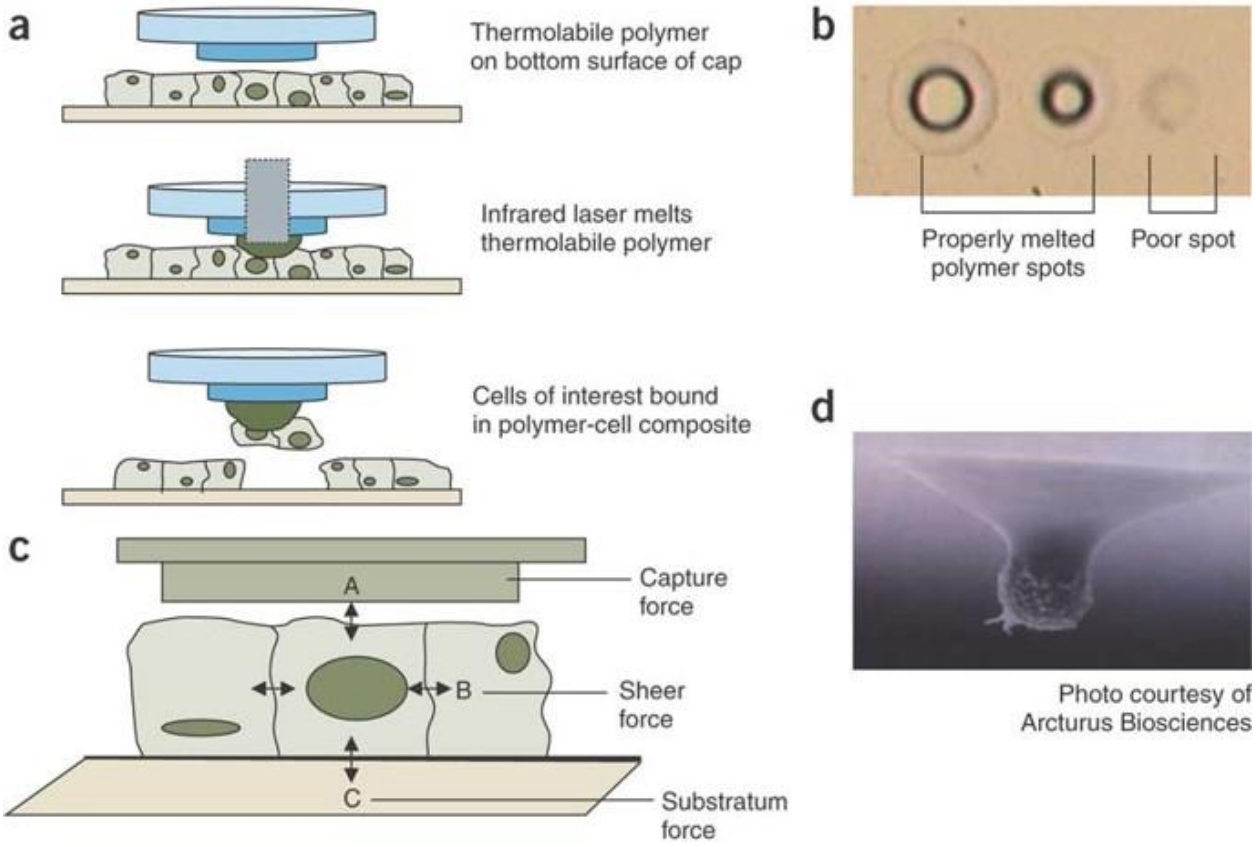

Figure is reproduced and modified with permission from ref.,[18]

Figure 1.2. The mechanics of Laser Capture Microdissection:

A) A thermolabile polymer is placed on a tissue section on a glass slide. An infrared laser melts the polymer in the vicinity of the laser pulse. The resulting polymer-cell composite is removed from the tissue. B) Properly melted polymer spots have a dark outer ring and a clear center, indicating that the polymer has melted and is in direct contact with the slide. Only cells lying within the diameter of the black melted polymer will be targeted for microdissection with each laser pulse. Poor spots have a fuzzy appearance, lacking a distinct black ring. C) Physical forces involved in LCM include an upward adhesive force between the substratum and the tissue, lateral forces between the cells, and a downward adhesive force between the polymer and the cells. D) A single cell is bound to the thermolabile polymer following microdissection with the infrared laser-capture technique.

1.4 Biophysical analysis: An emerging field in detecting, predicting, and understanding tumor migration and metastasis

1.4.1 Using biomaterials to predict tumor migration and metastasis by mimicking the tumor microenvironment

Due to the lack of universally applicable biomarkers to predict invasive and metastatic potential of solid tumors, biophysical analysis has made itself an attractive option for characterizing tumor invasive potential[83]. Because biophysical assays interrogate cellular properties such as size, deformability, circularity, etc. these assays are more broadly applicable in their ability to predict cellular behavior. These data have given considerable insight into which cell properties are important during the metastatic process, and serve as a more sensitive, accurate, and rapid indicator of cell migratory and metastatic phenotype when compared to traditional monitoring modalities.

One approach to analyzing cell biophysical characteristics is the use of engineered biomimetic materials in order to interrogate how cellular physical interaction with its microenvironment is indicative of its migratory phenotype. For example, it has been well documented that both epithelial mammary tumors and glioblastoma tumors exhibit an increase in mechanical stiffness compared to the surrounding tissue stroma[84–86]. In addition, analysis of mammary tumor and GBM microenvironment has demonstrated that these changes in tissue mechanics are due to an increase in the deposition, and remodeling of, structural ECM proteins[87–

[91]. Furthermore, it has been well described that these changes in fibronectin, collagen and Tenascin C only transform the topography of the tumor microenvironment, but serves as both a durotactic and receptor-signaling cue to enhance cellular migration into the surrounding tissue stroma[84,88–92].

In order to understand how these changes in the tumor microenvironment affect tumor cell behavior, in-vitro recapitulation of these biophyscial cues (such as increased matrix rigidity) have been performed[93,94]. Analysis of tumor niche biophysical changes have shed light on the tumor migratory and metastatic process, showing that those migratory and metastatic mammary tumor cells are sensitive to, and take advantage of, these structural changes in the tumor niche[92]. Specifically, these data indicate that migratory and metastatic tumor cell populations initiate a tension-induced response where, in response to this increase in matrix rigidity, cells increase focal adhesion assembly, and cellular contractility[10,95]. In mammary tumors, these cellular responses couple with signaling mechanisms such as extracellular signal-regulated kinase (ERK) downstream of the mechano-sensing as well as key transcription factors such as Twist family bHLH transcription factor 1 (TWIST1) to drive cells toward a migratory and invasive epithelial-to-mesenchymal phenotype transition (EMT) (Fig 1.3)[96,97].

Although interrogation of cellular mechano-sensitivity has both demonstrated the efficacy of cellular biophysical analysis, and illuminated some of the mechanisms involved in understanding cell migratory and metastatic potential there are also some limitations. First, is the technically challenging and time-consuming nature of the aforementioned assays both from a characterization and implementation perspective[98,99]. Specifically, prior to analyzing cellular biophysical response to differences in ECM properties, those tumor microenvironments must be

characterized in ECM composition and in mechanical properties (i.e. stiffness)[25,100]. This characterization is neither trivial nor rapid, and can require time and effort-intensive analysis such as immunofluorescent imaging (IF), immunohistochemical imaging (IHC) and atomic force Microscopy (AFM)[100–105]. In addition, ECM components, physical properties, and topographies must not only be recapitulated in-vitro, but also may not translate between tumor types. These restrictions require constant characterization of various tumor types, as well as extensive expertise in the materials and techniques necessary to fabricate, develop, and run such assays. Most importantly, the utilization of biomimetic materials to recapitulate the tumor niche is extremely low throughput, being limited by the number of cells whose migration can be observed and characterized by microscopy. In short, though mimicking cellular microenvironment is able to predict tumor cell migration and metastatic phenotype and is useful for understanding the mechanisms and pathways responsible for tumor cell behavior in a biomarker-independent manner, its implementation clinically is limited.

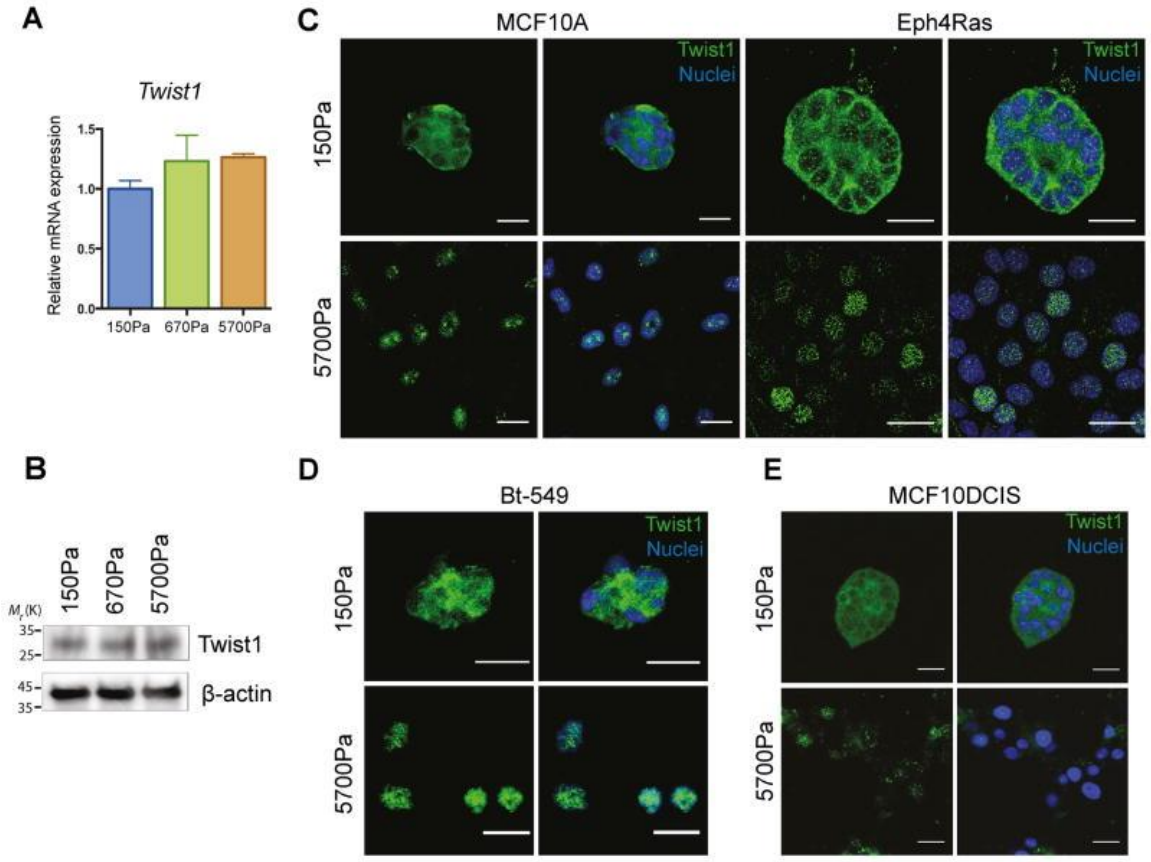

Figure is reproduced and modified with permission from ref.,[96]

Figure 1.3. Matrix stiffness regulates TWIST1 nuclear localization:

A) qPCR analysis of MCF10A cells grown in 3D culture on polyacrylamide hydrogels with the indicated rigidities (not significant, unpaired two-tailed t-test with Welch's correction, n = 3 independent experiments, statistics source data can be found in Supplementary Table 1; error bars represent s.d.). B) Cell lysates from MCF10A cells grown in 3D culture on polyacrylamide hydrogels with the indicated rigidities were analyzed by SDS–PAGE and probed for TWIST1 and β-actin. Unprocessed original scans of the blots are shown in Supplementary Figure 7. C–E) Eph4Ras, MCF10A (C), Bt-549 (D) and MCF10DCIS (E) cells were cultured in 3D culture with the indicated rigidities for 5 days and stained for TWIST1 (green) and nuclei (blue; scale bars, 25 μm).

1.4.2 Capturing circulating tumor cells

Although the use of biomaterials does predict tumor migration and metastatic propensity independent of the need for a biomarker, it is time-consuming, low throughput, and prohibitively complex to implement in a clinical setting. In order to more rapidly detect metastatic tumor cells as well as interrogate their biophysical properties, the use of turbulent flow microfluidics has been implemented[106]. Detection of circulating tumor cells (CTCs) is a clear metric of tumor initiation, growth and recurrence, because throughout tumor development, cells detach themselves from the primary tumor, and migrate into the surrounding stroma[107,108]. Once in that stroma, tumor cells migrate toward and intravasate into the vasculature in order to initiate metastasis to other organs. Moreover, these cells serve as a reservoir of tumor cells for tumor recurrence[3,4]. As a result, the presence of CTCs in the blood stream serves as an early indicator of tumor formation, and in addition, increased CTC prevalence is an indicator of increases in cell migration, tumor recurrence, and tumor metastasis[109].

In order to isolate tumor cells from patient blood, assays use either tumor-specific antigen labeling, or label-free methodologies, in conjunction with microfluidic principles[16,17,77,110]. In the case of tumor cells which express known antigens such as the rearrangement of ALK receptor, or chromosomal instability, these devices are able to rapidly and efficiently label those CTCs for isolation them from patient blood[77,110–112]. Once labeled, the cells can then be subjected to appropriate separation modalities such as magnetic bead separation or surface immobilization and further analyzed[16,17,77,110]. By contrast, those marker-free devices utilize differences in cell properties such as dimension, paired with optical analysis, and microfluidics properties such as turbulent flow to isolate those CTCs from patient blood (Fig 1.4)[16,17,113].

The use of microfluidics to detect and isolate CTCs from patients has a multitude of benefits. In addition to allowing for the detection of CTCs in a biomarker-independent manner, CTC levels serve as a rapid, quantifiable, and sensitive metric for tracking tumor recurrence or metastasis[16,17,113]. Furthermore, once isolated from patient blood, CTCs are then subjected to both biophysical and genetic analysis in order to understand which properties contribute toward their increasing malignant phenotype[16,17]. More explicitly, by interrogating the differences in cell biophysical properties, such as cell membrane stiffness or deformability, we are able to gain a clearer understanding of those properties which play a key role in cell migration and metastasis.

As with all methods, however, there are also a number of limitations associated with the use of microfluidic-based CTC analysis. The first is the rarity of events that these devices are attempting to detect, specifically it has been suggested that CTC may exist at a rate of 3 cell per mL of blood[16,108,109], by contrast 1mL of blood has between 4 and 6 million non-tumor cells[114]. Second is the rate of CTC isolation which is limited by sample volume and which further decreases the signal to noise of downstream biophysical analysis. Most importantly, is the inability of these assays to predict tumor migratory and metastatic phenotypes from a primary tumor. More explicitly, although CTC isolation is a highly sensitive and rapid assay for detecting tumor cells progressing through metastasis, this process must still occur and cannot be predicted form the primary tumor. Additionally, not all tumors (such as GBM) metastasize to other organs in the body and as a result, detecting CTC's would not prove effective.

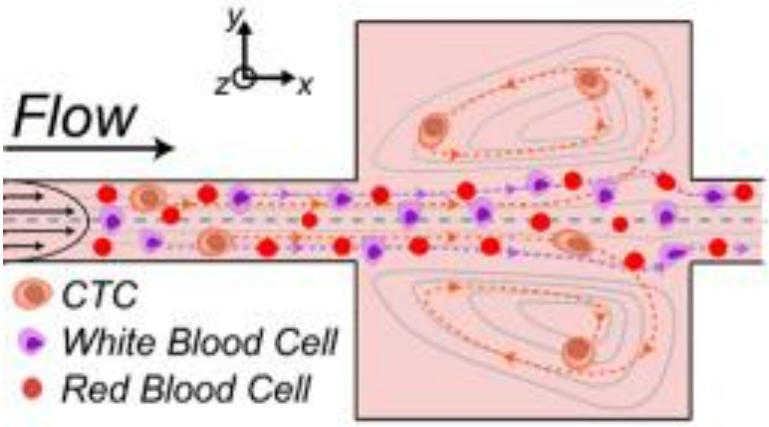

Figure is reproduced and modified with permission from ref.,[16]

Figure 1.4. Label-free isolation and enumeration of CTCs followed by downstream analysis:

The Vortex HT chip is used to capture CTCs in vortices formed in microfluidic reservoirs.

1.4.3 Directly interrogating biophysical properties of primary tumor cells

Due to the limitations associated with analyzing the presence of circulating tumor cells, new methodologies for directly interrogating primary tumor cell biophysical properties are being implemented. Specifically, in order to understand and predict tumor cell malignancy from the primary tumor, biophysical analysis of tumor cell properties such as membrane stiffness, nuclear rigidity, and migratory phenotype are being interrogated[19,22]. To assess these cell biophysical properties, cellular confinement and migratory assays have been utilized in order to understand differences between tumor cell populations[115]. These assays observe tumor cell biophysical properties as it migrates through a physically restrictive niche and assess which of those properties are critical to increasing cell malignancy. In addition, these assays can then be followed-up with genetic and molecular analysis in order to gain a mechanistic understanding of the genes and pathways driving these differences in tumor cell malignancy.

One example of interrogating cell biophysical properties directly is through the use of cellular confinement assays. Cellular confinement assays work on the principle of physically restricting tumor cell migration through a series of physical barriers and analyzing a cells ability to modify its physical properties in order to navigate around those barriers[116]. These assays are highly relevant to predicting tumor malignancy, because they directly measure cellular migration and observe biophysical characteristics, in the context of an assay which recapitulates the restrictive tumor microenvironment[20,117]. Through these analysis we are able to gain an understanding of how cellular biophysical characteristics enhance tumor cell malignancy[118].

One example of cellular confinement assays is the use of ECM coated polydimethylsiloxane (PDMS) pillars which are packed at a density which hinders cellular migration[19]. These assays

prevent migration of cells through without deformation of cell membrane, or in some cases disassembly, of the nuclear envelope (Fig1.5)[119]. This direct analysis of cell biophysical properties is a good predictor of cell malignancy, because it demonstrates the properties that a tumor cell must have in order to migrate into the healthy stroma. In addition, it directly examines cell migratory characteristics through live-cell microscopy of the tumor cells, and is able to analyze tumor cell populations to determine the proportions of malignant cells[19]. Furthermore, confinement chamber assays allow for post-assay analysis once cells are stratified by migratory and biophysical properties. Specifically, once cells are trapped in a specific region of the device (limited by their ability to deformed cell membrane or disassemble their nuclear envelop) they can then be analyzed by genetic or molecular methods to gain a mechanistic understanding of the pathways contributing to malignancy. Together, these metrics use of biophysical analysis via confinement and migration assays, along with genetic and molecular analysis, can be used to predict tumor cell migratory and metastatic potential in a mechanistic manner.

Though the confinement and migration assays are useful in their ability to analyze cell migratory and metastatic potential based on cell biophysical properties, they also exhibit some shortcomings. Specifically, though these assays allow for stratification of tumor cell populations based on migration characteristics, these assays require substantial investment in device design as well as a thorough understanding of PDMS fabrication methods. Furthermore, although these assays and can assess malignancy of a tumor, it is quite limited in the throughput of their analysis. More explicitly, the devices are limited to several hundred cells per assay, due to both physical restrictions of the device, and live-cell microscopy restrictions.

Cell confinement analysis has been very beneficial in expanding the biophysical and mechanistic understanding of malignant cell properties. Specifically, these assays have shed light on those cell properties (such as nuclear envelop disassembly) which tumor cells require in order to increase malignancy. These assays stratify tumor cell populations giving an accurate predictive analysis of malignancy in a tumor cell population, and can be paired with genetic and molecular assays in order to asses mechanism of action. However, the limitations of these devices prevent the implementation of cell confinement assays as a rapid and high-throughput methodology for assessing tumor migratory and metastatic potential.

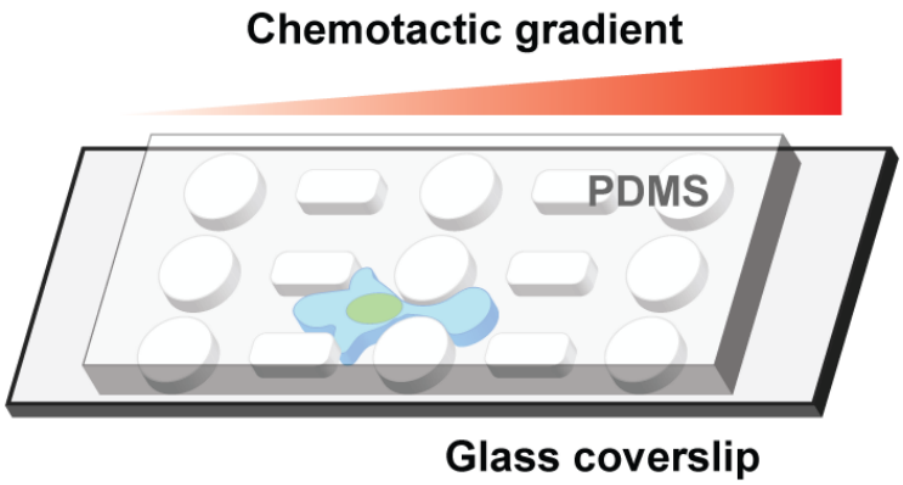

Figure is reproduced and modified with permission from ref.,[19]

Figure 1.5. Confined cell migration in microfluidic devices:

Schematic overview of the microfluidic device. Cells migrate along a chemotactic gradient through constriction PDMS channels, which provide precisely defined lateral and vertical confinement.

1.5 Utilizing cellular adhesion strength as a biophysical metric for tumor migratory and metastatic potential

1.5.1 Methodologies for interrogation of cellular adhesion strength

It has been well documented that cellular adhesion plays a vital role, and is altered, in many important biological processes such as development, proliferation, differentiation, and migration[120]. Furthermore, understanding how cellular adhesion strength is altered, and the effects that these changes have within the context of these fundamental biological processes, is crucial in shaping our understanding of biology[121].

In order to investigate how cellular adhesion strength changes and its consequences, a litany of assays have been developed to interrogate cell adhesion characteristics. Analysis of cell adhesion characteristics can range in scope and specificity, ranging from analysis of ECM-Receptor interactions to whole cell-ECM adhesion interrogation. For example, interrogation of ECM-Receptor interactions can be performed qualitatively through bead binding assays (e.g. biomembrane force probes and optical tweezers) as well as quantitatively through AFM analysis[122]. By contrast, whole cell-ECM interactions can be analyzed qualitatively through fluidic wash assays[123], as well as quantitatively through centrifugation assays[124].

These methods apply force to dissociate cell-ECM bonds shortly after initial attachment to the substrate even though it has been shown that fully adhered cells undergo adhesion strengthening by a complex interplay of integrin binding, focal adhesion assembly, and cell spreading over hours to days in culture[125]. Furthermore, these methods are either low in throughput but quantitative in their analysis, or are high in throughput and not quantitative.

Therefore, a methodology that permits quantitative assessment of large numbers of tumor cells simultaneously and in a manner that establishes and matures cell-ECM adhesion interactions is required.

A recent development in the field of cellular biophysical analysis is the application of fluidic shear stress as a quantitative and high-throughput method for determining cellular adhesion strength[126]. One methodology for analyzing cellular adhesion via quantitative fluidic shear is through spinning disk platform[126–128]. Spinning disk fluidic shear analysis exerts a range of shear stress in parallel to the surface the cells have adhered to, and which increases linearly with radial position defined by the following equation: $\tau = \frac{4}{5} r \sqrt{\rho \mu \omega^3}$ where r is the radial position from the center of the disk, ρ is the buffer density, μ is the buffer viscosity, and ω is the rotational speed of the disk. A complimentary assay for analyzing cellular adhesion strength by fluid flow is parallel plate flow analysis[129], which applies a defined shear stress across the cellular adhesion surface as described by the following equation: $\tau = \frac{6\mu Q}{wh^2}$ where μ is the buffer viscosity, Q is volumetric flow rate, h is chamber height, and w is chamber width.

1.5.2 Application of quantitative fluidic shear to interrogate cellular adhesion strength as a metric for tumor migratory and metastatic potential

Classically, fluidic shear has been applied to investigate cell biophysical characteristics within the context of cytoskeletal remodeling[87,130], and the effect of extracellular cues on cell adhesion[131]. Until recently, quantitative analysis of cell adhesion strength as a metric for tumor cell migratory and metastatic characteristics had not been implemented. However, given the delicate interplay between cellular adhesion and cellular migratory potential, changes in cellular

adhesion characteristics bode well as a biophysical marker for cell migratory and metastatic potential[132]. In order to evaluate cellular adhesion strength, the previously mentioned fluidic shear assays are utilized to interrogate cell biophysical properties. In addition, these assays are paired with genetic and molecular analyses in order to illuminate the mechanisms responsible for those differences in adhesion[133].

In order to perform cell adhesion analysis, spinning disk fluidic shear stress assays are conducted on sterile substrates functionalized with a structural ECM protein of interest[126]. Post-functionalization, the substrate is blocked to prevent deposition of cellular matrix components, and cells are seeded on to the substrates to allow for the initiation and maturation of cellular adhesion assemblies[127]. Once cells are adhered, they are subjected to fluidic shear (as defined by the equations above), fixed, imaged, and analyzed to determine the shear stress at which the normalized cell density has been reduced to half (Fig 1.6). This analysis allows for the rapid and quantitative determination of cellular adhesion strength, which has been shown to be an accurate metric for cell migratory and metastatic potential due to the inverse relationship between cellular adhesion and malignancy[132].

Specifically, spinning disk shear assays are able to characterize a cell population adhesion strength rapidly and in a quantitative manner due to the large range of fluidic shear stress that can be applied to the adherent cells[126]. More explicitly, due to the radially increasing shear characteristics, cells on the same substrate experience a range of shear stresses increasing from the center of the coverslip. In addition, although cells must be seeded in single-cell suspensions such that there are no compounding effects from cell-cell interactions, substrate dimensions (i.e. 25mm diameter) allow for large numbers of cells to be analyzed simultaneously. Furthermore,

computational analysis allows for the combination of multiple shear stress conditions which more accurately describe the adhesion characteristics of the cell population[132]. Lastly, spinning disk assays also allow for interrogation of both ECM structural components (fibronectin vs collagen vs laminin) as well as soluble factors which may be involved in modulating cell biophysical characteristics. As a result, spinning disk platform demonstrated its applicability as a rapid, high-throughput, quantitative and marker-free based analysis of malignancy of a tumor cell population. However, it does not allow for the stratification of the heterogeneity in a cell from that population to understand which sub-set of cells is more or less adherent, nor does it allow for live-cell imaging during shear analysis[132]. This is where PPFC can be applied, to compliment spinning disk shear analysis.

As previously indicated, PPFC subjects cells to fluidic shear in a similar way that spinning disk analysis does, however looking at the equation above, it is obvious that for a single flow rate and chamber height, there is no continuously varying term in the equation and as a result the fluidic shear is uniform over the surface of the device. Although this inability to provide a range of shear stress prevents the utilization of PPFC as a device for characterizing cell adhesion in a population-based manner, it provides some advantages as well. Specifically, because PPFC allows for the interrogation of cell adhesion strength at discreet numbers (and collection of those cells post-shear), it can be used to stratify heterogeneous cell populations. More explicitly single shear stresses are able to isolate those cells on either extreme of adhesion strength and subject them to downstream analysis to understand what genetic and epigenetic alterations may be responsible for the difference in adhesion phenotype. Furthermore, PPFC analysis allows for the imaging of those cells during shear flow, this allowing for the direct verification of increased cell

migration characteristics based on adhesion differences[133]. Similar to spinning disk shear analysis, PPFC analysis is quantitative, rapid, high-throughput, and marker free demonstrating its utility in assessing tumor malignancy characteristics. In addition, (again similar to spinning disk analysis) PPFC assays allow for the analysis of both ECM structural and soluble components, allowing for higher-resolution understanding of the factors which contribute to tumor cell malignancy.

Both the spinning disk and PPFC assays serve as excellent metrics for understanding and predicting tumor cell migratory and metastatic characteristics. Although these assays can only provide limited characterization of the tumor cells individually, they can be used in concert with each other (as well as with other genetic and molecular assays such as scRNA-seq) to provide high-quality and rapid prediction of tumor malignancy characteristics. Together these assays allow for a very complete analysis of cell biophysical properties and serve as a rapid and quantitative indicator of cell migratory and metastatic phenotype.

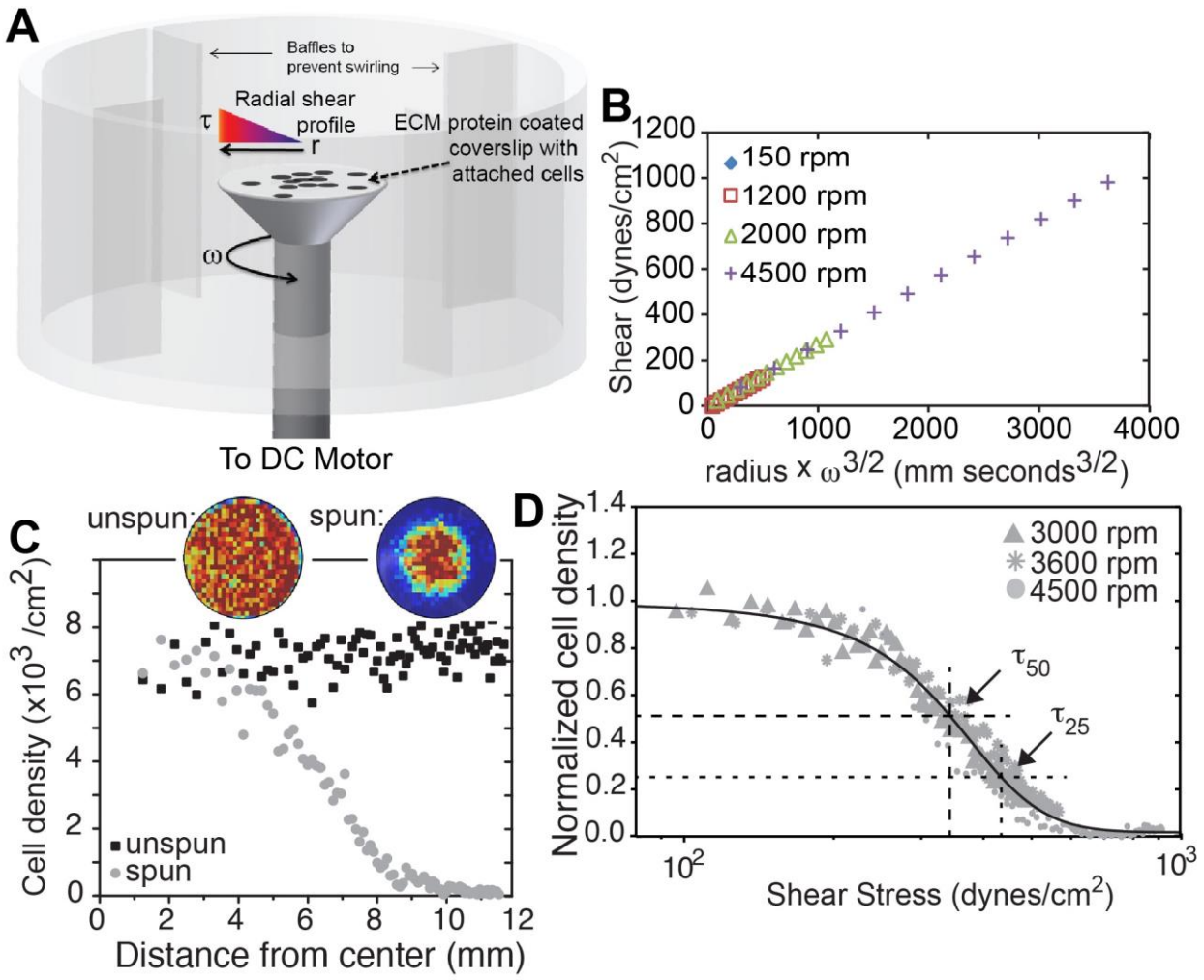

Figure is reproduced with permission from ref., [132]

Figure 1.6. Spinning Disc Assay Creates a Radially-dependent Shear Profile:

A) The spinning disc device is illustrated with cells attached to an extracellular matrix protein-coated coverslip mounted and rotating on a spinning rod in buffer. The radially-dependent shear profile is highlighted showing that cells at the center only rotate in place while those at the edge move around at a high linear velocity. B) The plot shows the relationship of radial position on the coverslip and angular velocity versus applied shear stress at a given point for the indicated velocities (in revolutions per minute; rpm). C) Plot of the relationship between radial position and cell density. Inset images show heat maps of cell density. Warm (red) and cool (blue) colors indicate high and low densities, respectively. D) Plot of cell density, normalized to the center of the coverslip, versus the applied shear. Data is plotted for the indicated velocities. τ25 and τ50, i.e. the shear to detach 25% and 50% of cells, respectively, are indicated in the plot and are 438 and 346 dynes/cm2, respectively.

1.6 Perspectives and conclusion

Analyzing, understanding, and predicting tumor migratory and metastatic characteristics is critical for improving patient survival through the tailoring of therapeutics to prevent the spread of tumor cells to other regions of the body. As the fields of tumor biology, and oncology continue to grow, more efficient and effective methodologies for predicting tumor behavior and assessing tumor malignancy are being developed. Some assays, such as genetic testing, are now being implemented in clinical setting and provide a clear picture of tumor driver mutations, and how these genetic alterations evolve during recurrence. In addition, genetic testing has been useful in identifying common genetic alterations (both in the tumor and germ-line cells) and determining the effects of those mutations on patient survival. These data have been instrumental in developing novel therapeutics for inhibiting those common mutations such as the use of osimertinib in treating T790M EGFR point mutations in non-small-cell lung cancer[134,135]. Although genetic testing has improved patient standard of care bulk tumor sequencing lacks the resolution to interrogate tumor heterogeneity or stratify highly malignant tumor cell populations. Furthermore, there is a lack of universally applicable markers which can predict tumor malignancy, limiting our ability to effectively target those cells which lead to tumor recurrence and metastasis.

These shortcomings demonstrated the need to design and develop assays which can analyze patient tumor samples at higher resolutions, and which do not rely on biomarkers to predict malignancy. In order to address these needs, biophysical assays such as ECM mimetic biomaterials, analysis of CTCs by microfluidics, and interrogation of cell rigidity characteristics have been developed. These assays provide a more universal approach to analyzing tumor

malignancy, and allow for the systematic analysis of downstream pathways in a reductionist manner. More explicitly, improved in-vitro tumor models allow for a more thorough understanding of tumor progression, as well as mechanism of action and opportunity of therapeutic intervention. For example, analysis of GBM microenvironment has shown that increases in ECM components such as tenascin c[95,136–138], result in increased tumor stiffness[139] and enhanced tumor migration phenotype[95,139–141] due to increased intracellular tension[142]. In-vitro recapitulation of these matrix conditions via biomimetic materials provides a mechanistic understanding behind increases cellular migration i.e. increased migratory phenotype stems from focal adhesion assembly due to integrin-based mechano-sensing of the extracellular environment[143]. These analyses are extremely important not only in establish a more accurate in-vitro model system, but also provide a platform to analyze the effects of inhibiting those pathways on cellular malignant phenotype[143].

Similarly, analyzing cell biophysical characteristics such as membrane rigidity, and their synergistic effects with ECM modifying enzymes is essential in understanding mechanism and limitations of cell motility. Cell motility through the tumor microenvironment is a complex process that involves a large variety of mechanisms and the use of confinement assays to interrogate these mechanisms is vital towards understanding and inhibiting those migration phenotypes[144]. One example of this is the use of microchannels to understand how tumor cells are able to migrate through spaces with a diameter 7-20μm where actomyosin contraction cannot be used[145]. The use of confinement assays indicated the use osmotic pressure-based migration through aquaporins at the leading edge of cells occurring independent of actin polymerization[24]. This novel migration modality provides a mechanism of action for

phenomenon which had not been understood and which groups are now targeting through the use of ion channel pump inhibitors[145].

The ability to assess tumor cell malignancy is critical for improving patient outcome because it will allow for the design of treatment regiments aimed at mitigating cell migration. The utilization of cell biophysical properties has emerged, in recent times, as a marker-free and broadly applicable indicator for predicting tumor cell migratory and metastatic potential. Furthermore, these assays provide insight into those properties that enhance tumor cell malignancy, and can stratify tumor and tumor cell populations to predict tumor aggression. To this point, fluidic shear has recently been utilized to analyze and stratify metastatic mammary epithelial tumor cells from a heterogeneous population[133]. These analyses demonstrated that decreased cellular adhesion and increased migration can be attributed to decreased focal adhesion assembly state, and increased contractility of the cytoskeleton, and that inhibition of actin assembly by nocodazole reverses these phenotypes. Furthermore, longitudinal characterization and RNA-seq analysis is now being performed on these stratified populations to determine the stability of weakly adherent cell phenotypes, and to gain a genetic understanding of the gene expression differences between the weakly and strongly adherent tumor cells respectively.

The use of biophysical analysis whether through biomaterials, confinement assays or fluidic shear has shown to be an effective toolset in understanding cell migratory and metastatic phenotypes from a novel perspective (Fig 1.7). Furthermore, the combination of biophysical assays with traditional genetic, molecular, and cellular analysis presents a new horizon in tumor analysis wherein samples can be rapidly characterized for malignancy, and therapeutic modalities

may be implemented to directly target those mechanisms. The application of these technologies is slowly being implemented in clinical settings toward the goal of improving patient outcome, and may soon serve as commonplace assays for informing personalized therapeutics.

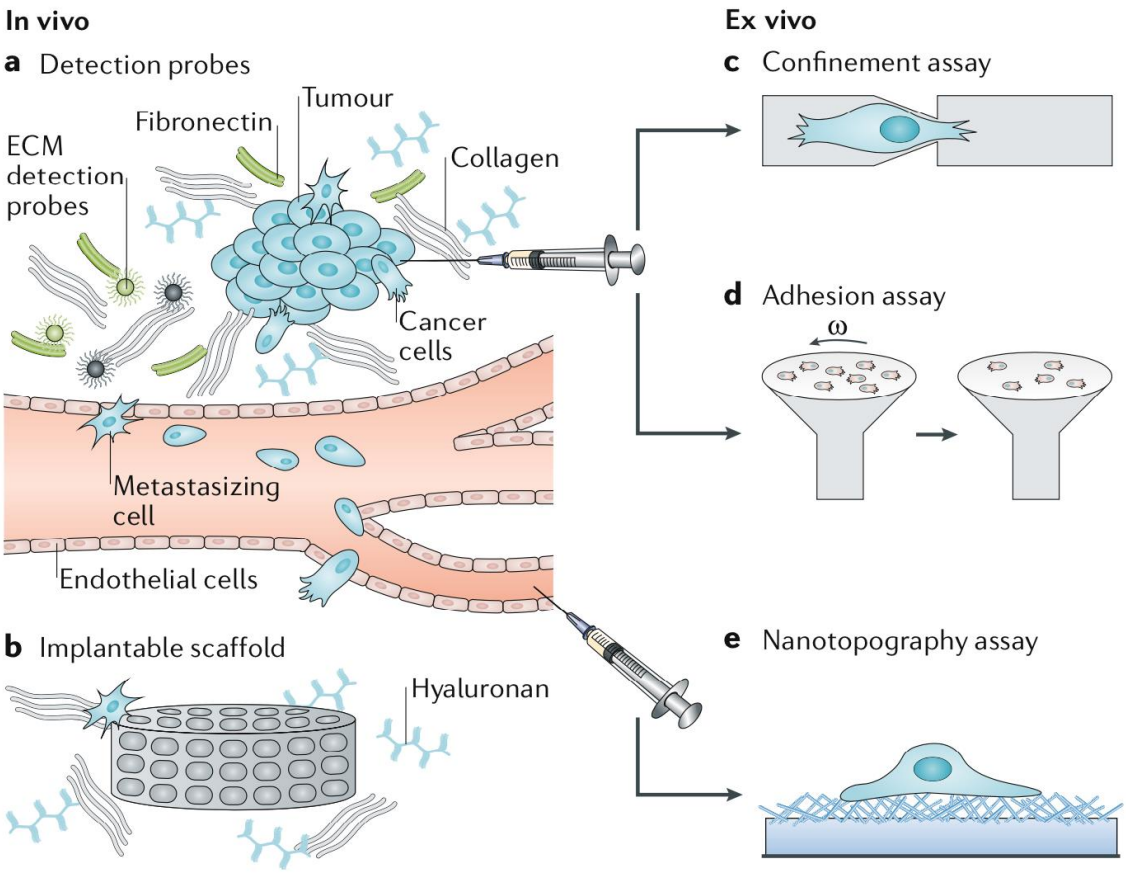

Figure is reproduced with permission from ref.,[27]

Fig 1.7. Next-generation material-based cancer technologies:

The specific interactions between cancer cells and the tumor stroma can be exploited for the detection of cancer cells: A) Magnetic resonance imaging (MRI) or positron emission tomography (PET) contrast agents can be conjugated with extracellular matrix (ECM)-affinity peptides to create specific probes to target the dense ECM of the tumor stroma for the detection of mature tumors in vivo. B) Implantable scaffolds can be used to recreate a pre-metastatic niche at the implant site, recruiting cells for capture and therapy and at the same time lowering the tumor burden in typical secondary metastasis sites. c,d) Confinement assays or adhesion assays can be applied to test cells obtained from tumor biopsy samples for their aggressiveness by measuring cellular deformation or adhesion to specific ECM molecules. Omega (ω) is the angular velocity that defines the shear stress applied to cells. E) Circulating tumor cells (CTCs) can be isolated from patient blood samples using nanotopography assays that take advantage of the affinity of CTCs for nano-roughed substrates.

1.7 Acknowledgements

Funding for this work was provided by US National Institutes of Health grants R01CA206880 (A.J.E. and J.Y.) and R21CA217735 (A.J.E.), a US National Science Foundation grant 1463689 (A.J.E.) and the Graduate Research Fellowship program (A.B.). Additional fellowship support was provided by Brazilian Federal Agency for Support and Evaluation of Graduate Education award 88881.135357/2016-01 (B.F.M.).

Chapter 2.

Metastatic state of cancer cells may be indicated by adhesion strength

2.1 Abstract

Cancer cells within a tumor are heterogeneous and only a small fraction are able to form secondary tumors. Universal biological markers that clearly identify potentially metastatic cells are limited, which complicates isolation and further study. However, using physical rather than biological characteristics, we have identified Mg^{2+}- and Ca^{2+}-mediated differences in adhesion strength between metastatic and nonmetastatic mammary epithelial cell lines, which occur over concentration ranges similar to those found in tumor stroma. Metastatic cells exhibit remarkable heterogeneity in their adhesion strength under stromal-like conditions, unlike their nonmetastatic counterparts, which exhibit Mg^{2+}- and Ca^{2+}-insensitive adhesion. This heterogeneity is the result of increased sensitivity to Mg^{2+}- and Ca^{2+}-mediated focal adhesion disassembly in metastatic cells, rather than changes in integrin expression or focal adhesion phosphorylation. Strongly adherent metastatic cells exhibit less migratory behavior, similar to nonmetastatic cell lines but contrary to the unselected metastatic cell population. Adhesion strength heterogeneity was observed across multiple cancer cell lines as well as isogenically, suggesting that adhesion strength may serve as a general marker of metastatic cells.

2.2 Introduction

Cancer cell dissemination is a highly coordinated process in which a cell detaches and migrates away from the primary tumor to form a secondary metastatic site[23]. However, only a small subset of cancer cells from a tumor or even from a cancer cell line are capable of causing secondary tumors in vivo[8]. Successful dissemination requires collagen fiber deposition, alignment, and cross-linking in the adjacent stromal matrix[9,10] to create tracks on which cells migrate. However, this will only occur in cells with labile adhesions[20]. Focal adhesion (FA) turnover permits the migration required of invasive cancer cells[146], which tend to have more dynamic FAs than noninvasive cancer cells[147,148]. Due to the lack of a consistent set of biomarkers that predict metastatic potential across solid tumors[11], a systematic quantification of adhesion strength could result in a unique biophysical metric to identify highly metastatic cells within a broader tumor cell population. Furthermore, a quantification of tumor cell adhesion strength could serve as a predictor of the metastatic potential of a solid tumor.

Population-based adhesion assays, e.g., the spinning-disk shear assay[127,128], can monitor FAs by measuring adhesion strength. Specifically, by analyzing the magnitude of shear needed to detach 75% of the cell population (denoted by τ_{25}), we are able to quantify the adhesion strength of a cell population and correlate it with FA assembly. In addition, the spinning-disk shear assay can capture adhesion heterogeneity within a population[131]. For example, by plotting a log shear stress versus linear cell density profile, we are able to analyze the logarithmic slope for the resulting sigmoidal curve. From these data, we are able to determine the attachment

heterogeneity of a cell type in a variety of conditions. In contrast, single-cell, single-shear, and wash assays cannot quantify these values[148–153]. Although some studies have shown a correlation between changes in adhesion and secondary tumor development[151–153], substantial phenotypic heterogeneity can exist even within a single cancer cell line[154]. Thus, understanding the adhesive heterogeneity within an invasive population may improve our ability to physically monitor cancer cells and predict invasive behavior. Population-based adhesion assays also provide a reductionist niche for determining sensitivity to culture conditions (e.g., cation concentration and matrix composition)[131]. This is especially important because breast tumors have higher magnesium (Mg) and calcium (Ca) concentrations than healthy breast tissue[155,156]. Clinically, lower stromal cation concentrations have been associated with increasingly metastatic[157] and aggressive[158] tumors. As cancer cells migrate into the stroma, lower Mg^{2+} and Ca^{2+} concentrations may decrease integrin activation[159] and clustering[160,161], thus favoring the labile adhesions required for cancer cell migration[20]. These data appear consistent with observations that integrin activation is inversely proportional to the metastatic potential of mammary cell lines[148], whereas traction forces are proportional[162]. These data collectively suggest that heterogeneity in the adhesion-strength profile in stromal conditions may act as a biophysical marker, indicating the presence of a subset of metastatic cancer cells that are capable of disseminating into the stroma with lower Mg^{2+} and Ca^{2+} concentrations. Thus, we hypothesize that strongly adherent cells within a metastatic cell line will be the least migratory, and that adhesion strength is regulated by the sensitivity of assembled FAs to stromal $Mg^{2+}$and Ca^{2+} concentrations.

To understand how Mg^{2+} and Ca^{2+} influences cancer cell adhesion, we performed a spinning-disk analysis on epithelial and invasive cancer cell lines across a spectrum of metastatic

potentials while varying the Mg^{2+} and Ca^{2+} levels. We observed a remarkable cellular heterogeneity and a decrease in cellular adhesion strength during the spinning-disk analysis. This was quantified by a decrease in logarithmic slope and a leftward shift in the τ_{25} value when shear stress was plotted versus cell density. This phenotype was only present in low Mg^{2+} and Ca^{2+} conditions for metastatic cell lines. These observations correlated with FA disassembly and were recapitulated in nonmetastatic cell lines that had been transformed to mirror their metastatic counterparts. The data further establish that metastatic cells with less labile adhesions and higher adhesion strength have reduced migration in collagen gels and transwell assays. These behaviors were independent of tumor and tissue type and were demonstrated isogenically. These results support the concept that adhesion strength may act as a universal biophysical regulator of metastasis.

2.3 Results

2.3.1 Mg^{2+} and Ca^{2+} concentrations influence the adhesion heterogeneity of metastatic cells

To disseminate from primary tumors, metastatic cancer cells must invade adjacent stroma, which requires a transition from stable to labile adhesion. Using a spinning-disk device (Figure S2.1), we measured the adhesion strength, τ_{25}, of mammary epithelial cell lines of varying metastatic potential. At physiological (serum) cation concentrations, i.e., 0.5 mM Mg^{2+} and 1 mM Ca^{2+} (denoted as PBS + MgCa), the adhesion strengths of nontumorigenic MCF10A cells, tumorigenic but not metastatic MCF7 cells, and tumorigenic and metastatic MDAMB231 cells to

fibronectin were very similar, with no dramatic differences (Figure 2.1, black). Mg^{2+} and Ca^{2+} concentrations differ between a healthy niche and tumor niche[155,156], and their removal during 5 min of shear application only slightly reduced the adhesion strength of MCF10A and MCF7 cells. However, the removal of Mg^{2+} and Ca^{2+} significantly reduced MDAMB231 cell adhesion strength (Figure 2.1, red) by more than an order of magnitude (Figure 2.1E). Notably, the cell adhesion strength of the latter metastatic cell line was very heterogeneously distributed, with a significantly lower logarithmic slope versus nonmetastatic lines (Figure 2.1F). Given the significant genetic differences between these lines, we also assessed the adhesion strength of H-Ras-transformed MCF10A cells (labeled MCF10AT cells), which give rise to invasive carcinoma in vivo[163,164]. As was the case with MDAMB231 cells, the MCF10AT cells showed Mg^{2+} and Ca^{2+} sensitivity, with lower τ_{25} and slightly more heterogeneity than MCF10A cells (Figure 2.1D, open versus closed data points). In contrast to fibroblasts[131], shear forces in the presence of Mg^{2+} and Ca^{2+} did not induce large changes in size for any of the cell lines tested. Furthermore, in the presence of Mg^{2+} and Ca^{2+}, variation in cell size across different cell lines was within the same order of magnitude. In these analyses, we visually assessed the cells to ensure that they were sufficiently spaced apart to prevent cell-cell interactions from disrupting the shear analysis (Figure S2.2).

Although these data were obtained over a wide range of Mg^{2+} and Ca^{2+} concentrations, concentration gradients likely exist between the tumor and adjacent stroma[155,156]sel. We found that homogeneous and strong adhesion strengths for metastatic cells, i.e., high τ_{25} and a logarithmic fit slope in density versus shear plots, could be gradually restored with increasing cation concentrations (Figure 2.2A), independently of cation type (Mg or Ca), with significant

sensitivity at tumor and adjacent stroma concentrations (Figure 2.2B). Mg^{2+}- and Ca^{2+}-dependent adhesion heterogeneity was also observed on type I collagen and could be gradually restored with increasing Mg^{2+} and Ca^{2+} concentrations (Figure 2.2, C and D). Conversely, adhesion strength changes were minimal for nontumorigenic cells, which always exhibited strong adhesion (Figure S2.3). Thus, metastatic mammary epithelial cells likely adhere in a metastatic- potential-dependent manner based on a subset of FA parameters.

Adhesive heterogeneity also extends beyond MDAMB231 cells to other metastatic cells. For comparison, we analyzed metastatic MDAMB468 and SUM1315 mammary cells by spinning-disk assay to determine the heterogeneity of their adhesion strength. The cells were sufficiently spaced apart to enable measurements of only the cell- matrix adhesion strength[130] (Figure S2.2). Although it was not as robust as that observed for MDAMB231 cells, their adhesion strength was also heterogeneously distributed in terms of a lower τ_{25} and logarithmic fit slope, especially in comparison with BT20, an invasive but non-metastatic mammary cell line, and BT549, a nonmalignant and nonmetastatic mammary cell line. PC-3 prostate carcinoma cells, a tumorigenic and highly metastatic cell line, also exhibited heterogeneously distributed adhesion (Figure S2.4), indicating that common FA parameters may make adhesion strength a unique biophysical metric of cell state.

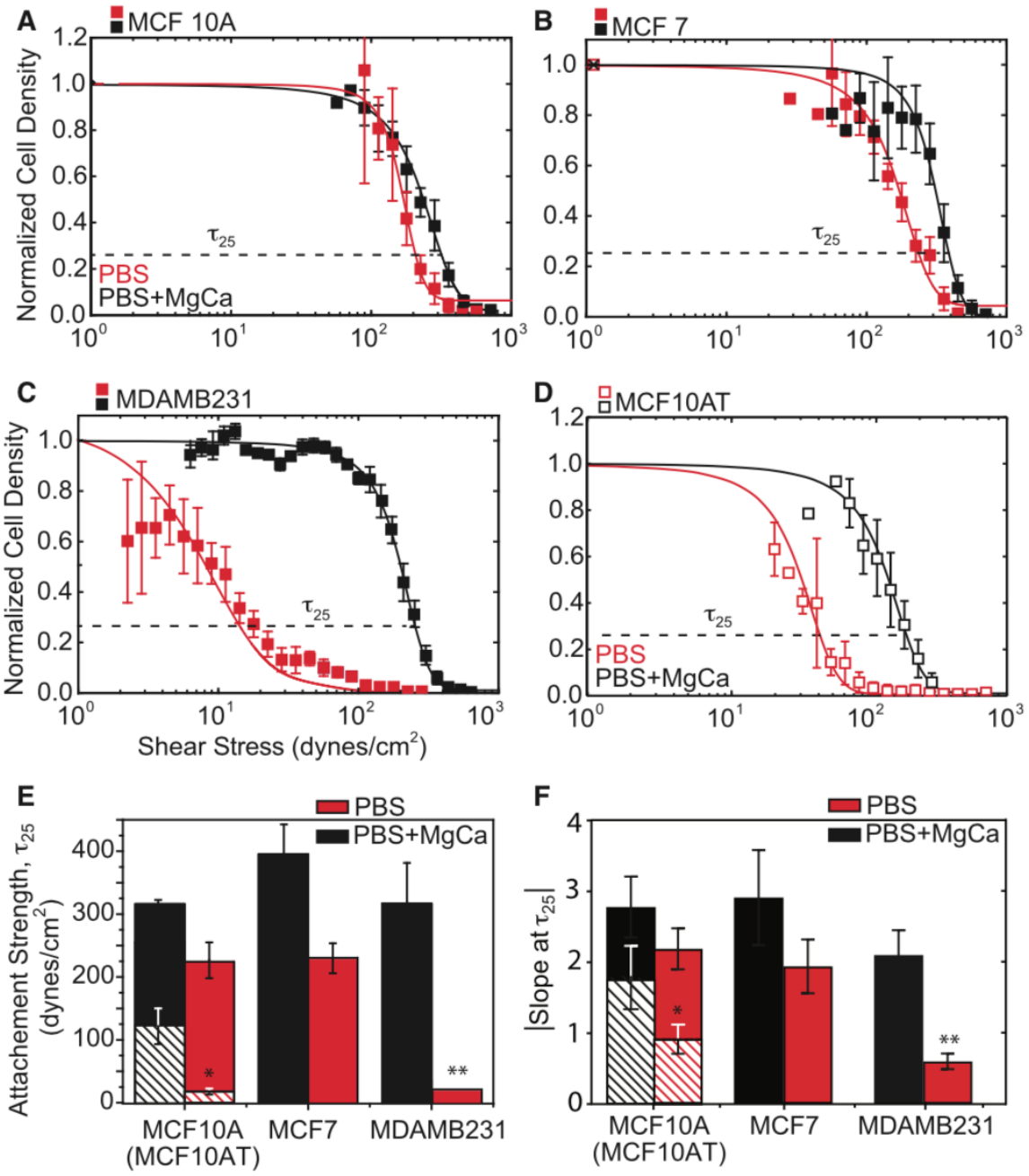

Figure 2.1. Adhesion strength is heterogeneous for metastatic mammary epithelial cells in a stromal-like niche:

(A–D) Normalized cell density is plotted versus shear stress for (A) MCF10A (closed) and MCFA10T (open), (B) MCF7, (C) MDAMB231, and (D) MCF10AT cells. Shear stress was applied in buffer with (black) and without (red) 0.5 mM Mg^{2+} and 1 mM Ca^{2+}. t25, i.e., the shear to detach 25% of cells (also referred to as adhesion strength) is indicated in each plot. (E) Plot showing the average adhesion strength for cells exposed to shear in PBS buffer with (black) and without (red) cations. Crosshatched bars indicate data from MCF10AT cells. (F) Plot of the absolute magnitude of the logarithmic fit slope for each cell line and cation condition. All shear plots represent binned averages from biological triplicate experiments performed across multiple, overlapping shear ranges. All adhesion-strength assays were performed using fibronectin-coated coverslips. All other plots have n > 3.

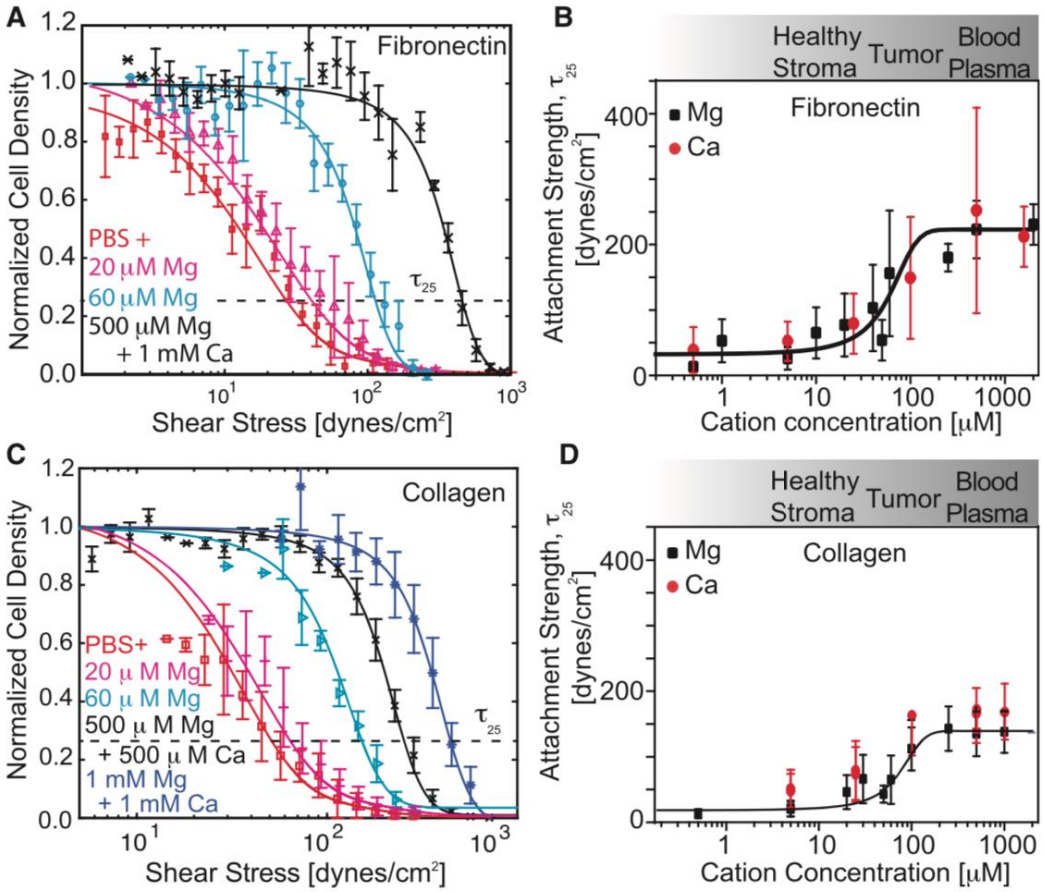

Figure 2.2. Adhesion strength can be titrated but is independent of the matrix ligand type:

(A) Representative plot for MDAMB231 cells bound to fibronectin-coated coverslips versus the applied shear. Each color corresponds to the indicated cation condition; τ_{25} is indicated. (B) Plot of the average τ_{25} adhesion strength for MDAMB231 cells bound to fibronectin-coated coverslips versus cation concentration. The data are plotted separately for modulation of Mg^{2+} (black squares) or Ca^{2+} (red circles), but the sigmoidal fit is for the combined data. The cation concentration range for the indicated tissue is provided for reference based on Seltzer et al.. (C) Representative plot for MDAMB231 cells bound to collagen type I-coated coverslips versus the applied shear. Each color corresponds to the indicated cation condition; τ_{25} is indicated. (D) Plot of the average τ_{25} adhesion strength for MDAMB231 cells bound to collagen type I-coated coverslips versus cation concentra- tion. The data are plotted separately for modula- tion of Mg^{2+} (black squares) or Ca^{2+} (red circles), but the sigmoidal fit is for the combined data. All shear plots represent binned averages from biological triplicate experiments performed across multiple, overlapping shear ranges. All other plots have n > 3.

2.3.2 Adhesion heterogeneity correlates with a migratory phenotype

Although metastatic mammary epithelial cells display adhesive heterogeneity in a niche with low concentrations of Mg and Ca, it remains unclear how adhesion differences affect migration. We assessed cell migration in cell media containing physiological Mg and Ca concentrations first by selecting for strongly adherent cells, as outlined in (Figure 2.3A). Migration appeared to change with relative adhesive heterogeneity in the absence of Mg and Ca; for example, minimal migration was observed for MCF10A cells and MDAMB231 cells selected with 45 dynes/cm^2 shear, whereas unselected MDAMB231 cells were significantly more motile (Figure 2.3B) and progressive in their migration. Migration of unselected MDAMB231 cells in collagen gels was increasingly persistent and linear with collagen concentration. Conversely, strongly adherent cells selected with high shear progressively lost their persistent, linear migration (Figure 2.3C). Other metastatic mammary cells, i.e., SUM1315, also demonstrated adhesive heterogeneity (Figure S2.4), exhibiting more persistent, linear migration on collagen-coated, planar substrates than on collagen hydrogels. Migration of unselected SUM1315 cells, however, was more persistent and linear on collagen hydrogels compared with strongly adhering cells (Figure S2.5A). Migration of PC3 prostate cancer cells was also more persistent and linear with the unselected cell population (Figure S2.5B). These data suggest that shear selection can selectively isolate highly adhesive, Mg- and Ca-independent MDAMB231 cells, which appear to be less migratory than unselected MDAMB231 cells. Cell migration was also assessed using a transwell assay over 48 h. Relative to MCF10A cells, twice as many unselected MDAMB231 cells migrated through the pores. Metastatic cells demonstrating a strongly adherent phenotype during shear selection also exhibited decreased migration in the transwell assay. Interestingly, a

significant number of MDAMB231 cells detached from the transwell insert and reattached to the chamber bottom. Significantly more MDAMB231 cells underwent this process compared with MCF10A (Figure 2.3D). Thus, the highly adhesive, Mg- and Ca-independent MDAMB231 cells appear to be less migratory than their unselected counterparts, which contain a highly migratory subpopulation.

2.3.3 Labile FAs reduce adhesion strength and enhance migration in metastatic cells.

Although these data illustrate adhesive differences and their correlation to a migratory phenotype, they do not suggest an origin for these differences. Strongly adherent MDAMB231 cells did not differentially express integrins (Figure 2.4A), nor did phosphorylation of FAK change between MCF10A and MDAMB231 cells as a function of shear exposure (Figure 2.4B), suggesting a structural mechanism. Consistent with their adhesion strength, MCF10A cells did not fully disassemble their FAs (Figure 2.4, C and D) and maintained their size and shape (Figure 2.4, E and F) after Mg^{2+} and Ca^{2+} removal in the absence of shear. Conversely, metastatic MDAMB231 cells disassembled their FAs (Figure 2.4, G and H) without significant changes in their size or morphology (Figure 2.4, I and J). Thus, Mg^{2+} and Ca^{2+} sensitivity in the absence of shear suggests that MDAMB231 adhesions are transient and independent of the amount of elapsed culture time before shear application.

Although MCF10A cells did not exhibit Mg^{2+}- and Ca^{2+}- sensitive adhesion, we next asked whether we could induce FA disassembly and adhesion strength heterogeneity in these cells. Cells were seeded onto a fibronectin-coated substrate and pretreated with the fibronectin integrin-blocking peptide RGD. When the fibronectin-binding integrins were blocked, cells without Mg^{2+} and Ca^{2+} exhibited statistically fewer FAs per area (Figure 2.5, A and B). These data

are consistent with fewer FAs but a different distribution from MDAMB231 cells (Figure 2.5B versus Figure 2.4H). When exposed to shear, RGD-treated MCF10A cells exhibited lower adhesion strengths but were not as heterogeneous as MDAMB231 cells (Figure 2.5C), possibly due to uniform integrin blocking with RGD ligand. Free RGD improved cell migration velocity (Figure 2.5D) to rates similar to those observed for MDAMB231 cells versus untreated nonmetastatic cells. Overall, these data suggest that FAs in metastatic cells are more Mg^{2+} and Ca^{2+} sensitive than those in non-metastatic cells and disassemble in stromal conditions (in contrast to nonmetastatic cells), thus driving the metastatic potential.

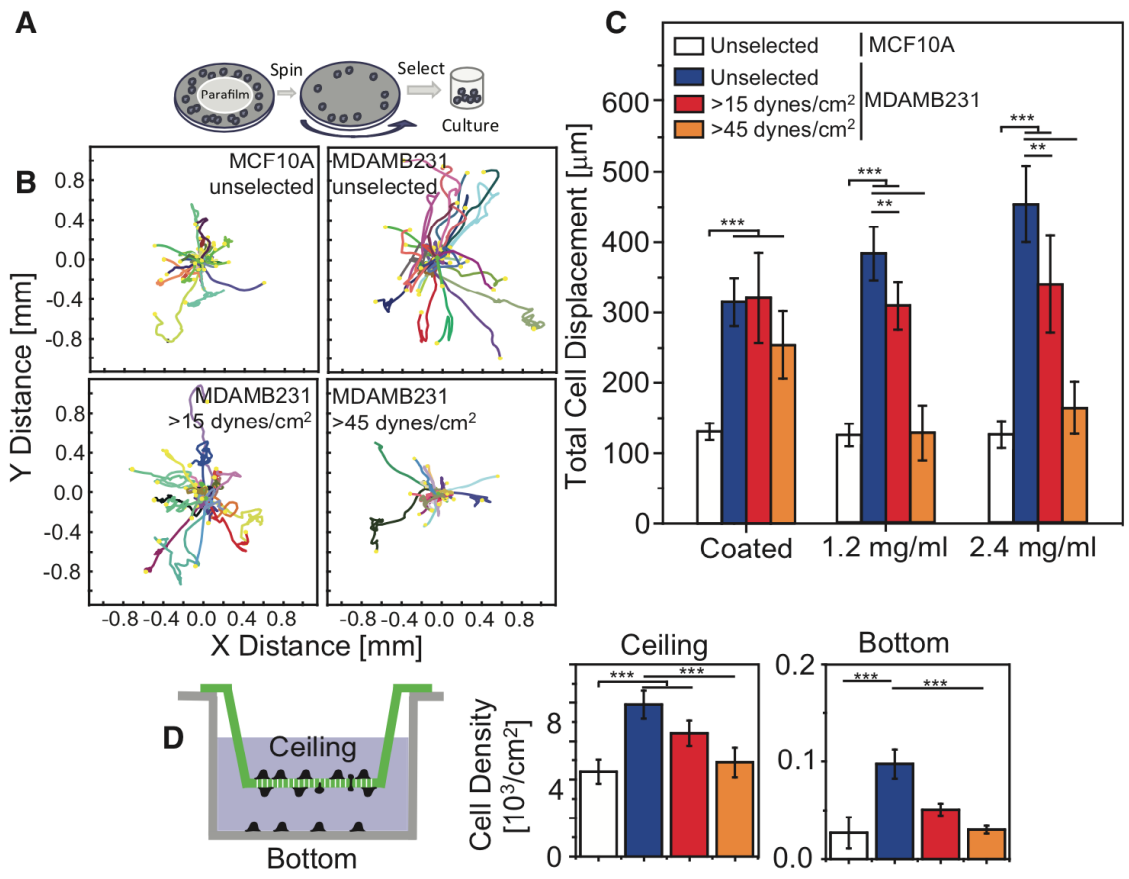

Figure 2.3. The weakly adherent subpopulation of MDAMB231 cells is highly migratory:

(A) Schematic of the selection assay, where Parafilm is used to block the center of the coverslip so that cells only adhere to regions exposed to high shear stress. After trypsinization from collagen- coated coverslips, the cells are re-plated in migration or transwell assays. (B) Rose plots of cell migration trajectories for the indicated cell lines and shear stress selection conditions. Each trajectory represents an individual cell path on a collagen-coated substrate, as observed over 24 h. (C) Total cell displacement over 24 h for the indicated cell lines, shear stress selection conditions, and substrates. Each bar represents experiments performed in biological triplicate with >20 per sample and with each cell trajectory quantified at 15 min intervals over 24 h of imaging. (D) At left is an illustration of the transwell migration assay, indicating cells that have migrated through the pores of the membrane (green; referred to as the ceiling) and those cells that subsequently detached and reattached to the bottom of the well (gray). At right are graphs of cell density for the indicated cell lines and shear stress selection conditions. Cell densities on the ceiling of the insert (top) and bottom of the well (bottom) are shown separately and represent the results of triplicate biological replicates. **$p < 0.01$, ***$p < 0.001$.

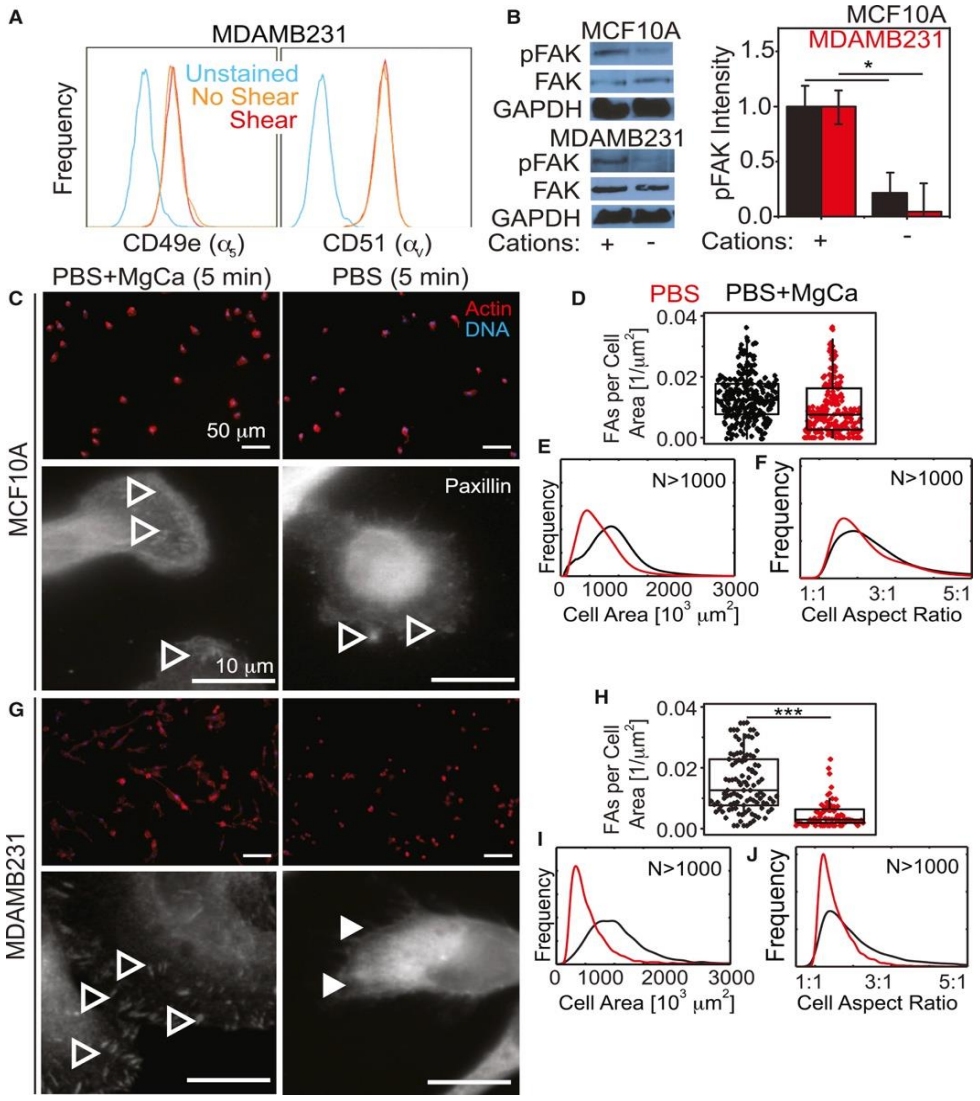

Figure 2.4. FAs are more Mg^{2+} and Ca^{2+} sensitive in MDAMB231 cells than in MCF10A cells:

(*A*) Flow-cytometry profiles for the indicated integrins of MDAMB231 cells that were previously exposed (*red*) or not exposed (*orange*) to shear stress in the absence of cations. Unstained controls (*blue*) are shown for reference. (*B*) Representative Western blots for pFAK, total FAK, and GAPDH are shown for the indicated cells exposed to the indicated cation conditions for 5 min. Quantification of band intensity, normalized to GAPDH and total FAK, is shown for MCF10A and MDAMB231 cells with and without Mg^{2+} and Ca^{2+}. (*C*) Images of MCF10A cells in the indicated buffer conditions for 5 min without shear. Upper images are lower magnification and show cells stained for actin (*red*) and DNA (*blue*). Lower images are at higher magnification for the same conditions as the upper images and were stained for paxillin (*green*), actin (*red*), and DNA (*blue*). (*D*) Scatter plot of MCF10A cells, counting the number of FA plaques per square micron. (*E* and *F*) Frequency plots of MCF10A cell area and aspect ratio. (*G*) Images of MDAMB231 cells in the same conditions indicated in (*C*) for MCF10A cells. Open and closed arrowheads in (*C*) and (*G*) indicate cells with and without visible FAs, respectively. (*H*) Scatter plot of MDAMB231 cells, counting the number of FA plaques per square micron. (*I* and *J*) Frequency plots of MDAMB231 cell area and aspect ratio. In (*D–F*) and (*H–J*), cells incubated with and without cations for 5 min before measurement are shown in black and red, respectively. The scale bar represents 50 μm for all images. All adhesion assays were performed with fibronectin-coated coverslips. $^{***}p < 0.001$. All frequency and dot plots represent triplicate experiments analyzing 500+ cells per condition.

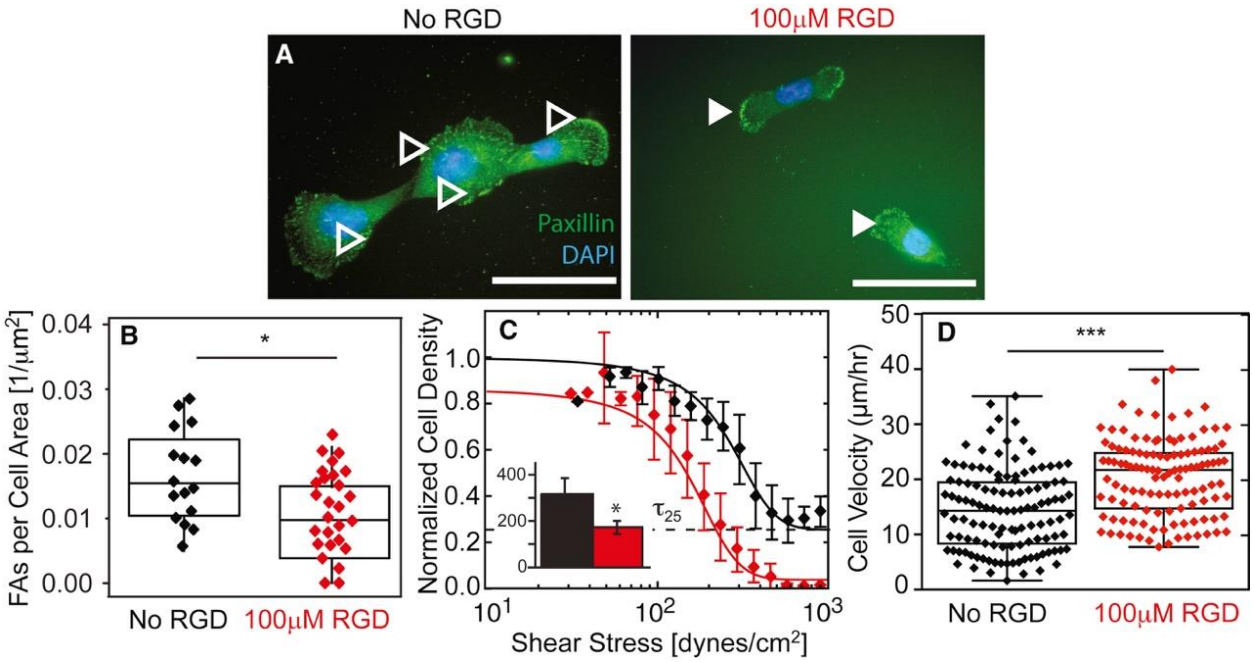

Figure 2.5: Integrin blocking reduces cation-dependent adhesion strength in nonmalignant cells:

(*A*) MCF10A cells were stained for paxillin (*green*) and nuclei (*blue*). Open and closed arrowheads indicate FAs for the indicated RGD culture condition. Scale bars, 100 μm. (*B*) Plot of the number of FAs per cell area for cells without (*black*) and with (*red*) RGD. (*C*) Normalized cell density is plotted versus shear stress for cells without (*black*) and with (*red*) RGD. The inset shows the average τ_{25} adhesion strength for each condition in dynes per square centimeter. $^{*}p <$ 0.05. All dot plots represent triplicate experiments analyzing >20 cells per condition. Shear plots represent binned averages from biological triplicate experiments performed across multiple, overlapping shear ranges. All adhesion-strength assays were performed using fibronectin-coated coverslips. (*D*) Plot of cell velocity, in micrometers per hour, for cells treated (*red*) or not treated (*black*) with RGD on fibronectin-coated coverslips. $^{***}p < 0.001$ for comparisons with unpaired *t*-test with Welch's correction. To see this figure in color, go online.

2.4 Discussion

Cancer is a heterogeneous disease, which can be observed in comparisons between tumors, across cell lines, and even within a single cancer cell population. Complex tumor genotyping has been used to predict metastatic risk[165,166], and although these predictions are successful for some tumor subclasses[167], they do not identify the functional mediators of metastasis[76]. Even in model cell lines, a subpopulation may develop increased metastatic potential under certain conditions that could inhibit metastasis for others. Rather than using biomarker(s) to predict metastatic potential[11], we tested a functional assay that allows the strength of cell adhesion to an underlying substrate to be observed ex vivo and in the appropriate context (i.e., with specific Mg^{2+} and Ca^{2+} concentrations to recapitulate tumor stroma)[155,156]. It has been observed that lower cation concentrations, akin to those found in tumor stroma, create labile adhesions[20] and lead to increased metastasis[157] and invasion[158]. We demonstrated that 1) a systematic quantification of metastatic versus nonmetastatic cells can reveal different adhesive phenotypes, and 2) that these differences are driven by changes in FA dynamics resulting from stromal niche conditions.

Cell-matrix adhesion is an exceedingly dynamic process[23]. To capture that complexity in a context-specific manner, a systematic quantification of adhesion under appropriate tumor and stromal cation conditions is required. Classic wash assays involve cells adhering for a short period of time (<1 h), with subsequent rinsing steps to remove unbound cells[150]. The undefined shear in such assays makes it difficult to quantitatively assess cancer cell adhesion. Although centrifugation and micropipette assays can impose a single shear amount per culture, they typically indicate that the number of bound cancer cells[151–153] and the amount of activated

integrin[148] is inversely proportional to the metastatic potential of those cells. However, with the spinning-disk device, force is applied in a quantifiable and reproducible manner across the population[127]. Furthermore, cation concentrations can also be probed directly since the cells remain in media[131]. Under conditions that recapitulate estimated tumor Mg^{2+} and Ca^{2+} concentrations, e.g., 0.1–0.5 mM[155,156], we found that several mammary cell lines had adhesion strengths be- tween 300 and 400 dynes/cm^2, regardless of the metastatic potential. At lower stromal cation concentrations, metastatic cells became significantly weaker and displayed adhesive heterogeneity, whether they originated from mammary (MDAMB231, SUM1315, and MDAMB468) or prostate (PC3) cancers. In contrast, nonmetastatic cell lines did not demonstrate significant adhesion strength heterogeneity. Moreover H-Ras transformation of a nonmetastatic cell line caused it to adopt adhesive heterogeneity only in Mg^{2+}- and Ca^{2+}-free conditions, indicating that independently of their genetic background, metastatic cell lines vary significantly in adhesion strength. Together with previous findings[151–153], these data establish an adhesion dependence on stromal-like conditions for a subset of metastatic cells.

The mechanism(s) behind adhesive heterogeneity and cation sensitivity in cells appears to be complex, whether the cells are selected by shear or not. Although metastatic behavior was previously linked to diminished integrin activation[148], we found no change in integrin expression or FAK phosphorylation that was independent of the buffer conditions used. However, blocking ion channels in meta- static mammary and prostate cancer cells artificially enhanced their adhesion in single-cell assays versus control cells[151], suggesting that cation effects are plausible. Indeed, we found that MCF10A adhesions were less cation sensitive than MDAMB231 adhesions, as their FA size and number changed less after Mg^{2+} and Ca^{2+} removal in comparison with the

MDAMB231 cells. Similarly, when MCF10A cell FA assembly was modulated by the addition of soluble RGD, the resulting changes in FAs reduced adhesion strength in a manner consistent with that observed for MDAMB231 cells. It should be noted that MCF10A cells were more sensitive to ligand type, although the sensitivity was always observed with adhesion strengths well above 100 dynes/cm^2. The sensitivity of MDAMB231 cells was observed at lower adhesion strengths and also induced heterogeneous adhesion, i.e., a shallow logarithmic slope. Under comparable matrix and cation conditions, MCF10A cells never exhibited heterogeneous adhesion. Together, these data suggest that assembly differences in low Mg^{2+} and Ca^{2+} conditions in the stroma could drive adhesion strength heterogeneity. As such, assembly changes have been equated to differences in turnover[147] and might be expected to create MDAMB231 cells with labile adhesions required for 3D protrusion and migration[168]. This interpretation is consistent with metastatic and invasive behaviors observed in low Mg^{2+}- and Ca^{2+}-containing stroma[158,159]. We also showed that shear selection of the strongly adhering subpopulation of MDAMB231 cells (>45 dynes/cm^2) suppressed their migration on collagen gels and their ability to migrate through transwells, such that they resembled the less cation-sensitive, nonmetastatic cells. Although the origin of increased FA cation sensitivity remains unclear, the mechanism is not specific to mammary cells, since adhesion-selected PC3 prostate cancer cells also failed to migrate on substrates and/or in transwell assays as did their unselected counterparts. Together, these data suggest that there is a common heterogeneous adhesive signature in cell lines described as having metastatic potential, and importantly, within this population is a subset of weakly adherent, highly migratory cells.

2.5 Conclusions

Given the heterogeneity and plasticity observed in the adhesive phenotype and the inverse correlation between migration and strongly adherent subpopulations, the data presented here emphasize the importance of therapeutically targeting as many cancer cell states as possible, instead of focusing on the largest population or most aggressive phenotypes. These data also suggest that the adhesive state, when measured in the appropriate stromal cation concentrations, could serve as a unique biophysical marker for highly migratory behavior in metastatic cells generally.

2.6 Methods

2.6.1 Cell culture

Cells were cultured in their respective media as indicated in Supplementary Table 2.6 in the Supporting Material, using typical formulations from Life Technologies (Carlsbad, CA) and the American Type Culture Collection (ATCC, Manassas, VA). When applicable, cells were selectively cultured with RGD peptides (Sigma, St. Louis, MO). All cells were cultured at 37C in a humidified incubator containing 5% CO_2. Unless otherwise noted, cell culture products were purchased from Life Technologies. All cells were obtained from the ATCC cell bank and verified to be mycoplasma free. Cells were also authenticated by the ATCC based on morphology, growth curve analysis, and isoenzyme analysis, and were passaged for <6 months after resuscitation.

2.6.2 Cell adhesion-strength assay

Glass coverslips (25 mm, Fisher Scientific, St. Louis, MO) were sonicated in ethanol and pure water before incubation with 10 mg/mL human fibronectin (isolated from serum[169]) for 60 min at room temperature. All adhesion-strength assays were performed on fibronectin-coated coverslips unless otherwise noted, and 20 mg/mL type I collagen (rat tail; BD Biosciences, Franklin Lakes, NJ) was used. Under regular conditions, cells were allowed to attach for 24 h at 37C and 5% CO_2 using cation-containing media. The coverslips were then mounted on a custom-built spinning-disk de- vice and dipped into temperature-controlled spinning buffer (37C)[131]. Phosphate-buffered saline (PBS; without magnesium and calcium or with 0.5 mM $MgCl_2$ and 1 mM $CaCl_2$ (Cellgro, Manassas, VA)) was used as the spinning buffer. All spinning buffers contained 4.5 mg/mL dextrose. Once immersed in the spinning buffer, the coverslips were spun for 5 min at defined angular velocities and then the culture was continued or the cells were fixed with 3.7% formaldehyde immediately after spinning.

To select for strongly attaching cells, the center of the coverslips was covered with Parafilm that had been circularly cut with a crafting punch (The Punch Bunch, Temple, TX) and removed before shear application to ensure that all cells were subjected to a minimum shear. After 5 min of shear application, cells were allowed to recover in cell culture media for 1–2 h. The remaining cells were then trypsinized and re-plated on regular petri dish plastic. Control cells were treated likewise but without application of shear (i.e., 0 rpm).

2.6.3 Quantification of adhesion strength

Shear stress, t, by radial fluid motion over the surface of the coverslip was calculated[127,130] such that:

$$\tau = \frac{4}{5} r \sqrt{\rho \mu \omega^3},$$

where r is the radial position from the center of the disk, ρ is the buffer density, μ is the buffer viscosity, and ω is the rotational speed. To obtain quantitative information about the adhesion strength, whole 25 mm coverslips were imaged at 10X magnification on a Nikon (Melville, NY) Ti-S microscope (~1000 individual images stitched together with Metamorph 7.6 soft- ware and custom macros) and analyzed using a custom-written MATLAB (The MathWorks, Natick, MA) program. In brief, in this approach, the user defines the outer circle of the coverslip from a stitched overview image and the software then finds the position of each nucleus relative to the center of the coverslip. Cell densities, as a function of radial position and subsequently shear, are stored and combined with other measurements, e.g., those obtained at different RPMs. A sigmoidal decay fit is used to quantify values of adhesion strength and the logarithmic slope, i.e., the fit parameter in the sigmoid for curve steepness.

2.6.4 Migration assays

For two-dimensional migration experiments, tissue-culture-treated 12- and 24-well plates were coated with soluble rat-tail type I collagen in acetic acid (BD Biosciences) to achieve a coverage of 20 mg/cm^2 and incubated at room temperature for 1 h. For two-dimensional migration, collagen matrices at 1.2 and 2.4 mg/mL concentrations were prepared as described elsewhere[168]. In brief, collagen was mixed with ice-cold PBS and 1 M NaOH was then added to normalize the pH to 7.0. Cells were imaged with a Nikon Eclipse Ti-S microscope equipped with a motorized temperature- and CO_2-controlled stage. Cells were imaged at 10X in bright field at multiple positions every 15 min for up to 48 h. Most of the migration data were analyzed by Time

Lapse Analyzer, a freely available MATLAB program for cell migration analysis[170]. Samples that could not be analyzed by the automated software (due to gel swelling and/or z-migration of the cells) were tracked manually with ImageJ (NIH, Bethesda, MD).

Additional migration experiments utilized six-well plates with transwell permeable supports (8 mm polycarbonate membrane; Corning, Corning, NY) that were seeded with 100,000 cells. After cells adhered to the permeable support, media was added to the whole well. Cells were allowed to migrate through the membrane for 24 h and then fixed and stained for nuclei (DAPI). Cells that successfully migrated through the membrane were counted on the bottom of the permeable support (ceiling). Additionally, cells that dropped off the support and adhered to the bottom of the six-well plate were also counted (bottom).

2.6.5 Immunofluorescence staining and focal adhesion analysis

Fixed cells were incubated for 10 min with 0.25% Triton X-100 followed by 1% albumin overnight at 4^{o}C for blocking. Primary paxillin antibody (1:2000; ab32084, Abcam, Cambridge, UK) was applied for 2 h at room temperature. Then, a secondary Alexa Fluor 488-conjugated antibody (1:2000, Invitrogen, Carlsbad, CA) was applied for 1 h or rhodamine phalloidin (1:2000, Invitrogen) and Hoechst 33342 (3.2 mM, Invitrogen) were applied for 30 min at room temperature. The cells were subsequently mounted with Fluoromount-G (Southern Biotech, Birmingham, AL). All buffers contained 1 mM $MgCl_2$. The samples were imaged with the use of a CARV II confocal (BD Biosciences) Nikon Eclipse Ti-S microscope equipped with a motorized, programmable stage using a Cool-Snap HQ camera (Photometrics, Tucson, AZ) and controlled by Metamorph 7.6 (Molecular Devices, Sunnyvale, CA). A custom-written MATLAB program was

used to quantify cell area and FA number and size[131]. All FA metrics were computed across the entire cell to avoid regional biases.

2.6.6 Western blotting

Cell lysates were collected in mRIPA buffer (50 mM HEPES (pH 7.5), 150 mM NaCl, 1.5 mM $MgCl_2$, 1% Triton X-100, 1% Na-DOC, and 0.1% SDS) with 1 mM EGTA, 1 mM Na_3VO_4, 10 mM $Na_4P_2O_7$, and 1 mM phenylmethanesulfonylfluoride for Western blots. Samples were run in 10% SDS-PAGE gels at 150 V until proteins were separated and then transferred onto polyvinylidene fluoride membranes (Bio-Rad, Hercules, CA) to be run at 100 V for 1 h 15 min in the transfer apparatus (Bio- Rad). The membranes were washed in buffer A (25 mM Tris-HCl, 150 mM NaCl, and 0.1% Tween-20) 5% bovine serum albumin overnight at $4^{o}C$ and then incubated for 2 h with the following antibodies: FA kinase (FAK; ab40794) at 1/500 and pFAK anti-phospho Y397 (ab4803) at 1/500 (both from Abcam), and glyceraldehyde 3-phosphate dehydrogenase (GAPDH; MAB374) at 1/250 (Millipore, Billerica, MA). After three 10-min washes with buffer A, secondary goat anti-rabbit horseradish peroxidase (Bio-Rad) and anti-mouse horseradish peroxidase (Abcam) were used for incubation for 30 min. Immunoblots were visualized using enhanced chemiluminescence reagent (Thermo Fisher, Waltham, MA).

2.6.7 Fluorescence-activated cell sorting analysis

Cells were detached from fibronectin-treated coverslips by incubation for 5–10 min with PBS without cations at $37^{o}C$ and gentle pipetting. After re-suspension in flow-cytometry buffer (DPBS, 2.5% goat serum, 1 mM EDTA (pH 7.4)), the cells were incubated with fluorescent-conjugated antibodies against CD49e (phycoerythrin) and CD51 (fluorescein isothiocyanate)

(Biolegend, San Diego, CA) for 30 min on ice. Cells were analyzed using a FACScan flow cytometer (BD Biosciences).

2.6.8 Statistical analysis

Nonparametric Kruskal-Wallis analysis of variance tests were used for all statistical analyses unless indicated otherwise. All data in shear plots are expressed as mean 5 SD. All experiments were performed at least in biological triplicate, and analyses represent hundreds of cells per condition.

2.7 Supplementary Figures

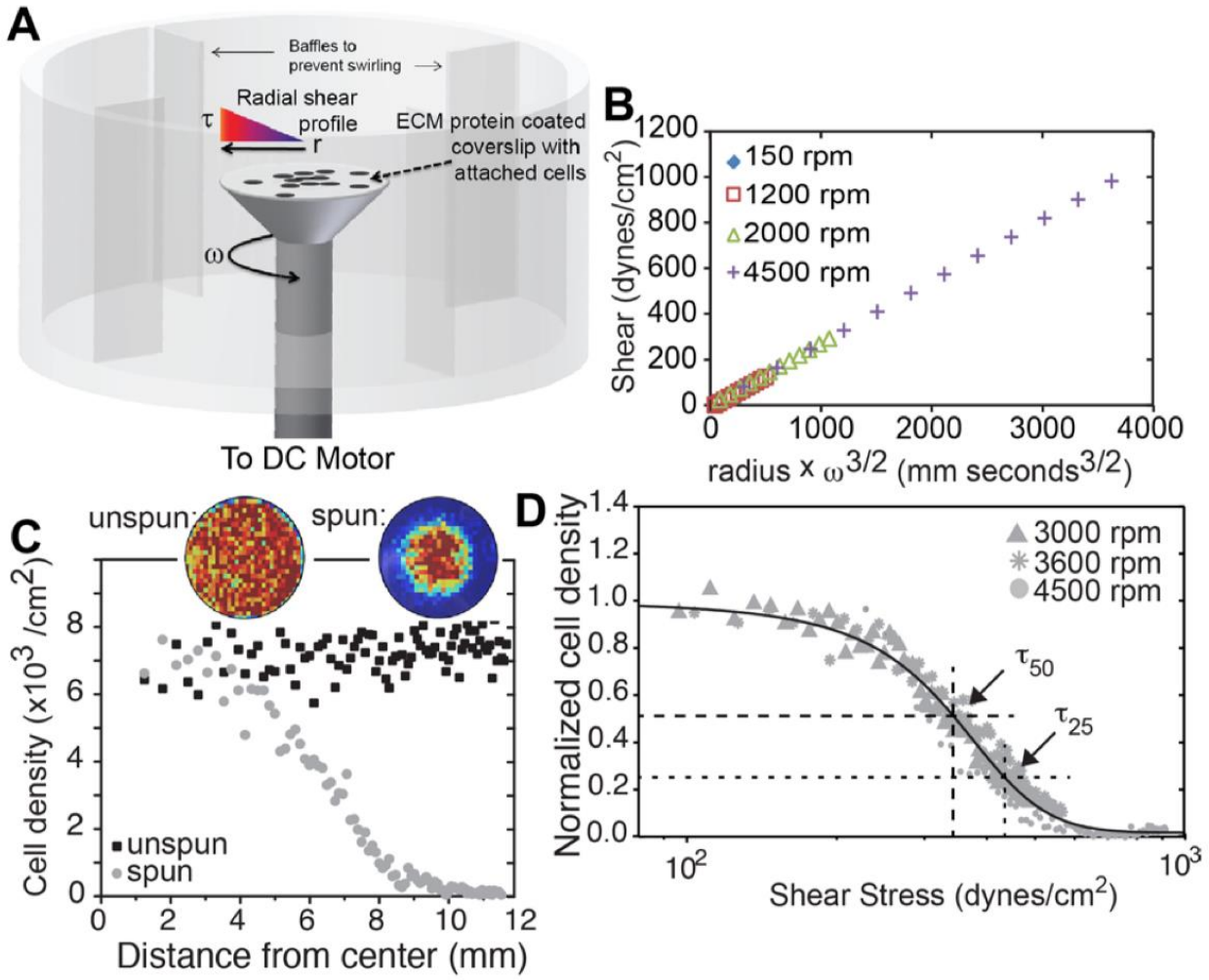

Supplementary Figure 2.1. Spinning Disc Assay Creates a Radially-dependent Shear Profile:

(A) The spinning disc device is illustrated with cells attached to an extracellular matrix protein-coated coverslip mounted and rotating on a spinning rod in buffer. The radially-dependent shear profile is highlighted showing that cells at the center only rotate in place while those at the edge move around at a high linear velocity. (B) The plot shows the relationship of radial position on the coverslip and angular velocity versus applied shear stress at a given point for the indicated velocities (in revolutions per minute; rpm). (C) Plot of the relationship between radial position and cell density. Inset images show heat maps of cell density. Warm (red) and cool (blue) colors indicate high and low densities, respectively. (D) Plot of cell density, normalized to the center of the coverslip, versus the applied shear. Data is plotted for the indicated velocities. τ25 and τ50, i.e. the shear to detach 25 and 50% of cells, respectively, are indicated in the plot and are 438 and 346 dynes/cm2, respectively.

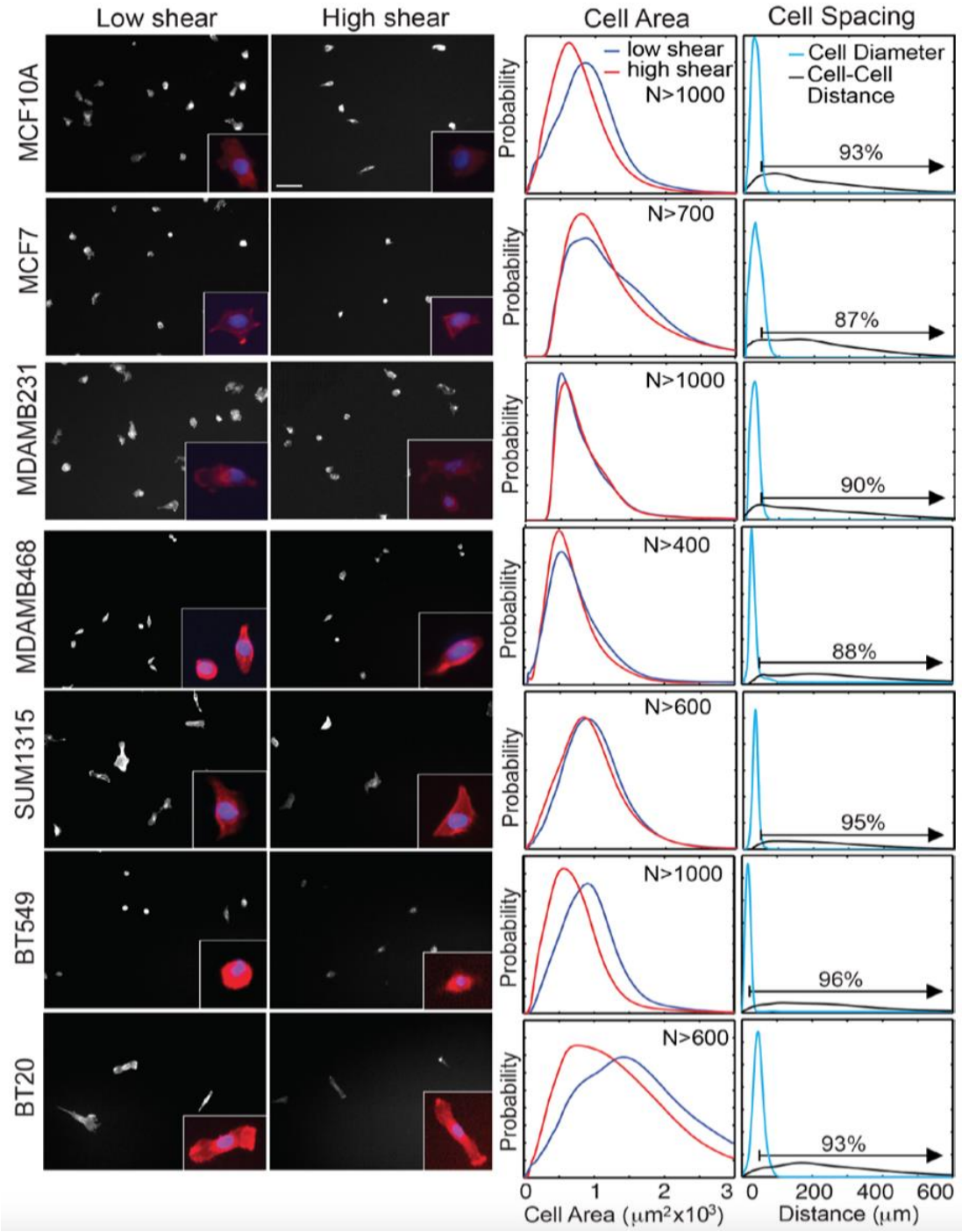

Supplementary Figure 2.2. Cell Morphology and Distribution are Independent of Mammary Epithelial Cell Line:

At the left are low magnification images of MCF10A, MCF7, MDAMB231, MDAMB468, SUM1315, BT549, and BT20 cells at low and high shear, which were stained with Rhodamine-Phalloidin. Inset images at higher magnification were also stained with DAPI. At right are plots of cell area (blue and red lines indicating high and low shear) and cell-to-cell spacing frequency for the indicated number of cells (N). Indicated within the plots is the percentage of cells spaced further apart than the average diameter of each cell line.

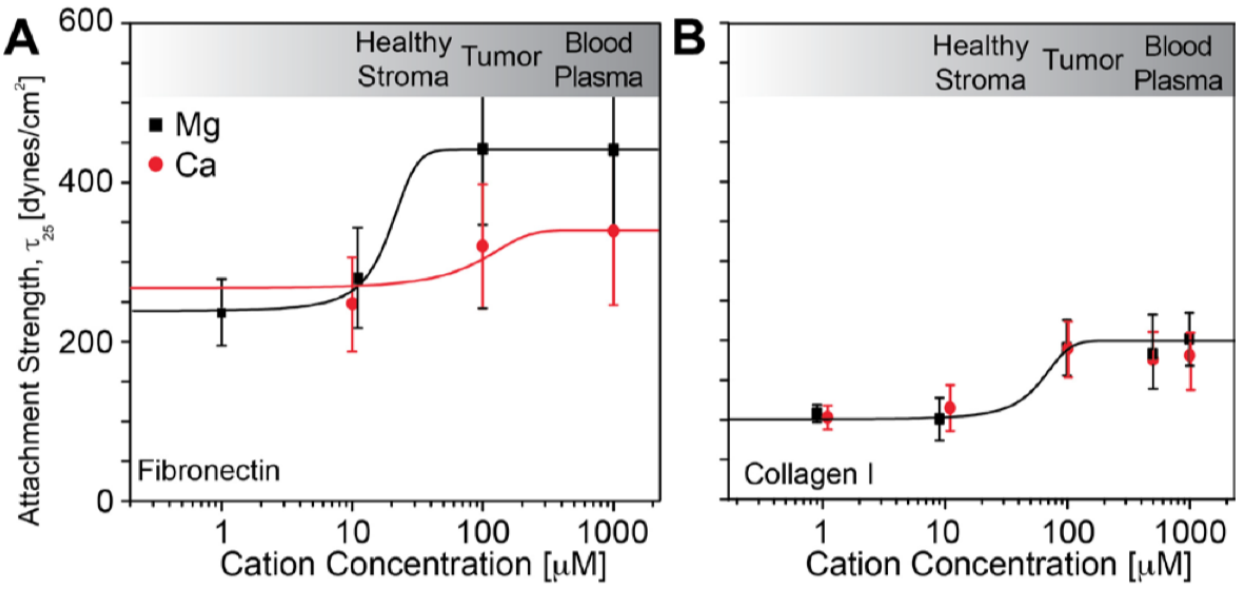

Supplementary Figure 2.3. MCF10A Cells Exhibit Cation-Sensitive Change in Attachment Strength:

MCF10A, cells had homogeneous and strong attachment strengths, i.e. τ25, as plotted versus cation concentration for Mg2+ (black squares) and Ca2+ (red circles) for cells bound to (A) collagen type I-coated and (B) fibronectin-bound coverslips. Cation concentration range for the indicated tissue is provided for reference. A sigmoidal fit for each cation is shown in panel A but they are combined in panel B.

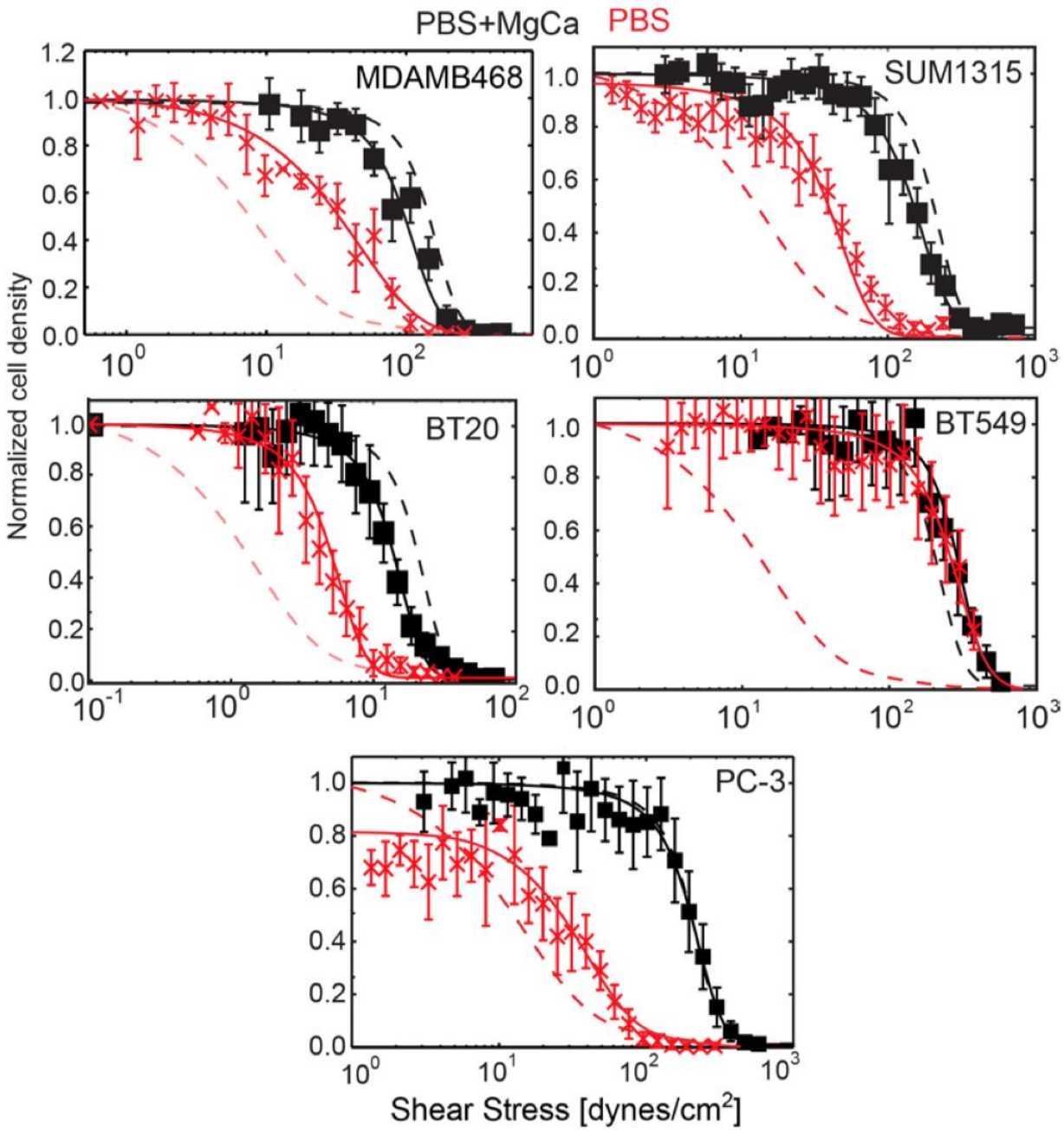

Supplementary Figure 2.4. Attachment Strength is Heterogeneous for Additional Mammary Epithelial Cells and Prostate Cancer Cells in Stromal-like Niche:

Normalized cell density is plotted versus shear for MDAMB468, SUM1315, BT20, BT549 and PC-3 cells. Cells were tested with (black) and without (red) media containing cations as defined in Figure 1. Dashed lines in each plot indicate the fits for MDAMB231 cells with (black) and without (red) media containing cations.

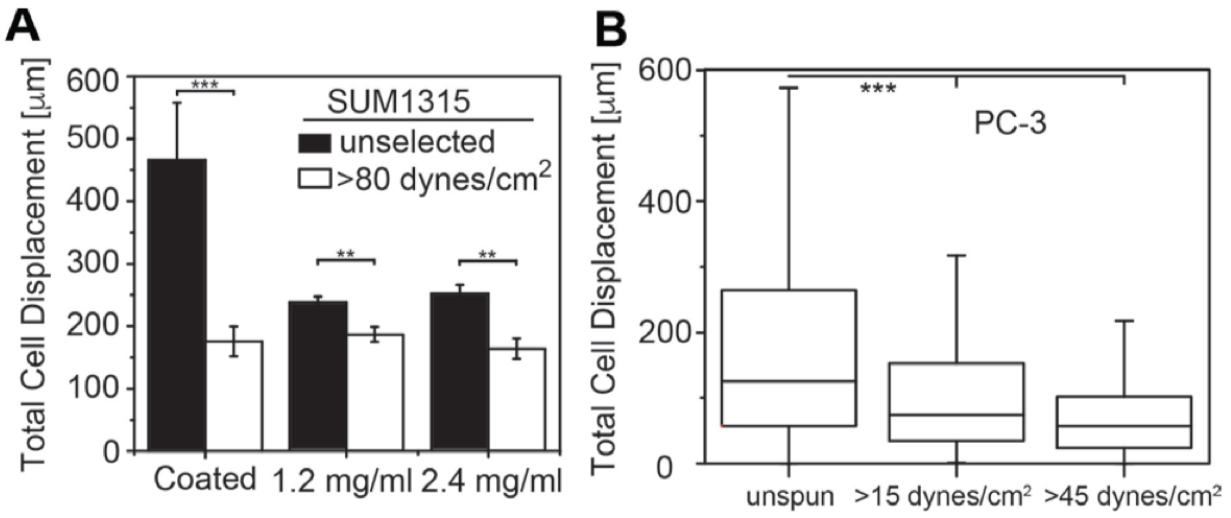

Supplementary Figure 2.5. Migration for SUM1315 and PC-3:

(A) SUM1315 cells, either unselected (blue) or selected with 80 dynes/cm2 (orange), plated onto collagen-coated, planar substrates (left) and 1.2 mg/ml (center) and 2.4 mg/ml (right) collagen hydrogels were plotted for the total distance migrated over 24 hours post-plating. Note that the migration of many unselected cells on planar surfaces exceeded the viewable window of the microscope over 24 hours, and thus these data represent a minimum distance traveled. (B) Total cell displacement over 24 hours for PC3 cells are plotted for the indicated shear stress selection conditions on collagen-coated substrates. PC-3 cell migration is more heterogeneous and thus displayed in a box and whisker plot **p <0.01, ***p < 0.001.

Supplementary Table 2.6. Media formulations for the indicated cell lines:

Cell Line	Base Media	Serum	Antibiotics	Others
MCF10A, MCF10A T	DMEM/ F12	5% HS	100 units/ml Penicillin, 100 µg/ml Streptomycin	0.5 µg/ml Hydrocortisone, 20 ng/ml hEGF, 10 µg/ml Insulin, 100 ng/ml Cholera toxin
MCF7	DMEM	10% FBS	100 units/ml Penicillin, 100 µg/ml Streptomycin	10 µg/ml Insulin
MDAMB231, MDAMB468, BT20	DMEM	10% FBS	100 units/ml Penicillin, 100 µg/ml Streptomycin	
SUM1315	DMEM/ F12	5% FBS	100 units/ml Penicillin, 100 µg/ml Streptomycin	5µg/ml hEGF, 5 µg/ml Insulin
BT549	DMEM	10% FBS	100 units/ml Penicillin, 100 µg/ml Streptomycin	1 µg/ml Insulin
PC3	F-12K	10% FBS	100 units/ml Penicillin, 100 µg/ml Streptomycin	

2.8 Acknowledgements

The authors thank Drs. Caroline Damsky and David Strom for antibodies obtained via the Developmental Studies Hybridoma Bank under the auspices of the National Institute of Child Health and Human Development, and maintained by the University of Iowa (Iowa City, IA). The authors also thank Dr. Philippe Gascard for a helpful review of the manuscript. The spinning-disk device was designed and manufactured by Jeremy Riley, Ryan Tam, Joe Shu, and the UC San Diego Campus Research Machine Shop.

This work was supported by grants from the National Institutes of Health (DP2OD006460 and U54CA143803-03 to A.J.E.), the Department of Defense (W81XWH-13-1-0133 to A.J.E.), and the National Science Foundation Graduate Research Fellowship Program (to A.B. and P.B.).

Chapter 2, in full, is a reprint of the material as it appears in Fuhrmann, A., Banisadr, A., Beri, P., Tlsty, T.D., and Engler, A.J. “Metastatic State of Cancer Cells may be indicated by Adhesion Strength.” *Biophys J*, 2017. 112(4): 736-745. The dissertation author was a corresponding author of this paper.

Chapter 3.

Cell adhesiveness serves as a biophysical marker for migratory potential

3.1 Abstract

A lack of biological markers has limited our ability to identify the invasive cells responsible for Glioblastoma multiforme. To become migratory and invasive, cells must down regulate matrix adhesions, which could be a physical marker of invasive potential. Murine astrocytes were engineered with common GBM mutations, e.g. Ink4a (Ink) or PTEN deletion and expressing a constitutively active EGF receptor truncation (i.e. EGFRvIII), to elucidate their effect on adhesion. While loss of Ink or PTEN did not affect adhesion, counterparts expressing EGFRvIII were significantly less adhesive. EGFRvIII reduced focal adhesion size and number, and these cells with more labile adhesions displayed enhanced migration. Regulation appears dependent not on physical receptor association to integrins but rather on the receptor's kinase activity resulting in transcriptional integrin repression. Interestingly, EGFRvIII intrinsic signals can be propagated by cytokine crosstalk to wildtype EGFR cells, resulting in reduced adhesion and enhanced migration. These data identify potential intrinsic and extrinsic mechanisms that gliomas use to invade surrounding parenchyma.

3.2 Introduction

Although the prevalence of brain tumors is lower than other tumor types, e.g. mammary or prostate[61,171], the mortality rate for brain tumors is much higher (5-year survival rate is 35% vs >90%); patient outcomes are even more drastic for Glioblastoma multiforme (GBM), a stage-4 astrocytoma characterized by infiltration into healthy parenchyma, tumor heterogeneity, resistance to apoptosis, and genomic instability[172]. GBM accounts for ~45% of all invasive brain cancers and >12,800 new cases annually in the US[173]. Average GBM patient survival is low (12-15 months[174]) despite standard of care i.e. tumor resection, radiation therapy and treatment with the DNA alkylating agent temozolomide[175,176]. Poor prognosis is due in part to GBM's poorly margined, highly invasive phenotype, recurring anywhere within 1 cm of the original lesion to the other side of the corpus callosum[3,4], thus prohibiting a surgical cure. Tumor cell invasion requires conversion away from a proliferative phenotype[3,4] and is characterized by a significant increase in migration and interaction with, and degradation of, multiple brain ECM proteins[5–7]. Despite advances in our understanding of glioma invasion and migration, little is known about the molecular mechanisms that regulate this switch and if these mechanisms are cell intrinsic, extrinsic or a combination of both.

The presence of multiple invasive mechanisms may be due to significant intratumoral genetic heterogeneity[177]. GBM tumors with the worst prognoses typically have mutations in one or more of three genes: cell cycle regulator Ink4a/Arf (p16) deletion[178,179], tumor suppressor Pten deletion[180,181], and epidermal growth factor receptor (EGFR) amplification and truncation[70,182,183]. For example, changes in EGFR occur in approximately 60% of GBM[184,185], and its most common EGFR variant–truncation of exons 2-7, i.e. EGFRvIII–causes constitutive self-phosphorylation,

pathway activation[186,187] and reduced apoptosis[188]. None of these properties are conferred to cells overexpressing wild-type EGFR (wtEGFR), which cannot drive glioma formation alone[179,189,190]. We have previously found that EGFRvIII-positive cells, which are often scattered diffusely within a tumor[191], actively educate neighboring wtEGFR cells[49,70,192], hinting that inter-clonal communication could illustrate a paradigm for cooperativity of GBM cells. However, the mechanisms that EGFR alterations individually or collectively use to drive GBM migration and invasion are less clear.

To ensure dissemination into healthy tissue, cells at the invasive front must detach from the tumor mass, changing adhesion from largely cell-cell to cell-matrix. For epithelial tumors, invasive potential and adhesion strength are inversely correlated[132] due to altered focal adhesion assembly[131] and turnover[147] allowing cells to move through the tissue effectively. As a result, cancer cell adhesion to ECM proteins is becoming a more accepted metric for metastatic potential[150,152]. While this relationship is not clear for GBM, the studies mentioned above suggest that EGFR variants could play an intrinsic role in directly binding to and indirectly modifying signaling pathways that affect adhesion. Conversely, wtEGFR cells could cooperatively invade with EGFRvIII cells that recruit and convert them epigenetically. Using a spinning disc assay[126,132] which subjects cell populations to radially increasing shear stress, we interrogated these possibilities using an isogenic mouse glioma cell line containing combinations of Ink4a/Arf (p16) deletion[179], Pten deletion[180], and with wtEGFR or EGFRvIII overexpression[70,183]. We found that combinations of Ink4a/Arf deletion, Pten deletion and EGFR overexpression did not reduce cell adhesion across a population of cells, but EGFRvIII overexpression did reduce adhesion. EGFRvIII reduced focal adhesion formation via canonical GBM pathways resulting in repression of integrin

expression, suggestive of an intrinsic adhesion mechanism. Given the lower frequency of these cells in heterogeneous tumors[178,181] we further found EGFRvIII expressing cells produced cytokine signals which, when applied to wtEGFR cells, could reduce their adhesion and increase their migration. Together these data suggest that EGFRvIII creates cell intrinsic signals that regulate adhesion strength as well as extrinsic signals that instruct heterogeneous tumor cell populations to invade the surrounding parenchyma.

3.3 Results

3.3.1 GBM Driver Mutations Reduce Adhesion Strength and Increase Migration

Tumor recurrence post-resection suggests that some subset of GBM cells have transitioned from a proliferative[3,4] to an invasive and migratory phenotype[4,175] using cell-matrix adhesions. To determine which of the most common mutations could affect adhesion, we utilized low passage isogenic murine astrocytes expressing combinations of Ink4A/arf deletion, Pten deletion, or EGFR alterations, i.e. overexpression of wild-type receptor or a constitutively active truncation mutant (Table S1)[189]. Cell genotypes were confirmed by western blot analysis (Figure 3.1A) and then adhesion characterized by spinning disk assay[127,128] i.e. a quantitative population-based assay where cells are detached from a fibronectin-coated coverslip by radially increasing shear stress (Figure S3.1). In the absence of cations, each line exhibited similar adhesion strength (Figure 3.1B, striped bars), yet in the presence of cations, adhesion strength was lower only for lines containing EGFRvIII (Figure 3.1B, solid bars). This difference may indicate that EGFRvIII plays a significant role in modulating cation-dependent astrocyte adhesion, regardless of other

mutations or wild-type receptor overexpression; conversely, epithelial tumor adhesion is reduced in the absence of cations[132].

Adhesion changes likely manifest themselves in migration differences[132,133], so we next determined whether reduced EGFRvIII cell adhesion improved migration speed and persistence on fibronectin in cation-containing media. Cells expressing EGFRvIII had significantly longer pathlength and migrated at a significantly faster speed compared to Ink-/- and were somewhat faster than wtEGFR expressing cells, i.e. EGFR amplification is beneficial for tumor cell migration but not as much as receptor truncation (Figure 3.2A-B; Figure S3.2). wtEGFR cells had significantly greater average displacement resulting in more processive motility compared to Ink-/- cells, whereas EGFRvIII cells had slightly lower displacement and thus less processive migration (Figure 3.2 C-D; Figure S3.2), indicating that they explored a greater area than cells simply with EGFR amplification. Therefore, these data indicate that EGFRvIII cells tend to rapidly investigate a larger portion of their environment consistent with GBM invasivity.

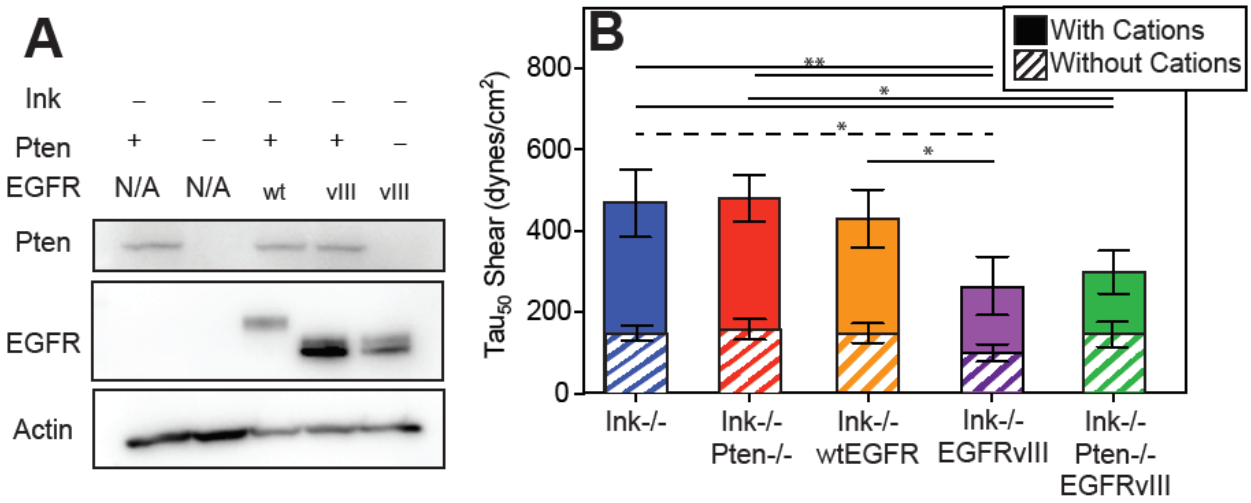

Figure 3.1. Cation-Dependent Astrocyte Adhesion is Reduced by EGFRvIII:

(A) Western blot of indicated genotypes for Pten, EGFR, and Actin. (B) Shear stress at which 50% of the population detaches, i.e. adhesion strength of τ_{50}, is plotted for the indicated genotypes. Cells assayed in buffer with (solid bars) and without (hatched bars) cation-containing media are shown. *p<0.05, and **p<0.01 by paired student t-test (n=4 per genotype and condition; solid and dashed lines indicate comparisons of cells with and without cation-containing media, respectively).

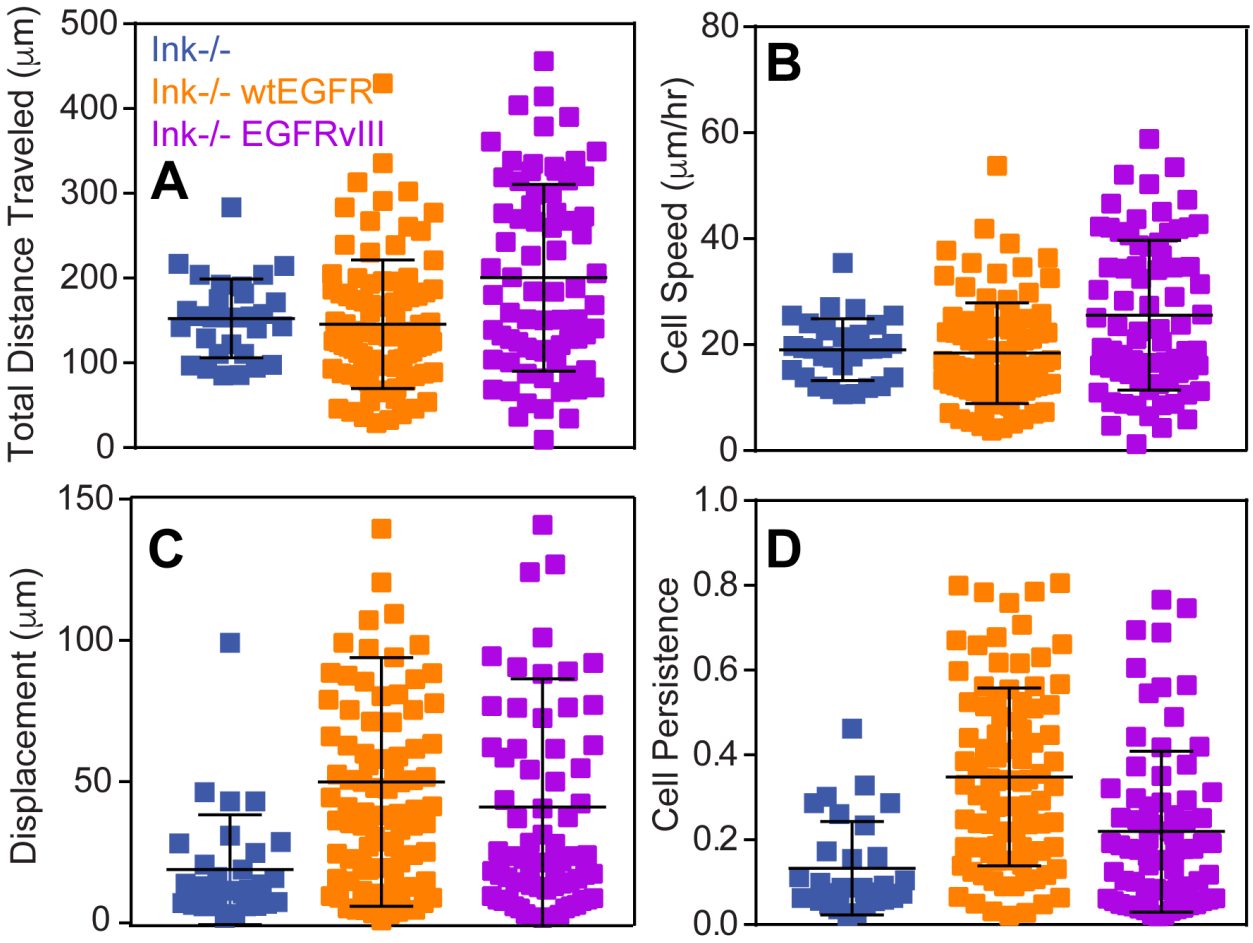

Figure 3.2. Migratory Characteristics Scale with Adhesion and Depend on EGFR:

(A) Total cell migration distance, (B) speed, (C) displacement, and (D) persistence over 24 hours is plotted for the indicated genotypes (n=3). *p<0.05, **p<0.01, ***p<0.001, and ****p<0.0001 by paired student t-test (n=30, 91, and 74 cells for Ink-/-, wtEGFR, and EGFRvIII cells).

3.3.2 Weakly Adherent Cells Display a Decrease in Focal Adhesion Assembly State

The link between diminished cation-dependent adhesion strength and migration further suggests that EGFRvIII could in some manner affect focal adhesion dynamics. Thus, we interrogated focal adhesion assembly on fibronectin-coated coverslips via immunofluorescence and found significant assembly differences between EGFRvIII and wtEGFR cells (Figure 3.3A-B). When normalized to cell area, EGFRvIII cells were nearly 2-fold fewer and had smaller focal adhesions per cell area (Figure 3.3C-E). Moreover, EGFR is enriched in the plasma membrane at focal adhesions for cells expressing EGFRvIII (Figure 3.3F), suggesting that there could be direct regulation of integrins by EGFR amplification and truncation which in turn could reduce cell adhesion strength and increase migration speed.

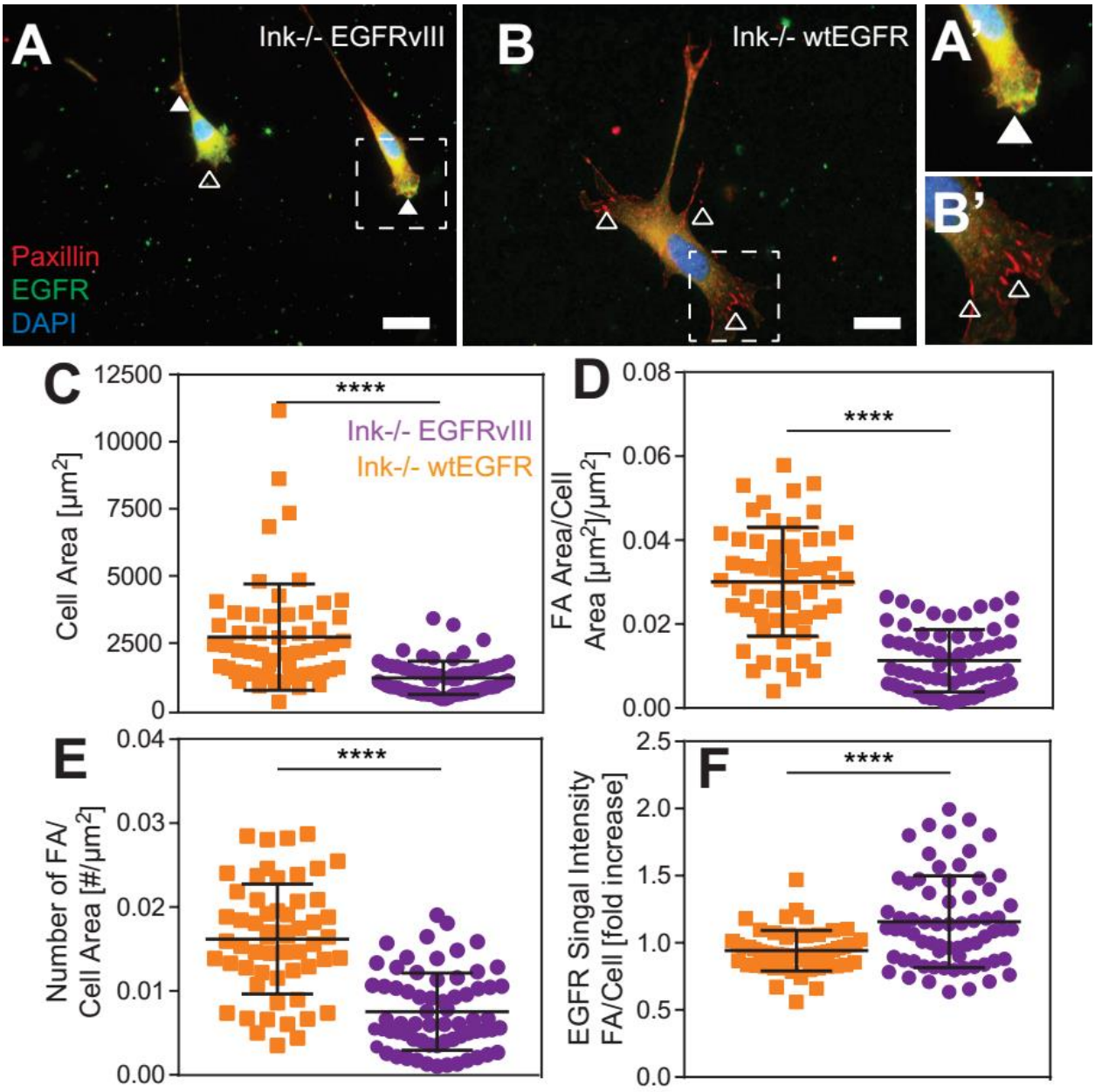

Figure 3.3. Focal Adhesion Assembly is Suppressed by EGFRvIII:

Immunofluorescent images of (A) EGFRvIII and (B) wtEGFR cells stained for paxillin (red), EGFR (green), and nucleus (blue). Dashed boxes indicate regions shown in inset images A' and B', which are related from panels A and B, respectively. Filled and open arrowheads indicate regions of diffuse and assembled adhesion complexes. Scale bar is 10 microns. (C) Cell area, (D) focal adhesion area to cell area, (E) focal adhesion number to cell area, and (F) EGFR signal intensity within a focal adhesion per average cell intensity are plotted for both EGFRvIII (orange) and EGFR (purple) (n=3). ****p<0.0001 by paired student t-test (n=68 and 57 cells for wtEGFR and EGFRvIII cells).

3.3.3 Labile Focal Adhesions are the Result of Intrinsic Kinase-Dependent Signaling

Although EGFRvIII appears to be more localized at adhesion sites than their receptor amplified counterparts, it is unclear if the receptor's constitutively active kinase activity[179] or if its proximity to or potential interactions with integrin[193] create more labile adhesions. To determine if physical associations between EGFRvIII and integrins reduce adhesion, αV and β3 integrins were observed by western blot, and consistent with staining, were found to be less expressed in EGFRvIII vs. wtEGFR cells. Yet when the receptors were immunoprecipitated, we were unable to find any association between either receptor and either integrin (Figure 3.4A). These data indicate that, despite enhanced co-localization, EGFRvIII does not directly interact with integrins and rather may indirectly regulate adhesion via enzymatic activity of its kinase domain and downstream signaling effectors. Western blot of phosphorylated EGFR, however, did confirm the receptor's constitutively active kinase activity for EGFRvIII (Figure 3.4B), which suggests that adhesion regulation could be kinase-dependent.

To determine if this was the case, a kinase defect mutant receptor was created by lysine to methionine substitution (K721M)[194] within the receptor's catalytic domain (Figure S3.3A), i.e. EGFRvIII kinase dead (EGFRvIIIKD), and validated by FACS sorting (Figure S3.3B) and western blot to confirm equal EGFR protein expression and loss of autophosphorylation for EGFRvIIIKD (Figure S3.3C). Although EGFRvIII reduced adhesion strength, loss of kinase activity in EGFRvIIIKD restored adhesion to native wtEGFR levels (Figure 3.4C). Similarly, cell migration speed, which increased with EGFRvIII, decreased in EGFRvIIIKD cells as did the distance traveled (Figure 3.4D; Figure S3.4). These data indicated that constitutive activation of the vIII receptor, and not it its residence on the cell surface[195], is responsible for altered adhesion.

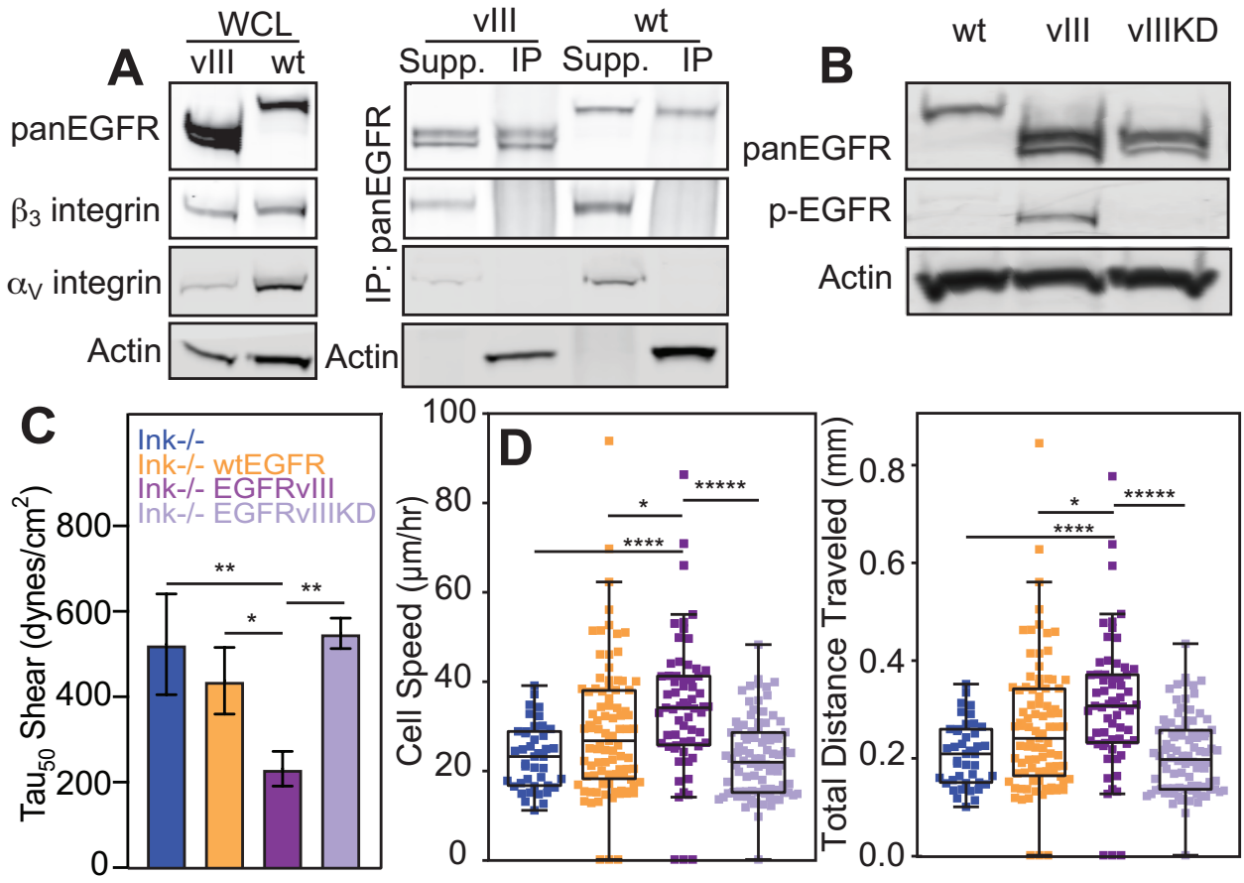

Figure 3.4. Adhesion Strength is Modulated by Kinase-Dependent Mechanism(s):

(A) Western blots of whole cell lysate (WCL; left) confirm genotypes and integrin expression pattern. Additional blots (right) for EGFRvIII and wtEGFR show the results of EGFR immunoprecipitation with supernatant (supp.) and pulldown (IP) lanes for the indicated integrins and Actin. (B) Western blot for total EGFR, phosphorylated EGFR, and Actin for wtEGFR, EGFRvIII, and EGFRvIIIKD. (C) Adhesion strength, i.e. τ_{50}, was plotted for the indicated genotypes. *p<0.05, and **p<0.01 by paired student t-test (n=4 for each genotype). (D) Cell speed and total migration distance for the same genotypes in panel C. *p<0.05, and ****p<0.0001 by paired student t-test (n=4 biological replicate analyzing 39, 88, 65, and 93 cells for Ink-/-, wtEGFR, EGFRvIII, and EGFRvIIIKD cells, respectively).

3.3.4 Intrinsic transcriptional variation in microtubule proteins contributes to increased migration of weakly adherent cells.

Although kinase-dependent, it is uncertain which downstream signaling effectors result in focal adhesion disassembly, thus we assessed adhesion protein expression and phosphorylation status in EGFRvIII cells compared to the Ink-/- and wtEGFR cells. We found that there were no phosphorylation or protein expression differences in FAK or vinculin but there were marked decreases in fibronectin binding integrins αV, α5 and β1 and increases in paxillin and talin in EGFRvIII cells (Figure 3.5A). Consistent with smaller focal adhesions in EGFRvIII cells, these data could indicate that the truncated receptor prevents integrin production, but that cells attempt to compensate by overexpressing adhesion components.

To better understand at what point integrins are downregulated, we first assessed transcript levels, finding that EGFRvIII cells downregulated αV and β1 integrins (Figure 3.5B), which are some of the strongest binding integrins (Bharadwaj et al., 2017). Next because constitutive receptor activation induces a plethora of downstream signaling exclusive to EGFRvIII[196], we assessed which kinase-dependent signals could result in adhesion changes by detecting and perturbing these signals. Along with differential expression of those adhesion proteins above, we observed differential phosphorylation of SHC, Jun kinase (JNK) and c-Jun, SRC, Stat3, and MEK in the EGFRvIII cells as compared to wtEGFR or EGFRvIIIKD cells (Figure 3.5C).

To validate these pathways, we first chose to block phosphorylation of EGFR/SHC (Erlotinib), and MEK (Trametinib), as shown by western blotting (Figure 3.5D). Small molecule inhibition of EGFR via Erlotinib and of MEK via Trametinib decreased signaling by 58% and 56%, respectively. To determine their effect on adhesion, cells were treated with inhibitor for 48hrs.

We found that blocking EGFR signaling to SHC via Erlotinib increased adhesion strength and in addition, we found that MEK inhibition also increased adhesion strength (Figure 3.5E), implicating its involvement in adhesion modulation and potentially intrinsic signaling that transcriptionally represses integrins to increase EGFRvIII cell migration.

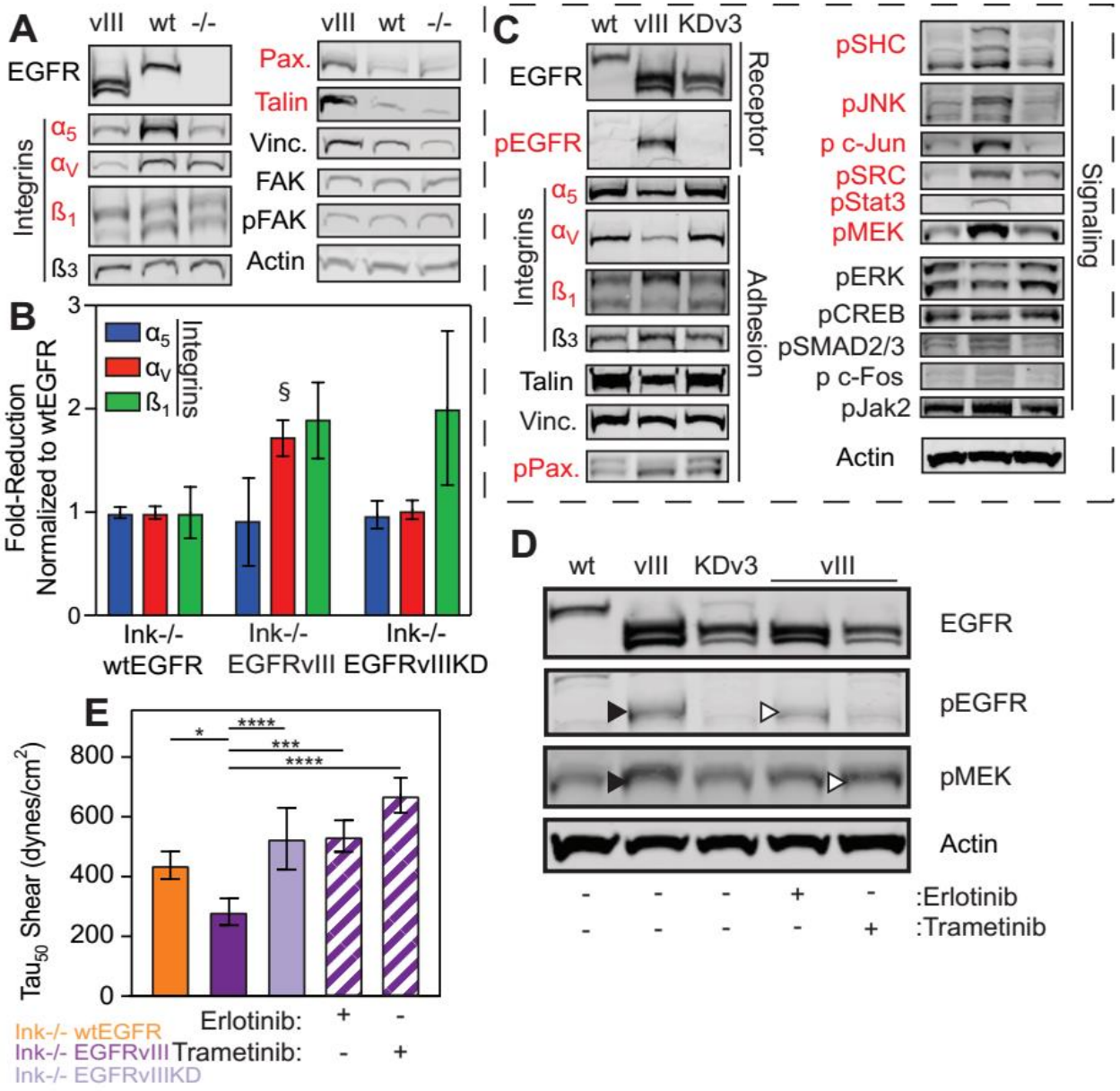

Figure 3.5. Kinase Signaling Downstream of EGFR Transcriptionally Silences Integrins:

(A) Western blots of indicated adhesive proteins expressed in EGFRvIII, wtEGFR, and Ink-/- cells. Those that show differential expression with EGFRvIII being different from the other isogenic cell lines are colored in red. (B) Plot of transcript expression of the indicated integrin genes showing the fold reduction of EGFRvIII cells normalized to wtEGFR cells, i.e. truncated and amplified receptor normalized to amplified receptor only. $^{\S}p<0.1$ by paired student t-test (n=6 biological replicates). (C) Western blots of indicated receptor, adhesive, and signaling proteins expressed in wtEGFR, EGFRvIII, and EGFRvIIIKD cells. (D) Western blots of indicated signaling proteins expressed in wtEGFR, EGFRvIII, and EGFRvIIIKD cells as well as EGFRvIII when treated by the indicated drugs and concentrations. (E) Adhesion strength, i.e. τ_{50}, was plotted for the indicated genotypes, including those selectively treated for the indicated drugs (EGFRvIII hatched bars; n=3 biological replicates). *p<0.05, ***p<0.001, and ****p<0.0001 by paired student t-test between the indicated comparisons.

3.3.5 Extrinsic crosstalk "educates" the adhesion of receptor amplified cells

Given that GBM tumors are exceedingly heterogeneous and can contain cells with all of the mutations studied here thus far, we next sought to determine if cell extrinsic communication, which has been previously observed for wtEGFR and EGFRvIII[70,192], could alter the adhesion of cells with amplified EGF receptor alone. To first determine if paracrine communication was sufficient, we treated wtEGFR cells with EGFRvIII conditioned media for 24 hours to "educate" them prior to shear exposure. When wtEGFR cells were conditioned, cell adhesion strength was reduced to near EGFRvIII levels. However, for Ink-/- and EGFRvIIIKD cells, exposure to conditioned media did not affect adhesion strength (Figure 3.6A). These data indicate that the receptor's kinase activity is necessary to affect adhesion strength, but it does not identify the specific cytokine(s) required to alter the cellular adhesion strength.

Although IL-6 and LIF have been suggested[70] as cytokines involved in the extrinsic alteration of cellular phenotype, we performed a cytokine screen on EGFRvIII and wtEGFR conditioned media to broadly determine components necessary for "education." Limiting hits to cytokines with a greater than 2-fold change, we identified a subset of candidates with differential secretion in EGFRvIII conditioned media (vIII CM), including TNF-α (Figure 3.6B).

To determine to what extend TNF-α signaling affects adhesion strength of wtEGFR expressing cells, EGFRvIII conditioned media was treated with either a neutralizing antibody for TNFα or rabbit IgG prior to dosing wtEGFR cells. TNF-α inhibition eliminated the decrease in adhesion strength conveyed by EGFRvIII CM. In contrast, dosing with rabbit IgG did not reverse the decrease (Figure 3.6C). These data indicate that TNF-α, among possible other cytokines, is necessary for cell crosstalk and cooperative adhesion modulation of neighboring cells expressing

wtEFGR. These findings suggest that not only does EGFRvIII modulate adhesion strength intrinsically, but it modulates the adhesion strength of non-EGFRvIII expressing cells via secretion of TNF-α (Figure 3.7)

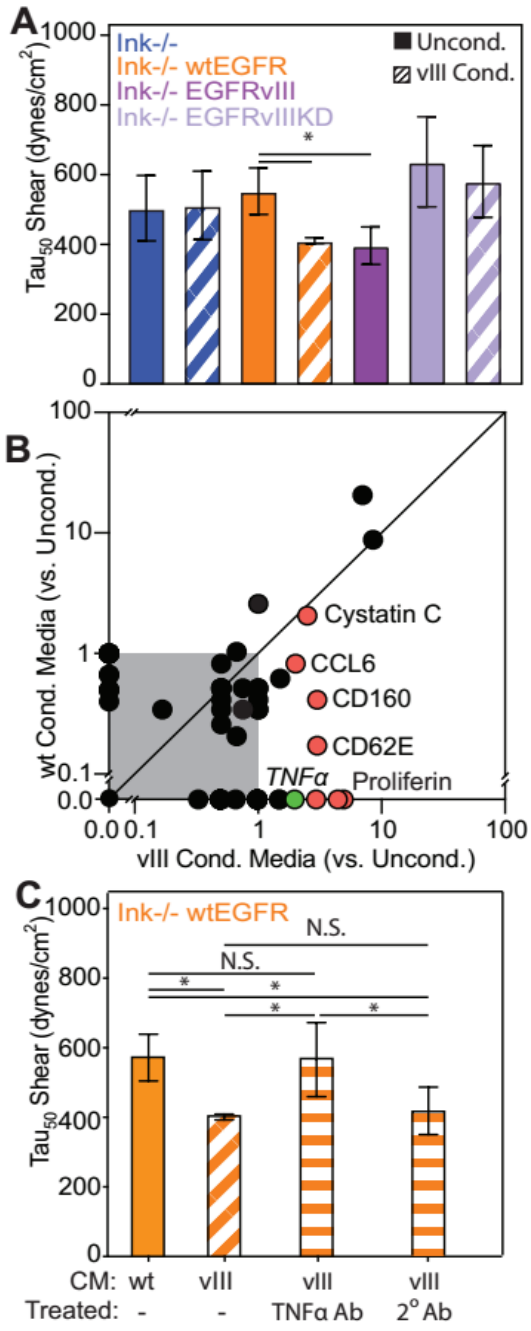

Figure 3.6. Cell Extrinsic Cytokines from EGFRvIII Reduces Adhesion of wtEGFR cells:

(A) Adhesion strength was measured for cells from the indicated genotypes in unconditioned (solid bars) or EGFRvIII conditioned media (hatched bars; n=3 biological replicates). (B) Cytokine production was measured by microarray and plotted for wtEGFR and EGFRvIII conditioned media as normalized to unconditioned media. Gray box indicates all cytokines measured below a ratio of 1. Unity line is shown to illustrate those cytokines differentially expressed in wtEGFR or EGFRvIII conditioned media. Data points highlighted in red and with labels indicate cytokines overproduced in EGFRvIII conditioned media. (C) Adhesion strength, i.e. τ_{50}, was plotted for wtEGFR cells selectively cultured in the indicated conditioned media that was pre-treated with the indicated antibodies (hatched bars represent cells treated with EGFRvIII conditioned media; n=3 biological replicates). *p<0.05 by paired student t-test between the indicated comparisons.

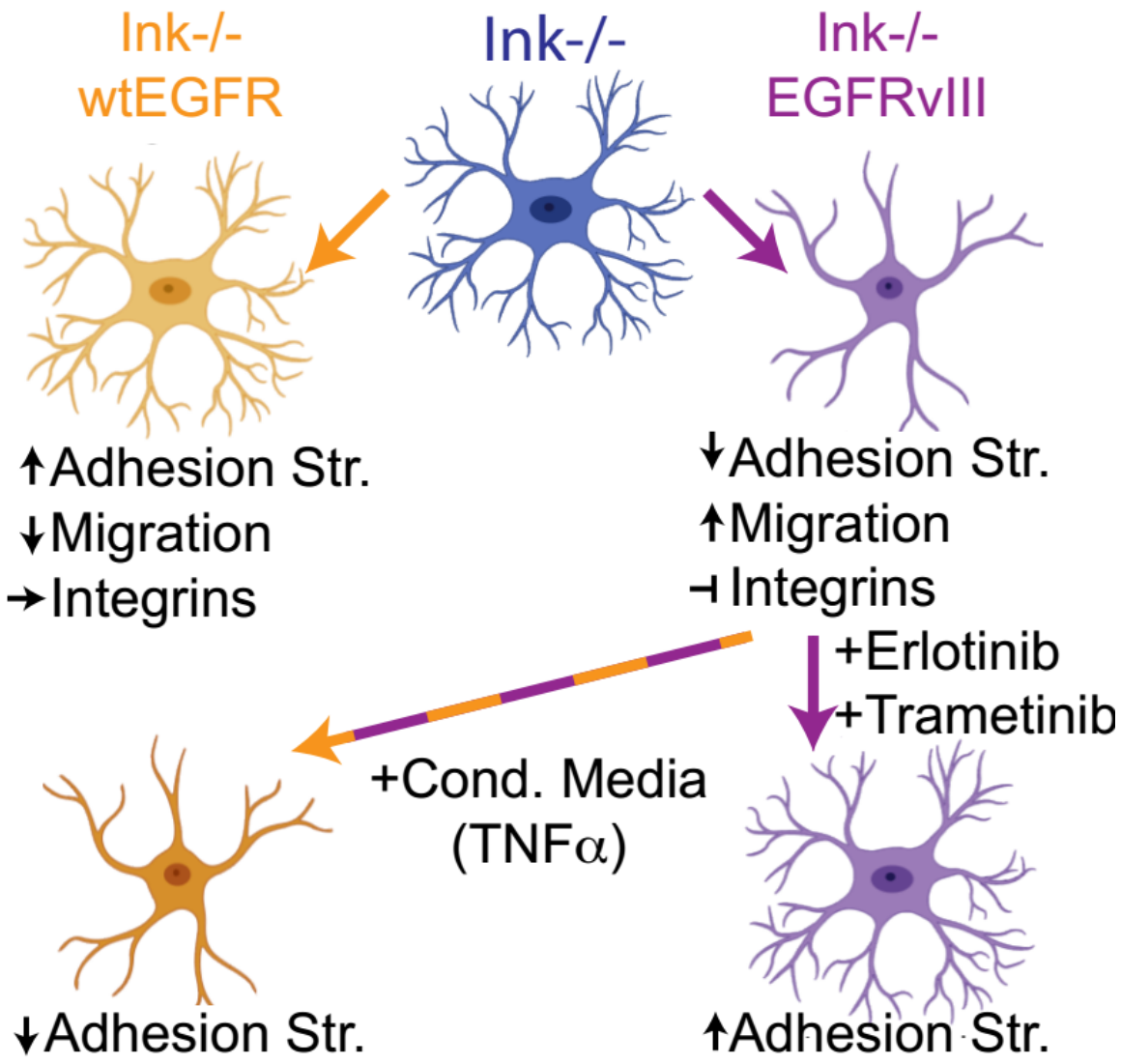

Figure 3.7. Proposed Mechanism of Action:

Schematic depicting how EGFR expression and vIII variant in the Ink-/- parental line affects cell functions and integrin expression. Indicated drug treatments that affect the EGFR-MEK signaling axis alter adhesion of EGFRvIII cells whereas cytokines from those cells can affect adhesion of wtEGFR expressing cells.

3.4 Discussion

Tumor heterogeneity and complex cooperative signaling between cells have impaired our ability to dissect the signaling pathways that promote GBM's highly invasive nature in vivo[3,4]. While crosstalk between cells in this heterogenous mass certainly occurs[49,70,192], current in vivo methods to elucidate pathway details in GBM, e.g. laser capture microdissection[82], have been limited in throughput and cannot resolve crosstalk between individual cells. On the other hand, dissemination cues are not limited to biochemical signals; as cells detach from the tumor mass to invade, significant adhesive changes must occur that should be ubiquitous for solid tumors.

Biophysical analyses have correlated adhesion with cell migration and metastatic potential[132]. Such assays also stratify tumor heterogeneity and provide a clearer understanding of the molecular mechanisms responsible for cancer cell migration[133]. Here for example, we applied a spinning disk shear assay to engineered murine astrocytes, finding that cells expressing the EGFRvIII mutation had decreased adhesion strength relative to those expressing similar wild type receptor levels, regardless of additional mutations. Cell adhesion scales inversely with migration and is the result of EGFRvIII kinase-mediated integrin transcriptional repression. These data demonstrate the utility of biophysical analyses to predict cell migration and shows that they serve as effective means of determining which cell populations may affect tumor recurrence.

While the cell-intrinsic role of EGFRvIII in astrocyte adhesion has not been examined previously, it has been studied elsewhere. Generally, EGFR kinase-dependent autophosphorylation activates downstream growth and cell survival pathways[197]. For cell adhesion, migration, and invasion of surrounding parenchyma, however, little is known about the impact of amplified levels or receptor truncation. EGFRvIII does modulate adhesion as shown

in ovarian cancer cells[198,199], but its adhesion effects in glioblastoma are uncertain. Given that nearly 60% of GBM exhibit EGFR alterations[184,185], this would appear to be a significant gap in our understanding of how biophysical changes in astrocytes affect disease progression. Adhesion data here identifies a unique role for EGFRvIII in transcriptional silencing of fibronectin-binding integrins via kinase signaling, which results in more labile adhesions capable of enhancing migration. The reliance on kinase-dependent signaling is consistent with GBM literature[187] but different from epidermoid carcinomas where EGFRvIII appears to directly associate with α2β1 ¬integrins[200]. So, while there is precedent for interactions elsewhere, we believe these data establish a new function for the vIII variant in glioma.

While intrinsic signaling can modulate a cell subtype, glioma invasion is rarely the result of a single subtype and is more likely the result of cooperative signals. EGFR-expressing astrocytes are not tumorigenic upon intracranial injection unless super-physiological levels of EGF ligand are infused into the injection site[189]. Amplified wild-type receptor can also respond to EGFRvIII-secreted cytokines to cooperatively invade into healthy parenchyma[70,192]. We found that these extrinsic signals may modulate adhesion of wild type receptor counterparts to cooperatively invasion. A variety of cytokines such as IL6, LIF, IL8, and TNF-α are differentially expressed by EGFRvIII cells. TNF-α has been linked to more aggressive and migratory phenotypes in other tumors[201], and our analysis indicated that not only was TNF-α differentially expressed, it is a necessary component in modulating the adhesion strength of cells overexpressing wtEGFR. These data highlight the importance of cell-extrinsic factors in modulating adhesion and thus migration and gives us insight into possible cooperative behaviors that lead to larger, collective migration of tumor cells.

GBM is a heterogeneous disease, and these data suggest that additional attention should be paid to how certain receptor variants modulate adhesion and subsequent migration intrinsically as well as how they recruit other cells to cooperatively migrate and locally invade adjacent parenchyma. Similar to epithelial tumor cells[133], GBM cell adhesion strength is inversely correlated with migration, and thus adhesion may serve as a physical means of stratifying tumors and an alternative to genetic markers. The most aggressive gene variants may dominate their behavior, e.g. EGFRvIII, but the plasticity we observed in adhesion strength for wtEGFR cells when exposed to conditioned media suggests that stratification by genetics alone may only explain a part of tumor outcomes; cell state plasticity has recently been shown to give rise to tumor diversity[202], so it is conceivable that cytokine crosstalk could drive phenotype and possible epigenomic changes that reduce adhesion strength throughout a population, as observed here. Overall, these data are supportive of a shift to more collective migration which has recently been thought to be a significant mode in which tumors invade in vivo[203].

3.5 Methods

3.5.1 Cell lines, media, and mutagenesis

Mouse astrocytes, mAstr-Ink4a/Arf-/-, mAstr-Ink4a/Arf-/--wtEGFR, mAstr-Ink4a/Arf-/--EGFRvIII, were obtained and cultured as previously described[70,189,204]. Briefly, cells were cultured in media composed of high glucose DMEM supplemented with L-Glutamine4 (ThermoFisher Scientific, Prod#: 11965), 10% fetal bovine serum (Gemini Bio-Products, Prod#: 900-208), 1% Penicillin/Streptomycin (10,000 u/mL, ThermoFisher Scientific, Prod#: 15140122), and 1% L-Glutamine (200mM, ThermoFisher Scientific Prod#: 25030081). All cells were cultured at 37°C in

a humidified incubator containing 5% CO2, and all media was sterile filtered. Cells were grown on tissue-culture treated polystyrene (TCPS) substrates unless otherwise indicated. Cells were passaged every 2-3 days depending on confluency using 0.25% Trypsin (ThermoFisher Scientific Prod#: 25200056), were neutralized by media, and were resuspended in fresh complete media at dilutions appropriate for each line.

For conditioned media, EGFRvIII cells were seeded overnight, media subsequently removed, and fresh media added for 24 hours. Conditioned media was collected, filtered using a 0.22 µm steriflip (MilliporeSigma Prod#: SCGP00525), and used immediately or frozen at -80°C in specific assays described below.

To briefly describe the generation of mAstr-Ink4a/Arf-/--EGFRvIIIKD cells, EGFRvIII in pBABE-puro[192] was altered by site directed mutagenesis to generate lysine 721 to methionine (K721M)[194] within the receptor's kinase domain (Figure S3.3A). To produce retrovirus, 293T cells were plated and adhered for ~18 hr before transfection by Lipofectamine 2000 (ThermoFisher Scientific Prod#: 11668019) along with retrovirus packaging construct pCL10A1 and the kinase dead receptor construct pBABE-puro EGFRvIII kinase dead. Retroviral supernatant was then harvested up to 48 hr post transfection, filtered and used to transduce mAstr-Ink4a/Arf-/-. Following overnight incubation, transduced cells were selected with 2 µg/ml puromycin for 4 days.

To ensure equivalent EGFRvIIIKD and EGFRvIII expression, cells were sorted via fluorescence-activated cell sorting (Figure S3.3B). Cells were grown to ~80% confluency under selection of puromycin (5 µg/mL, ThermoFisher Scientific Prod#: A1113802), and detached with Verscene (ThermoFisher Scientific Prod#: 15040066). Cells were counted, pelleted, and

resuspended in flow-cytometry buffer (FACS buffer, 1x DPBS, 2% BSA, 1 mM EDTA (pH 7.4)) at a concentration of 1x107 cells/mL. After resuspension, DH8.3 anti EGFRvIII (Novus Biologicals Prod#: NBP2-50599) primary antibody was added to the resuspended cells and incubated on ice for 1hr. Cells were then washed, labeled at 1:100 with Goat Anti-Mouse IgG H&L Alexa Fluor 488 (Abcam Prod#: ab150113), and then washed again. Propidium Iodide (1 mg/mL; ThermoFisher Scientific Prod#: P1304MP) was added at a 1:1000 ratio to differentiate live vs. dead cells prior to sorting. Sorting parameters were then set using non-EGFRvIII expressing and EGFvIII expressing cells, and kinase dead cells were sorted to an equivalent expression level of cell surface receptor using a SH800S Cell Sorter (Sony Biotechnology).

3.5.2 Cell adhesion-strength assay

In the spinning disk device[127], cells are seeded onto 25 mm glass coverslips functionalized with 10 μg/mL human fibronectin (isolated from serum5) for 60 min and blocked with media (10% FBS) for 60 min at room temperature; all adhesion-strength and cellular-migration assays were performed on fibronectin-coated coverslips unless otherwise noted. Cells were seeded at a density 10,000 cells/cm^2 to minimize cell-cell contact. Cells attached to coverslips for a minimum of 12 hrs using cation-containing media at which time they were then mounted on a custom-built spinning-disk device and submerged into temperature-controlled phosphate-buffered saline spinning buffer containing (PBS+MgCa; Corning Prod#: 20-030-CV) or lacking cations (PBS; Corning Prod#: 20-031-CV), supplemented with 4.5 g/L of dextrose, and warmed to 37°C. Cells were exposed to a range of fluid sheer–depending on rotational speed–for 5 min.

Once spun, cells were then fixed with 3.7% formaldehyde. Cell nuclei were then stained with 4',6-Diamidino-2-Phenylindole (DAPI, 1:2500, ThermoFisher Scientific Prod#: D1306) and

mounted on slides with Fluoromount-G (Southern Biotech, cat # 0100-01). Slides were then imaged using a CSU-X1 confocal scanner unit (Yokogawa), QuantEM:512SC camera (Photometrics, Tucson, AZ), and MS-2000-WK multi-axis stage controller (Applied Scientific Instrumentation) on a Nikon (Melville, NY) Ti-S microscope. Metamorph 7.6 software and a custom-written MATLAB (Mathworks) program was used to stitched together 1500 individual images of nuclei and quantify average cell adhesion, i.e.τ50, which is defined as the shear stress at which 50% of the initial cell population is removed by fluid sheer stress[132]. Thus was calculated based on equation 1:

$$\tau = \frac{4}{5} r \sqrt{\rho \mu \omega^3} \quad (1)$$

where r is the radial position from the center of the disk, ρ is the buffer density, μ is the buffer viscosity, and ω is the rotational velocity. To compare cell adhesion characteristics, cellular adhesion strength was analyzed in a minimum of triplicate and compared using a paired student t-test. All code associated with image analysis can be obtained at: https://github.com/englea52/Englerlab.

3.5.3 Co-Immunoprecipitation Protocol (co-IP)

EGFR was covalently crosslinked to other proteins, isolated from cell lysate, and analyzed for integrin association. Briefly, cells were washed and treated with of either 2 mM DTSSP or DSP (ThermoFisher Scientific Prod#: 21578, 22585 respectively) for 60 min to covalently crosslink interacting proteins; Tris Buffered Saline (TBS) was added to neutralize remaining crosslinker. Cells were then removed from the dish using a cell scraper (Corning, Prod#: 3010) and pelleted.

After TBS rinse, cells were resuspended in 200 µL of non-denaturing lysis buffer (20 mM Tris HCL pH 8, 137 mM NaCl, 0.5% Trition X-100, 2 mM EDTA) to lyse cell without destroying protein conformation. Lysate was vortexed and then centrifuged to pellet debris. The supernatant was collected to determine protein concentration via BCA Assay (ThermoFisher Scientific Prod#: 23225).

Next, protein G Dynabeads™ (ThermoFisher Scientific Prod#: 10007D) were functionalized with mouse Anti-EGF Receptor Clone 13 antibody (BD Biosciences Prod#: 610017) with or without BS3 crosslinker to covalently bind the antibody to the bead. To immunoprecipitate EGFR, samples containing 37 µg of protein were added to functionalized beads, pipetted to resuspend, and incubated overnight @ 4°C to allow antigen binding. Samples were magnetically pelleted and the supernatant decanted and saved for parallel analysis. Protein was eluted from the beads using denaturing gel loading buffer/dye, 50 mM DTT DTT, 1x Laemmli Sample Buffer (Biorad Prod#:1610747) and filled to 30 µL with mRIPA (50 mM HEPES, 150 mM NaCl, 1.5 mM MgCl2, 1 mM EDTA, 1% Triton, 10% glycerol, 25 mM sodium deoxycholate, 0.1% SDS, Roche Complete Protease Inhibitor (SigmaAldrich, Prod#: 11697498001) and PhosSTOP (Sigma-Aldrich, Prod#: 4906845001)). Samples were heated for 5 min at 95ºC, IP solution was separated from beads and a western blot was run on all samples to determine EGFR-integrins association.

3.5.4 Immunoflourescent Staining

Cells fixed in 3.7% formaldehyde in solution A (1x DPBS with 0.5 mM MgCl2 and 1 mM $CaCl_2$) for 15 min were washed and stained with deep red CellMask (ThermoFisher Scientific Prod#: C10046) to label cell membranes. Cells were washed again, permeabilized, blocked (0.3M

Glycine, 10% Goat Serum, 15 BSA, 0.1% BSA) for 1hr at room temp, and stained 1:500 with primary antibody Mouse anti EGFR ((BD Biosciences Prod#: 610017)) and Rabbit anti Paxillin (abcam Prod#: ab32084) at 4oC. Cells were washed and incubated 1:1000 with secondary antibodies goat anti-rabbit 568nm (ThermoFisher Scientific Prod#: A11011) and goat anti-mouse 488nm (ThermoFisher Scientific Prod#: A11001) at room temperature. Cells were finally washed, stained 1:2000 with Hoechst 33342 (ThermoFisher Scientific Prod#: H3570) at room temperature, and mounted with Fluoromount-G (Southern Biotech, Prod#: 0100-01).

Samples were imaged using the 60x objective on a Nikon Eclipse TI fluorescent microscope with a CSU-X1 confocal scanner unit (Yokogawa), QuantEM:512SC camera (Photometrics, Tucson, AZ), MS-2000-WK multi-axis stage controller (Applied Scientific Instumentation), and controlled by Metamorph 7.6 (Molecular Devices). A custom-written ImageJ script was then used to quantify cell area and FA number and size. All FA metrics were computed across the entire cell to avoid regional biases.

3.5.5 Measuring percent detachment versus migratory capability

12-well glass bottom plates with high performance #1.5 cover glass (Cellvis Prod#: P12-1.5H-N) were coated with 1.5 mL of fibronectin in DPBS at a concentration of 10 µg/cm2. Plates were incubated at room temperature for 1hr to allow for fibronectin adsorption and then blocked with 10% FBS for 1hr at room temperature. Cells were then seeded at a density of 300 cells/cm2 and allowed to adhere for 4 hours prior to live-cell imaging for 12 hours. Cells were imaged with a Nikon Eclipse Ti-S microscope equipped with a motorized stage (MS-2000-WK multi-axis stage controller (Applied Scientific Instumentation), as well as a temperature, humidity, and CO2-controlled live cell chamber (Pathology Devices Inc., LiveCell). Cells were imaged at 10x in bright

field at multiple positions every 15 min for 9 hrs. Cell migration data were analyzed using a combination of Image J (NIH, Bethesda, MD) or a custom matlab script (Github repository:byeoman-eng/CellTracking, MathWorks, Natick, MA) to determine cellular migration characteristics. Cellular speed, pathlength, displacement and persistence were calculated and plotted in rose plots for each individual cell and grouped in scatter plots.

3.5.6 Western Blotting

Protein was collected by isolating cells from an 80% confluent plate using a cell scraper (Corning, Prod#: 3010) and pelleted. Cells were resuspended in mRIPA buffer (50 mM HEPES, 150 mM NaCl, 1.5 mM MgCl2, 1 mM EDTA, 1% Triton, 10% glycerol, 25 mM sodium deoxycholate, 0.1% SDS) containing Roche Complete Protease Inhibitor (Sigma-Aldrich, Prod#: 11697498001) and PhosSTOP (Sigma-Aldrich, Prod#: 4906845001). Lysate concentrations were determined using a Pierce BCA Protein Assay kit (ThermoFisher Scientific, Prod#: 23225). 12 µg of protein from each sample was combined with 50 mM DTT, 1x Laemmli Sample Buffer (Biorad Prod#: 1610747) and heated to 95°C for 5 minutes to denature the lysates.

Protein mixtures were electrophoretically separated on reducing and denaturing gradient Bis-Tris gels (ThermoFisher Scientific, Prod#: NW04120BOX). Protein was transferred via nitrocellulose membrane using the iBlot 1 semi-dry transfer system (ThermoFisher Scientific, Prod#: IB1001) and membrane cassettes (ThermoFisher Scientific, Prod#: IB301001). Membranes were incubated with 5% Seablock blocking buffer (ThermoFisher Scientific Prod#: 37527) in Tris buffered saline with Tween (TBS-T, 150 mM NaCl, 15 mM Tris-HCl, 20 mM Tris Base, 0.1% Tween) and probed with primary antibodies. Membranes were washed, incubated with goat anti-rabbit 790nm (ThermoFisher Scientific, Prod#: A11374) and goat anti-mouse 680nm (ThermoFisher

Scientific, Prod#: A10038) secondary antibodies. Membranes were washed and imaged utilizing the Odyssey CLx Imaging System and ImageStudio (Licor) software. Immunoblots were normalized to loading control proteins to ensure accurate loading of protein samples.

3.5.7 Phospho-kinase Antibody Array

Media was analyzed using the Proteome Profiler Mouse XL Cytokine Array (R&D Systems, cat # ARY028). Briefly, membranes were blocked for 1 hour using array buffer, and media was then combined with array buffer overnight at 4ºC with rocking. Membranes were washed, incubated with the antibody cocktail diluted for 1 hour, washed, and incubated with streptavidin-HRP for 30 minutes, and finally treated with chemiluminescent reagent mix; membranes were exposed to film and imaged. Pixel quantification was performed in ImageJ and normalized to positive and loading controls. Conditioned media was normalized to unconditioned media to allow for accurate comparison across conditions.

3.5.8 Real-Time Quantitative Reverse Transcription PCR

Cells were grown to 80% confluency, RNA extracted by Trizol-chloroform (ThermoFisher Scientific, Prod#: 15596), and concentration measured via nanodrop 2000 (ThermoFisher Scientific, Prod#: ND-2000). 2 µg RNA was reverse transcribed using Super Script III Reverse Transcriptase (Thermo Scientific, Prod#: 18080093). Quantitative PCR was performed using the iQ SYBR Green Supermix (Bio-Rad Laboratories, Prod#: 1708880) using a 7900HT Fast Real-Time PCR System (ThermoFisher Scientific, Prod#: 4329001) green (45 cycles, 95°C for 15 seconds followed by 60°C for 1 min) with the primer sets described in Table S2. Analysis of gene expression was performed compared to actin gene expression via the ΔΔCT method.

3.5.9 Small molecule treatment

To understand if small molecule inhibition of EGFRvIII as well as its downstream pathways was able to modulate cellular adhesion, cells were exposed to select inhibitors prior to spinning. In brief, 25 mm glass coverslips were functionalized with fibronectin prior as previously described. Cells were then seeded at a density of 2,000 cells/cm2 and allowed to adhere overnight in media without inhibitor. Once adhered, cells were incubated with either 10 µM Erlotinib (LC Laboratories, Prod#: T-8123) to inhibit constitutive EGFR activation or 15 nM Trametinib (LC Laboratories, Prod#: T-4007) to inhibit downstream MEK activation for 48 hours prior to spinning. Cells were compared to DMSO dosed controls then spun, fixed, stained, imaged and analyzed as previously described. To confirm the effect of the inhibitors on pathway activation, cells were seeded for western blot analysis in parallel to the spinning disk assay. Similar to the spinning disk methodology, cells were seeded into 10 cm tissue culture dishes at a density of 10,000 cells/cm2 and allowed to adhere overnight before being exposed to their respective inhibitors (Erlotinib, Trametinib) and were incubated for 48 hrs prior to collection and analysis as previously described.

3.6 Supplementary Figures

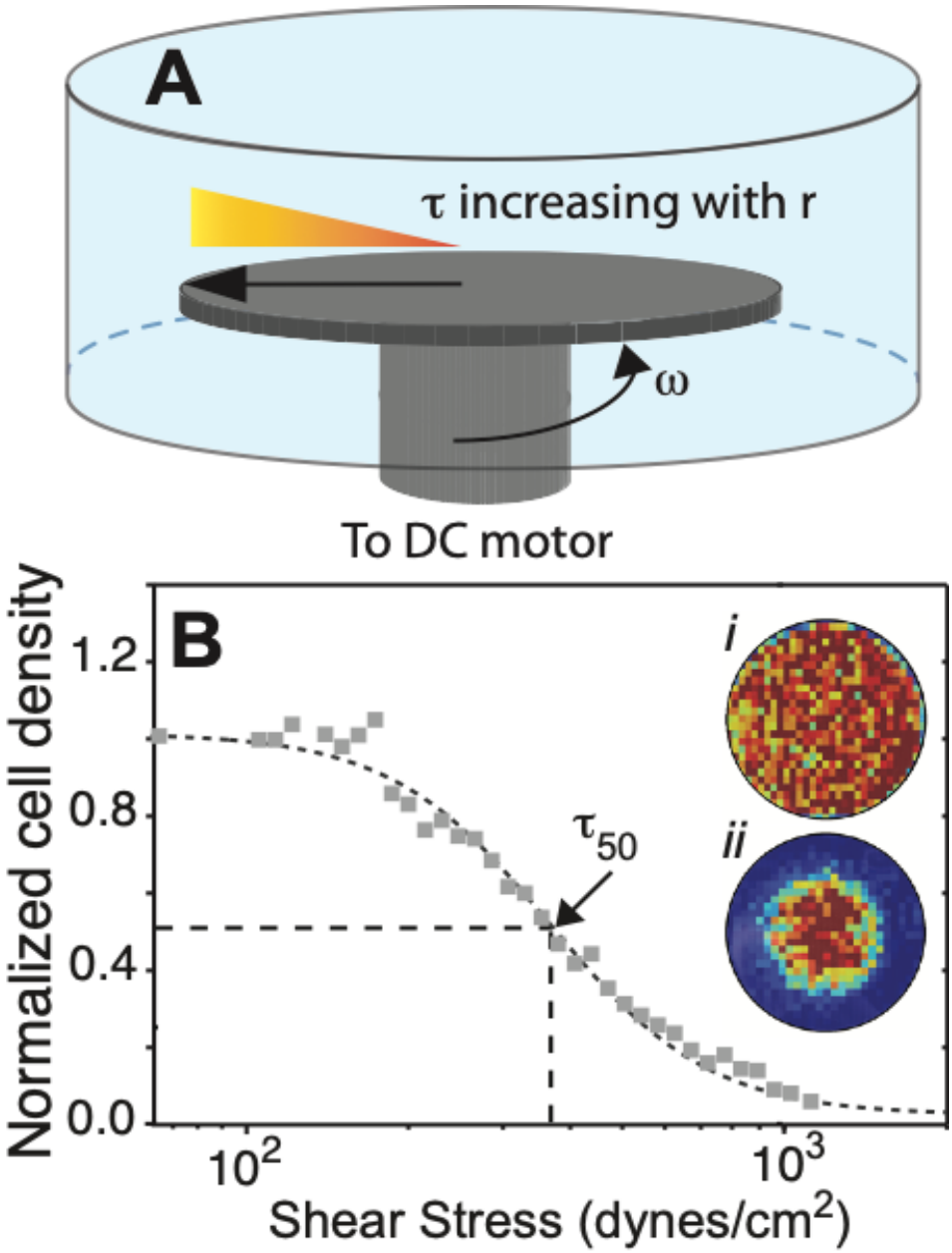

Supplemental Figure 3.1. Spinning Disc Creates a Radially-dependent Shear Profile:

(A) An illustration of the spinning disc device is shown indicating the radially-dependent shear profile (red to yellow gradient) created by the angular velocity, which causes lineage velocity at the center to effectively be zero while those at the edge move around at a high linear velocity. (B) Plot of cell density, normalized to the center of the coverslip, versus the applied shear. Data is plotted for the indicated velocities. τ_{50}, i.e. the shear to detach 50% of cells, is indicated in the plot. Inset images show heat maps of cell density. Warm (red) and cool (blue) colors indicate high and low densities, respectively.

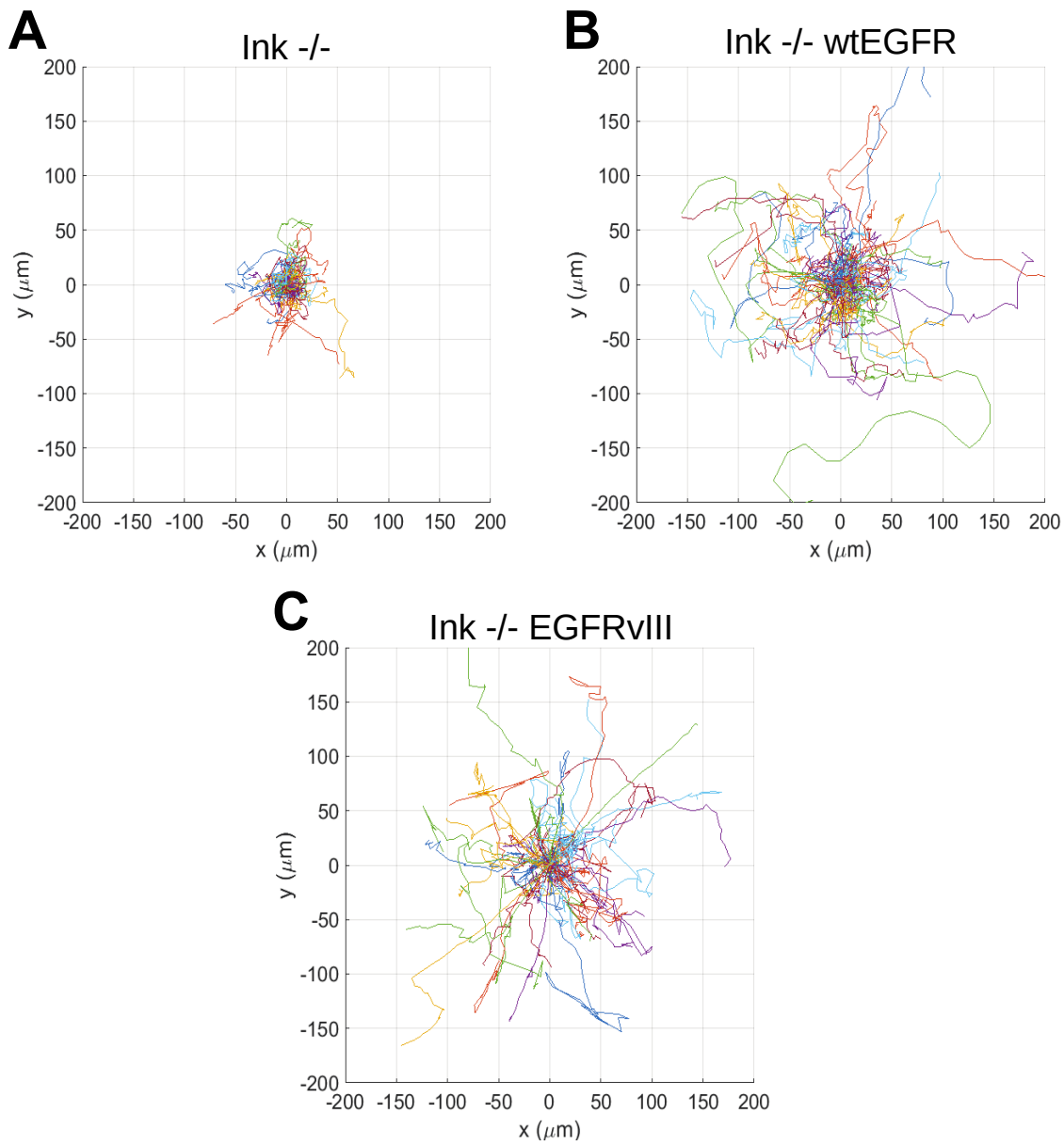

Supplemental Figure 3.2. Migration is Driven by Receptor Truncation:

Rose plots are shown for individual cells of a common genotype (each colored differently). Path length, distance traveled, and velocity were all measured from these traces. For ease of view, a limited number of traces are shown.

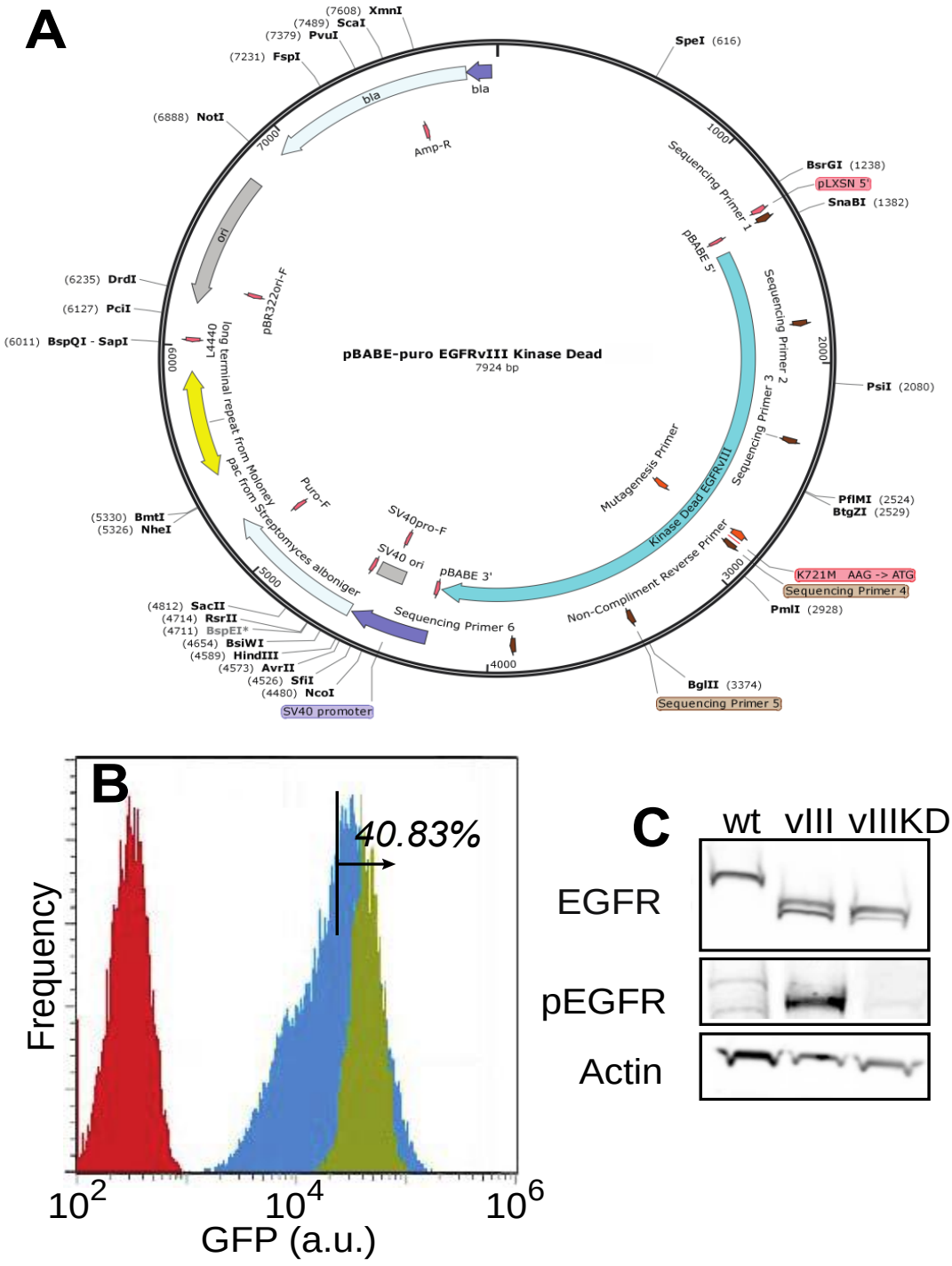

Supplemental Figure 3.3. Construction of Isogenic EGFRvIIIKD cell line:

(A) Plasmid map of the puromycin-selectable lysine to methionine substitution (K721M) construct for EGFR. (B) EGFR fluorescently-labeled cells were analyzed by flow cytometry for IgG only EGFRvIII (red), dual-labeled EGFRvIII (gold) and dual-labeled EGFRvIIIKD (blue). The gate indicates those cells that were serially sorted and puromycin-selected to establish a stable population. (C) Western blots of wtEGFR, EGFRvIII, and EGFRvIIIKD cells for EGFR, phosphorylated EGFR, and actin.

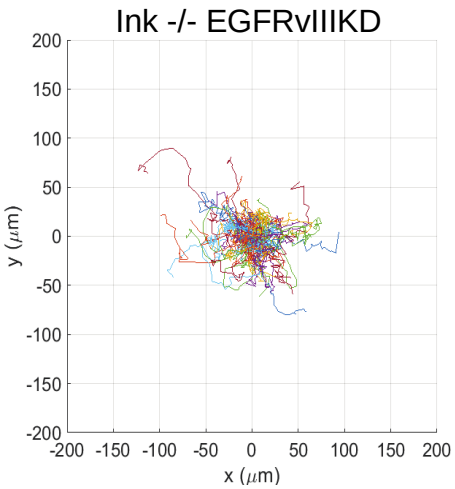

Supplemental Figure 3.4. Migration of Isogenic EGFRvIIIKD:

Rose plot is shown for individual cells of EGFRvIIIKD. Path length, distance traveled, and velocity were all measured from these traces. For ease of view, a limited number of traces are shown.

Supplemental Table 3.5. Mouse Astrocyte Lines:
This table shows the genotypes of each line.

Ink4a/Arf	**Pten**	**EGFR**	**Tumor Characteristics**
-/-	+/+	N/A	Non-Tumorigenic
-/-	-/-	N/A	Tumorigenic
-/-	+/+	wt	Tumorigenic
-/-	+/+	vIII	Tumorigenic Invasive
-/-	-/-	vIII	Tumorigenic Invasive
-/-	+/+	Kinase Dead vIII	Tumorigenic

Supplemental Table 3.6. PCR Primers:
This table shows all of the qPCR primers and in which figure each primer was used.

Primer Name	5'-Primer Sequence-3'
Kinase Dead EGFRvIII Forward Mutagenesis Primer	GCT ATC ATG GAA TTA AGA GAA GCA
Kinase Dead EGFRvIII Forward Mutagenesis Primer	TTT AAC TTT CTC ACC TTC TGG GAT CCA GAG T
Kinase Dead EGFRvIII Sequencing Primer 1	TTT ATC CAG CCC TCA CTC CTT CTC TAG
Kinase Dead EGFRvIII Sequencing Primer 2	GGG TTT TTG CTG ATT CAG GCT TGG
Kinase Dead EGFRvIII Sequencing Primer 3	CAG ACA ACT GTA TCC AGT GTG CCC
Kinase Dead EGFRvIII Sequencing Primer 4	AAC ATC TCC GAA AGC CAA CAA GG
Kinase Dead EGFRvIII Sequencing Primer 5	TCC ATC CTG GAG AAA GGA GAA CGC
Kinase Dead EGFRvIII Sequencing Primer 6	AAA CCA GTC CGT TCC CAA AAG G
Mouse Integrin AlphaV Forward Primer	CCG TGG ACT TCT TCG AGC C
Mouse Integrin AlphaV Reverse Primer	CTG TTG AAT CAA ACT CAA TGG GC
Mouse Integrin Alpha5 Forward Primer	CTT CTC CGT GGA GTT TTA CCG
Mouse Integrin Alpha5 Reverse Primer	GCT GTC AAA TTG AAT GGT GGT G
Mouse Integrin Beta1 Forward Primer	ATG CCA AAT CTT GCG GAG AAT
Mouse Integrin Beta1 Reverse Primer	TTT GCT GCG ATT GGT GAC ATT
Mouse Integrin Beta Actin Forward Primer	GGC TGT ATT CCC CTC CAT CG
Mouse Integrin Beta Actin Reverse Primer	CCA GTT GGT AAC AAT GCC ATG T

3.7 Acknowledgements

The authors wish to thank Mana Abbasinik, Tristian Saucedo, Bryanna Harris, and Shao Chi Chen for technical assistance. The authors declare no competing interests. Funding was provided by direct support from the Ludwig Institute for Cancer Research, National Institutes of Health (R01CA206880 and R21CA217735 to A.J.E. and R01NS080939 to F.F.), and the National Science Foundation (CMMI-1763139 to A.J.E.) along with the National Science Foundation Graduate Research Fellowship program (to A.B.).

Chapter 3, in full, is a preprint of material submitted for publication in Banisadr, A., Eick, M., Beri, P., Parisian, A. D., Yeoman, B., Placone, J., Engler, A.J., Furnari, F. “EGFRvIII contributes to glioblastoma migration by cell intrinsic and cooperative mechanisms that reduce cell-matrix adhesion.” (2020). The dissertation author was the primary author of this paper.

Chapter 4.

Conclusions

4.1 Introduction

Understanding and predicting tumor migratory and metastatic phenotype is critical in improving patient diagnosis, developing novel therapeutics, and preventing tumor recurrence either within the same tissue or systemically. The field of tumor biology has grown rapidly, with new assays and novel technologies improving our understanding of tumor development, tracing tumor evolutions, and predictive of tumor cell behavior. In particular, as demonstrated in chapter 1, the ability to analyze tumor malignancy through molecular, genetic, and biophysical properties has seen an exponential growth in the past decade. These assays have proven to be extremely effective in elucidating the multitude of variables which contribute to tumor cell malignancy from loss of tumor suppressors, to constitutive signaling of mutant receptors, and novel cell motility mechanisms such as osmotic engines. Of particular importance is the development and application of fluidic shear assays in assessing cellular adhesion characteristics. As demonstrated throughout this dissertation, the ability of these assays to predict tumor migratory and

metastatic characteristics, as well as interrogate the mechanisms involved in those phenotypes demonstrates their utility and importance.

4.2 Metastatic cancer cell populations display decreased adhesion strength and more labile focal adhesions compared to non-metastatic counterparts

Mammary epithelial tumors exhibit a large amount of heterogeneity in their migratory and metastatic characteristics between patients. This variability is due to a plethora of genetic diversity between patients in both within the tumor and at the germ-line. As a result of this heterogeneity, there is an inability to determine a universal biomarker which is capable of predicting tumor malignant potential from a primary tumor. As indicated in Chapter 1, in lieu of biomarkers, the use of cell biophysical properties is now being utilized as a more universal metric for interrogating cell migratory and metastatic potential. These assays vary in methodology, speed, throughput, and data output, but are more universal in their predicting tumor behavior and provide a much more thorough insight into the mechanisms involved in cell malignancy. In chapter 2 we were able to interrogate cellular adhesion strength as a biophysical metric for mammary epithelial tumor migratory and metastatic characteristics. Cellular adhesion strength analysis by the quantitative and population-based spinning disk fluidic shear assay served to differentiate the properties of metastatic MDA-MB-231 from non-metastatic MCF10A breast cancer lines. It has been previously shown that mammary tumors chelate Mg^{2+} and Ca^{2+} away from the surrounding tissue stroma, causing a gradient of divalent cations from the blood vessel

to the tumor. In order to recapitulate the extracellular conditions found in the tumor microenvironment, cellular adhesion strength was evaluated in the presence or absence of divalent cations (Mg^{2+} and Ca^{2+}). Cellular adhesion characteristics indicated that in the presence of divalent cation concentrations which mimic healthy tissue those MDA-MB-231 and MCF10A cells exhibited similar adhesion strength characteristics. Conversely, in the absence of Mg^{2+} and Ca^{2+} MDA-MB-231 cells show a marked decrease in adhesion, whereas the MCF10A cells maintained strong adhesion characteristics. In addition, this decrease in cellular adhesion correlated with an increase in cellular migration through transwells, in 2D collagen coated substrates, and on collagen gels. The mechanism responsible for this decrease in adhesion strength and increased cell migration in the metastatic MDA-MD-231 cells, is due to a loss of focal adhesion assembly state. In addition, focal adhesion disassembly, decrease in adhesion strength, and increase in migration can be recapitulated in the MCF10A cells by exposing the cells with cyclic RGD peptide prior to analysis. All together these data indicate that decreased cellular adhesion strength is indicative of tumor cell metastatic potential, in the context of proper extracellular cues, and that this decrease in adhesion strength is due to more labile focal adhesions which disassemble more readily in metastatic cells.

4.3 EGFRvIII expressing astrocytes exhibit decreased adhesion strength due to receptor-mediated integrin suppression, and decrease adhesion strength of wtEGFR expression cells through TNF-α paracrine signaling

As previously described in chapter 2, the utilization of fluidic shear stress to measure cellular adhesion strength demonstrates a clear correlation between decreased adhesion strength and increased tumor malignancy in epithelial tumors. However, in order to understand if cellular adhesion strength analysis may be implemented as a more universal marker of tumor cell migratory and metastatic potential, application to other tumor types needed to be validated. In chapter 3 we address this through the analysis of isogenic murine astrocytes which were engineered to express those genetic alterations most commonly found in glioblastoma tumors. These GBM tumor model systems presented an ideal candidate for analysis for several reasons. First is the astrocytic derivation of GBM tumors, which presented the opportunity to determine if adhesion strength analysis in a different tissue type and which is directly recapitulated in the murine astrocyte model. Second is the isogenic nature of the cells which allows for a systematic and reductionist approach to evaluating the impact of those most common GBM genetic alterations. Third, is the highly migratory nature of GBM tumors, which have been shown to cross the corpus callosum, and which are the cause of tumor recurrence in patients. Characterization of cellular adhesion strength as a metric for migratory characteristics was performed in a quantitative and population-based manner by spinning disk shear assay. Analysis of these data

showed a decrease in adhesion strength for those cells where the EGFRvIII mutation was present, regardless of the presence of other gene alterations (i.e. loss of Pten). Furthermore, live cell microscopy demonstrated an increase in migratory phenotype of those EGFRvIII expressing cells, further validating the correlation between decreased cell adhesion strength and increased cell migration. Molecular analysis of these cells by immunofluorescent microscopy indicated that the decrease in cell adhesion was due to a lack of focal adhesion assembly, a key component of adhesion strength properties, compared to wtEGFR expressing sister cells. In order to interrogate the mechanism by which the mutated receptor induces these changes, a cell line expressing the kinase dead version of the EGFRvIII (kdEGFRvIII) was generated and analyzed for both properties. Adhesion strength and molecular analysis of kdEGFRvIII cells showed a restoration of cellular adhesion strength properties, and an increase in ECM receptor integrins compared to kinase-competent sister astrocytes. Together, these data implicating the kinase-dependent mechanism of action in the EGFRvIII expressing cells. Furthermore, increased cellular adhesion strength was observed in the EGFRvIII cells when kinase function of the receptor, or downstream MEK pathways, was achieved by the small molecule inhibitors Erlotinib or Trametinib, respectively. Furthermore, education of wtEGFR expressing astrocytes by the soluble factor TNF-α secreted from EGFRvIII expressing cells induced a decrease in cellular adhesion strength of those wtEGFR cells. This study reveals the effects of EGFRvIII on cellular adhesion, not only intracellularly through the suppression of integrins through signaling of the receptor, but intercellularly through the secretion of cytokine TNF-α.

4.4 Future directions

Although the results and conclusions of this dissertation have demonstrated the applicability of adhesion strength as a biophysical marker of cancer cell malignancy, further analysis is needed to understand the implications of these findings. In chapter 3 we demonstrated that EGFRvIII expressing cells demonstrate a decrease in cellular adhesion strength compared to wtEGFR expressing cells, and that the EGFRvIII cells can modulate the adhesion strength of the wtEGFR cells through the secretion of cytokines. The next step in analyzing the impact EGFRvIII mutations on cell adhesion is two-pronged. First is to perform an analysis of EGFRvIII expressing cell adhesion heterogeneity to understand what mechanisms are responsible for differences in adhesion for genetically identical cells. Second is to investigate the mechanism of action by which TNF-α from the EGFRvIII cells is able to affect wtEGFR cell adhesion properties.

To investigate these adhesion differences in a heterogeneous EGFRvIII expressing cell population isolation of those cells exhibiting the weakest and strongest adhesion phenotypes must be performed. In order to achieve this, we would utilize the parallel-plate flow chamber fluidic shear assay which has been utilized for similar experiments in mammary epithelial tumors. This device works on the same principle of attaching cells to an ECM-coated coverslip, however, those cells in the device are exposed to a single uniform shear stress. This uniform application of fluidic shear allows us to tune the assay in such a manner which stratifies discreet cell populations by their adhesion strength. Furthermore, unlike the spinning disk device, the PPFC allows us to collect cells-post shear and perform analysis on these stratified cell populations. For example, in order to interrogate how epigenetic changes manifest as adhesion strength differences in the EGFRvIII cell population, we would expose cells to low fluidic shear and collect those most weakly

adherent cell populations. We would then apply extremely high shear to remove all but the most adherent cells, and then collect those strongly adherent cells through trypsinization of the coverslip. Once both cell populations were collected, we would submit them for RNA-seq analysis to determine gene expression differences that occur between the populations. Furthermore, in order to understand the *in vivo* effects of these gene expression and adhesion differences I would isolate weakly and strongly adherent populations as before. Cells would then be fluorescently labeled, and orthotopically inject them into mice to evaluate how adhesion and epigenetic heterogeneity affects *in vivo* tumor formation and invasion over a long-term period.

Secondly, in order to understand pathways that EGFRvIII activates or inhibits in the wtEGFR cell through the secretion of TNF-α, I would do phospho-mass-spec and RNA-seq of wtEGFR expressing cells in the presence and absence of EGFRvIII cell conditioned media. I would then analyze those gene ontologies and phosphorylation pathway for differences in cell adhesion pathways, contractility pathways, and cytoskeletal proteins.

References

1. Makubate, B., Donnan, P. T., Dewar, J. A., Thompson, A. M. & McCowan, C. Cohort study of adherence to adjuvant endocrine therapy, breast cancer recurrence and mortality. *Br. J. Cancer* 108, 1515–1524 (2013).

2. Dent, R.,Valentini, A., Hanna, W., Rawlins, E., Rakovitch, E., Sun, P., Narod, S. A.. Factors associated with breast cancer mortality after local recurrence. *Curr. Oncol.* 21, 418–425 (2014).

3. Cuddapah, V. A., Robel, S., Watkins, S. & Sontheimer, H. A neurocentric perspective on glioma invasion. *Nat. Rev. Neurosci.* 15, 455–465 (2014).

4. Demuth, T. & Berens, M. E. Molecular mechanisms of glioma cell migration and invasion. *J. Neurooncol.* 70, 217–228 (2004).

5. Bellail, A. C., Hunter, S. B., Brat, D. J., Tan, C. & Van Meir, E. G. Microregional extracellular matrix heterogeneity in brain modulates glioma cell invasion. *Int. J. Biochem. Cell Biol.* 36, 1046–1069 (2004).

6. Brösicke, N. & Faissner, A. Role of tenascins in the ECM of gliomas. *Cell Adhesion and Migration* vol. 9 131–140 (2015).

7. Rao, J. S. Molecular mechanisms of glioma invasiveness: The role of proteases. *Nature Reviews Cancer* vol. 3 489–501 (2003).

8. Quintana, E., Shackleton, M., Sabel, M. S., Fullen, D. R., Johnson, T. M., Morrison, S. J. Efficient tumour formation by single human melanoma cells. *Nature* 456, 593–598 (2008).

9. Levental, K. R., Yu, H., Kass, L., Lakins, J. N., Egeblad, M., Erler, J. T., Fong, S. F. T., Csiszar, K., Giaccia, A., Weninger, W., Yamauchi, M., Gasser, D. L., Weaver, V. M. Matrix crosslinking forces tumor progression by enhancing integrin signaling. *Cell* 139, 891–906 (2009).

10. Paszek, M. J., Zahir N., Johnson K.R., Lakins J.N., Rozenberg G.I., Gefen A., Reinhart-King C.A., Margulies S.S., Dembo M., Boettiger D., Hammer D.A., Weaver V.M. Tensional homeostasis and the malignant phenotype. *Cancer Cell* 8, 241–254 (2005).

11. Liu, Y., Nenutil, R., Appleyard, M. V., Murray, K., Boylan, M., Thompson, A. M., Coates, P. J. Lack of correlation of stem cell markers in breast cancer stem cells. 110, (2014).

12. Sun, X. X. & Yu, Q. Intra-tumor heterogeneity of cancer cells and its implications for cancer treatment. *Acta Pharmacologica Sinica* vol. 36 1219–1227 (2015).

13. Dagogo-Jack, I. & Shaw, A. T. *Tumour heterogeneity and resistance to cancer therapies*. *Nature Reviews Clinical Oncology* vol. 15 (Nature Publishing Group, 2018).

14. Civita, P., Franceschi, S., Aretini, P., Ortenzi, V., Menicagli, M., Lessi, F., Pasqualetti, F., Giuseppe A. N., Maria, M. C. Laser capture microdissection and RNA-seq analysis: High sensitivity approaches to explain histopathological heterogeneity in human glioblastoma FFPE archived tissues. *Front. Oncol.* 9, (2019).

15. Hwang, B., Lee, J. H. & Bang, D. Single-cell RNA sequencing technologies and bioinformatics pipelines. *Experimental and Molecular Medicine* vol. 50 1–14 (2018).

16. Dhar, M., Pao, E., Renier, C., Go, D. E., Che, J., Montoya, R., Conrad, R., Matsumoto, M., Heirich, K., Triboulet, M., Rao, J., Jeffrey, S. S., Garon, E. B., Goldman, J., Rao, N. P., Kulkarni, R., Sollier-Christen, E., Di Carlo, D. Label-free enumeration, collection and downstream cytological and cytogenetic analysis of circulating tumor cells. *Sci. Rep.* 6, 35474 (2016).

17. Che, J., Yu, V., Garon, E. B., Goldman, J. W., Di Carlo, D., Zhou, Y., Yue, D., Koehler, S. A., Ung, L. W., Heyman, J., Ren, Y., Ziblat, R., Chong, S., Weitz, D. A., Regev, A., McCarroll, S. A., Smith, K., Spuhler, P. S., Sullivan, J. P., Lee, R. J., Ting, D. T., Luo, X., Shaw, A. T., Bardia, A., Sequist, L. V., Louis, D. N., Maheswaran, S., Kapur, R., Haber, D. A., Toner, M. Biophysical isolation and identification of circulating tumor cells. *Lab Chip* 17, 1452–1461 (2017).

18. Espina, V., Wulfkuhle, J, D., Calvert, V. S., VanMeter, A., Zhou, W., Coukos, G., Geho, D. H., Petricoin, E. F., Liotta, L. A. Laser-capture microdissection. *Nat. Protoc.* 1, 586–603 (2006).

19. Denais, C. M., Gilbert, R. M., Isermann, P., McGregor, A. L., Te Lindert, M., Weigelin, B., Davidson, P. M., Friedl, P., Wolf, K., Lammerding, J. Nuclear envelope rupture and repair during cancer cell migration. *Science (80-.).* 352, 353–358 (2016).

20. Zaman, M. H., Trapani, L. M., Siemeski, A., MacKellar, D., Gong, H., Kamm, R. D., Wells, A., Lauffenburger, D. A., Matsudaira, P. Migration of tumor cells in 3D matrices is governed by matrix stiffness along with cell-matrix adhesion and proteolysis. *Proc. Natl. Acad. Sci. U. S. A.* 103, 10889–10894 (2006).

21. Swift, J., Ivanovska, I. L., Buxboim, A., Harada, T., Dingal, P. C. D. P., Pinter, J., Pajerowski, J. D., Spinler, K. R., Shin, J. W., Tewari, M., Rehfeldt, F., Speicher, D. W., Discher, D. E., Nuclear lamin-A scales with tissue stiffness and enhances matrix-directed differentiation. *Science (80-.).* 341, (2013).

22. Harada, T., Swift, J., Irianto, J., Shin, J. W., Spinler, K. R., Athirasala, A., Diegmiller, R., Dingal, P. C. D. P., Ivanovska, I. L., Discher, D. E. Nuclear lamin stiffness is a barrier to 3D migration, but softness can limit survival. *J. Cell Biol.* 204, 669–682 (2014).

23. Wirtz, D., Konstantopoulos, K. & Searson, P. C. The physics of cancer: The role of physical interactions and mechanical forces in metastasis. *Nature Reviews Cancer* vol. 11 512–522 (2011).

24. Paul, C. D., Mistriotis, P. & Konstantopoulos, K. Cancer cell motility: Lessons from migration in confined spaces. *Nature Reviews Cancer* vol. 17 131–140 (2017).

25. Li, Q. S., Lee, G. Y. H., Ong, C. N. & Lim, C. T. AFM indentation study of breast cancer cells. *Biochem. Biophys. Res. Commun.* 374, 609–613 (2008).

26. Cho, S., Vashisth, M., Abbas, A., Majkut, S., Vogel, K., Xia, Y., Ivanovska, I. L., Irianto, J., Tewari, M., Zhu, K., Tichy, E. D., Mourkioti, F., Tang, H. Y., Greenberg, R. A., Prosser, B. L., Discher, D. E. Mechanosensing by the Lamina Protects against Nuclear Rupture, DNA Damage, and Cell-Cycle Arrest. *Dev. Cell* 49, 920-935.e5 (2019).

27. Beri, P., Matte, B. F., Fattet, L., Kim, D., Yang, J., Engler, A. J. Biomaterials to model and measure epithelial cancers. *Nature Reviews Materials* vol. 3 418–430 (2018).

28. Types of Cancer Treatment - National Cancer Institute. https://www.cancer.gov/about-cancer/treatment/types.

29. Saquib, N., Saquib, J. & Ioannidis, J. P. Does screening for disease save lives in asymptomatic adults? Systematic review of meta-analyses and randomized trials. *Int. J. Epidemiol.* 264–277 (2015) doi:10.1093/ije/dyu140.

30. Pinker, K., Chin, J., Melsaether, A. N., Morris, E. A. & Moy, L. Precision Medicine and Radiogenomics in Breast Cancer: New Approaches toward Diagnosis and Treatment. *Radiology* 287, 732–747 (2018).

31. Mazurowski, M. A. Radiogenomics: what it is and why it is important. *J. Am. Coll. Radiol.* 12, 862–6 (2015).

32. Vardhanabhuti, V. & Kuo, M. D. Lung Cancer Radiogenomics. in *Journal of Thoracic Imaging* vol. 33 17–25 (Lippincott Williams and Wilkins, 2018).

33. Jemal, A., Siegel, R., Ward, E., Hao, Y., Xu, J., Murray, T., Thun, M. J. Cancer statistics, 2008. *CA. Cancer J. Clin.* 58, 71–96.

34. Mandelson, M. T. , Oestreicher, N., Porter, P. L., White, D., Finder, C. A., Taplin, S. H., White, E. Breast Density as a Predictor of Mammographic Detection: Comparison of

Interval-and Screen-Detected Cancers. *J. Natl. Cancer Inst.* 92, 1081–1087 (2000).

35. Kelly, K. M., Dean, J., Comulada, W. S. & Lee, S. J. Breast cancer detection using automated whole breast ultrasound and mammography in radiographically dense breasts. *Eur. Radiol.* 20, 734–742 (2010).

36. Zaha, D. C. Significance of immunohistochemistry in breast cancer. *World Journal of Clinical Oncology* vol. 5 382–392 (2014).

37. Abeloff, M., Armitage, J., Niederhuber, J., Kastan, M. & McKenna, W. *Abeloff's Clinical Oncology.* (Elsevier Health Sciences, 2008).

38. Connolly, J. L., Schnitt, S. J., Wang, H. H., Longtine, J. A., Dvorak, A., Dvorak, H. F. *Principles of Cancer Pathology*. (BC Decker, 2003).

39. Cancer Staging - National Cancer Institute. https://www.cancer.gov/about-cancer/diagnosis-staging/staging.

40. Onder, T. T., Gupta, P. B., Mani, S. A., Yang, J., Lander, E. S., Weinberg, R. A. Loss of E-cadherin promotes metastasis via multiple downstream transcriptional pathways. *Cancer Res.* 68, 3645–3654 (2008).

41. Jordan, V. C. Tamoxifen: A most unlikely pioneering medicine. *Nature Reviews Drug Discovery* vol. 2 205–213 (2003).

42. Jordan, V. C. Tamoxifen as the first targeted long-term adjuvant therapy for breast cancer. *Endocrine-Related Cancer* vol. 21 R235 (2014).

43. Sporn, M. B. & Lippman, S. M. Agents for Chemoprevention and Their Mechanism of Action. (2003).

44. Young, R. M., Jamshidi, A., Davis, G. & Sherman, J. H. Current trends in the surgical management and treatment of adult glioblastoma. *Annals of Translational Medicine* vol. 3 (2015).

45. Wilson, T. A., Karajannis, M. A. & Harter, D. H. Glioblastoma multiforme: State of the art and future therapeutics. *Surg. Neurol. Int.* 5, (2014).

46. Lara-Velazquez, M., Al-Kharboosh, R., Jeanneret, S., Vazquez-Ramos, C., Mahato, D., Tavanaiepour, D., Rahmathulla, G., Quinone-Hinojosa, A. Advances in brain tumor surgery for glioblastoma in adults. *Brain Sciences* vol. 7 (2017).

47. Garner, J. M., Ellison, D. W., Finkelstein, D., Ganguly, D., Du, Z., Sims, M., Yang, C. H., Interiano, R. B., Davidoff, A. M., Pfeffer, L.M. Molecular Heterogeneity in a Patient-Derived

Glioblastoma Xenoline Is Regulated by Different Cancer Stem Cell Populations. *PLoS One* 10, e0125838 (2015).

48. Klughammer, J., Kiesel, B., Roetzer, T., Fortelny, N., Nemc, A., Nenning, K.H., Furtner, J., Sheffield, N. C., Datlinger, P., Peter, N., Nowosielski, M., Augustin, M., Mischkulnig, M., Ströbel, T., Alpar, D., Ergüner, B., Senekowitsch, M., Moser, P., Freyschlag, C. F., Kerschbaumer, J., Thomé, C., Grams, A. E., Stockhammer, G. Kitzwoegerer, M., Oberndorfer, S., Marhold, F., Weis, S., Trenkler, J., Buchroithner, J., Pichler, J., Haybaeck, J., Krassnig, S., Ali, K. M., von Campe, G., Payer, F., Sherif, C., Preiser, J., Hauser, T., Winkler, P. A., Kleindienst, W., Würtz, F., Brandner-Kokalj, T., Stultschnig, M., Schweiger, S., Dieckmann, K., Preusser, M., Langs, G., Baumann, B., Knosp, E., Widhalm, G., Marosi, C., Hainfellner, J. A., Woehrer, A., Bock, C. The DNA methylation landscape of glioblastoma disease progression shows extensive heterogeneity in time and space. *Nat. Med.* 1 (2018) doi:10.1038/s41591-018-0156-x.

49. Bonavia, R., Inda, M. D. M., Cavenee, W. K. & Furnari, F. B. Heterogeneity maintenance in glioblastoma: A social network. *Cancer Research* vol. 71 4055–4060 (2011).

50. Bailey, M. H. Tokheim, C., Porta-Pardo, E., Sengupta, S., Bertrand, D., Weerasinghe, A., Colaprico, A., Wendl, M.C., Kim, J., Reardon, B., Ng, P.K., Jeong, K.J., Cao, S., Wang, Z., Gao, J., Gao, Q., Wang, F., Liu, E.M., Mularoni, L., Rubio-Perez, C., Nagarajan, N., Cortés-Ciriano, I., Zhou, D.C., Liang, W.W., Hess, J.M., Yellapantula, V.D., Tamborero, D., Gonzalez-Perez, A., Suphavilai, C., Ko, J.Y., Khurana, E., Park, P.J., Van Allen, E.M., Liang, H., Lawrence, M.S., Godzik, A., Lopez-Bigas, N., Stuart, J., Wheeler, D., Getz, G., Chen, K., Lazar, A.J., Mills, G.B., Karchin, R., Ding, L. Comprehensive Characterization of Cancer Driver Genes and Mutations. *Cell* 173, 371-385.e18 (2018).

51. Mardis, E. R. & Wilson, R. K. Cancer genome sequencing: a review. doi:10.1093/hmg/ddp396.

52. Gliomas, L. Comprehensive, Integrative Genomic Analysis of Diffuse Lower-Grade Gliomas. *N. Engl. J. Med.* 372, 2481–2498 (2015).

53. Palomba, G. Palomba, G., Colombino, M., Contu, A., Massidda, B., Baldino, G., Pazzola, A., Ionta, M., Capelli, F., Trova, V., Sedda, T., Sanna, G., Tanda, F., Budroni, M., Palmieri, G., Cossu, A., Contu, M., Cuccu, A., Farris, A., Macciò, A., Mameli, G., Olmeo, N., Ortu, S., Petretto, E., Pusceddu, V., Virdis, L. Prevalence of KRAS, BRAF, and PIK3CA somatic mutations in patients with colorectal carcinoma may vary in the same population: clues from Sardinia. *J. Transl. Med.* 10, 178 (2012).

54. Buenrostro, J., Wu, B., Chang, H. & Greenleaf, W. ATAC-seq: A Method for Assaying Chromatin Accessibility Genome-Wide. doi:10.1002/0471142727.mb2129s109.

55. Park, P. J. ChIP-seq: Advantages and challenges of a maturing technology. *Nature Reviews*

Genetics vol. 10 669–680 (2009).

56. Wang, Z., Gerstein, M. & Snyder, M. RNA-Seq: A revolutionary tool for transcriptomics. *Nature Reviews Genetics* vol. 10 57–63 (2009).

57. Belkadi, A., Bolze, A., Itan, Y., Cobat, A., Vincent, Q. B., Antipenko, A., Shang, L., Boisson, B., Casanova, J. L., & Abel, L. Whole-genome sequencing is more powerful than whole-exome sequencing for detecting exome variants. *Proc. Natl. Acad. Sci. U. S. A.* 112, 5473–5478 (2015).

58. Ginsburg, G. & Willard, H. *Genomic and Personalized Medicine*. *Genomic and Personalized Medicine* vols 1–2 (2013).

59. Jamieson, N. B. & Maker, A. V. Gene-expression profiling to predict responsiveness to immunotherapy. *Cancer Gene Therapy* vol. 24 134–140 (2017).

60. Goodman, A. M., Kato, S., Bazhenova, L., Patel, S. P., Frampton, G. M., Miller, V., Stephens, P. J., Daniels, G. A., & Kurzrock, R. Tumor mutational burden as an independent predictor of response to immunotherapy in diverse cancers. *Mol. Cancer Ther.* 16, 2598–2608 (2017).

61. American Cancer Society. Cancer Facts & Figures 2015. (2015) doi:10.3322/caac.21254.

62. Psifidi, A., Dovas, C. I., Bramis, G., Lazou, T., Russel, C. L., Arsenos, G., & Banos, G. Comparison of Eleven Methods for Genomic DNA Extraction Suitable for Large-Scale Whole-Genome Genotyping and Long-Term DNA Banking Using Blood Samples. *PLoS One* 10, e0115960 (2015).

63. Meyer, M. & Kircher, M. Illumina sequencing library preparation for highly multiplexed target capture and sequencing. *Cold Spring Harb. Protoc.* 5, (2010).

64. Yost, S., Ruark, E., Alexandrov, L. B. & Rahman, N. Insights into BRCA Cancer Predisposition from Integrated Germline and Somatic Analyses in 7632 Cancers. *JNCI Cancer Spectr.* 3, (2019).

65. Pavlick, A. C., Fecher, L., Ascierto, P. A. & Sullivan, R. J. Frontline Therapy for BRAF - Mutated Metastatic Melanoma: How Do You Choose, and Is There One Correct Answer? . *Am. Soc. Clin. Oncol. Educ. B.* 564–571 (2019) doi:10.1200/edbk_243071.

66. Arkenau, H. T., Kefford, R. & Long, G. V. Targeting BRAF for patients with melanoma. *British Journal of Cancer* vol. 104 392–398 (2011).

67. Pasquali, S., Hadjinicolaou, A. V., Chiarion Sileni, V., Rossi, C. R. & Mocellin, S. Systemic treatments for metastatic cutaneous melanoma. *Cochrane Database of Systematic*

Reviews vol. 2018 (2018).

68. Dagogo-Jack, I. & Shaw, A. T. Tumour heterogeneity and resistance to cancer therapies. *Nature Reviews Clinical Oncology* vol. 15 81–94 (2018).

69. Malric, L., Monferran, S., Gilhodes, J., Boyrie, S., Dahan, P., Skuli, N., Sesen, J., Filleron, T., Kowalski-Chauvel, A., Cohen-Jonathan Moyal, E., Toulas, C., & Lemarié, A. Interest of integrins targeting in glioblastoma according to tumor heterogeneity and cancer stem cell paradigm: an update. *Oncotarget* 8, 86947–86968 (2017).

70. Inda, M. M., Bonavia, R., Mukasa, A., Narita, Y., Sah, D. W., Vandenberg, S., Brennan, C., Johns, T. G., Bachoo, R., Hadwiger, P., Tan, P., Depinho, R. A., Cavenee, W., & Furnari, F. Tumor heterogeneity is an active process maintained by a mutant EGFR-induced cytokine circuit in glioblastoma. *Genes Dev.* 24, 1731–1745 (2010).

71. Patel, A. P., Tirosh, I., Trombetta, J. J., Shalek, A. K., Gillespie, S. M., Wakimoto, H., Cahill, D. P., Nahed, B. V., Curry, W. T., Martuza, R. L., Louis, D. N., Rozenblatt-Rosen, O., Suvà, M. L., Regev, A., & Bernstein, B. E. Single-cell RNA-seq highlights intratumoral heterogeneity in primary glioblastoma. *Science (80-.).* 344, 1396–1401 (2014).

72. Nagalakshmi, U., Waern, K. & Snyder, M. RNA-Seq: A Method for Comprehensive Transcriptome Analysis. *Curr. Protoc. Mol. Biol.* 1–13 (2010) doi:10.1002/0471142727.mb0411s89.

73. Phillips, H. S., Kharbanda, S., Chen, R., Forrest, W. F., Soriano, R. H., Wu, T. D., Misra, A., Nigro, J. M., Colman, H., Soroceanu, L., Williams, P. M., Modrusan, Z., Feuerstein, B. G., & Aldape, K. Molecular subclasses of high-grade glioma predict prognosis, delineate a pattern of disease progression, and resemble stages in neurogenesis. *Cancer Cell* 9, 157–173 (2006).

74. Wang, Q., Hu, B., Hu, X., Kim, H., Squatrito, M., Scarpace, L., deCarvalho, A. C., Lyu, S., Li, P., Li, Y., Barthel, F., Cho, H. J., Lin, Y. H., Satani, N., Martinez-Ledesma, E., Zheng, S., Chang, E., Sauvé, C. G., Olar, A., Lan, Z. D., … Verhaak, R. Tumor Evolution of Glioma-Intrinsic Gene Expression Subtypes Associates with Immunological Changes in the Microenvironment. *Cancer Cell* 32, 42-56.e6 (2017).

75. Kim, J., Lee, I., Cho, H. J., Lee, J. & Park, P. J. Spatiotemporal Evolution of the Primary Glioblastoma Genome Article Spatiotemporal Evolution of the Primary Glioblastoma Genome. *Cancer Cell* 28, 318–328 (2015).

76. Valastyan, S. & Weinberg, R. A. Tumor metastasis: molecular insights and evolving paradigms. *Cell* 147, 275–92 (2011).

77. Pailler, E., Adam, J., Barthélémy, A., Oulhen, M., Auger, N., Valent, A., Borget, I., Planchard,

D., Taylor, M., André, F., Soria, J. C., Vielh, P., Besse, B., & Farace, F. Detection of circulating tumor cells harboring a unique ALK rearrangement in ALK-positive non–small-cell lung cancer. *J. Clin. Oncol.* 31, 2273–2281 (2013).

78. Lareau, C. A., Duarte, F. M., Chew, J. G., Kartha, V. K., Burkett, Z. D., Kohlway, A. S., Pokholok, D., Aryee, M. J., Steemers, F. J., Lebofsky, R., & Buenrostro, J. D. Droplet-based combinatorial indexing for massive-scale single-cell chromatin accessibility. *Nat. Biotechnol.* 37, 916–924 (2019).

79. Humana Press. *Laser Capture Microdissection*. *Methods in Molecular Biology* vol. 2 (2011).

80. College tuition, other costs climb again this year. http://money.cnn.com/2012/10/24/pf/college/public-college-tuition/index.html.

81. Mariani, L., McDonough, W. S., Hoelzinger, D. B., Beaudry, C., Kaczmarek, E., Coons, S. W., Giese, A., Moghaddam, M., Seiler, R. W., & Berens, M. E. Identification and Validation of P311 as a Glioblastoma Invasion Gene Using Laser Capture Microdissection. *Cancer Res.* 61, 4190–4196 (2001).

82. Daubon, T., Guyon, J., Raymond, A. A., Dartigues, B., Rudewicz, J., Ezzoukhry, Z., Dupuy, J. W., Herbert, J., Saltel, F., Bjerkvig, R., Nikolski, M., & Bikfalvi, A. The invasive proteome of glioblastoma revealed by laser-capture microdissection. *Neuro-Oncology Adv.* 1, (2019).

83. Friedl, P., Alexander, S., Cancer Invasion and the Microenvironment: Plasticity and Reciprocity. *Cell* 147, 992–1009 (2011).

84. Barnes, J. M., Kaushik, S., Bainer, R. O., Sa, J. K., Woods, E. C., Kai, F., Przybyla, L., Lee, M., Lee, H. W., Tung, J. C., Maller, O., Barrett, A. S., Lu, K. V., Lakins, J. N., Hansen, K. C., Obernier, K., Alvarez-Buylla, A., Bergers, G., Phillips, J. J., Nam, D. H., Bertozzi C.R., Weaver V.M. A tension-mediated glycocalyx–integrin feedback loop promotes mesenchymal-like glioblastoma. *Nat. Cell Biol.* 1 (2018) doi:10.1038/s41556-018-0183-3.

85. Han, W., Chen, S., Yuan, W., Fan, Q., Tian, J., Wang, X., Chen, L., Zhang, X., Wei, W., Liu, R., Qu, J., Jiao, Y., Austin, R. H., & Liu, L. Oriented collagen fibers direct tumor cell intravasation. *Proc. Natl. Acad. Sci. U. S. A.* 113, 11208–11213 (2016).

86. Hambardzumyan, D., Bergers, G. Glioblastoma: Defining Tumor Niches. *Trends in Cancer* 1, 252–265 (2015).

87. Fuhrmann, A. & Engler, A. J. The Cytoskeleton Regulates Cell Attachment Strength. *Biophys. J.* 109, 57–65 (2015).

88. Sood, D., Tang-Schomer, M., Pouli, D., Mizzoni, C., Raia, N., Tai, A., Arkun, K., Wu, J., Black, L. D., 3rd, Scheffler, B., Georgakoudi, I., Steindler, D. A., & Kaplan, D. L. 3D extracellular

matrix microenvironment in bioengineered tissue models of primary pediatric and adult brain tumors. *Nat. Commun.* 10, 1–14 (2019).

89. Podgorny, O. V. Live cell isolation by laser microdissection with gravity transfer. *J. Biomed. Opt.* 18, 055002 (2013).

90. Pointer, K. B., Clark, P. A., Schroeder, A. B., Salamat, M. S., Eliceiri, K. W., & Kuo, J. S. Association of collagen architecture with glioblastoma patient survival. *J. Neurosurg.* 126, 1812–1821 (2017).

91. Coulter, W. H., Es, A. & Garc Ia, J. Dennis W. Zhou Measurement Systems for Cell Adhesive Forces. (2015) doi:10.1115/1.4029210.

92. Herrera-Perez, M., Voytik-Harbin, S. & Rickus, J. L. Extracellular matrix properties regulate the migratory response of glioblastoma stem cells in 3D culture. *Tissue Eng. Part A* 21, 2572–2582 (2015).

93. Lo, C. M., Wang, H. B., Dembo, M. & Wang, Y. L. Cell movement is guided by the rigidity of the substrate. *Biophys. J.* 79, 144–152 (2000).

94. Tse, J. R. & Engler, A. J. Preparation of Hydrogel Substrates with Tunable Mechanical Properties. *Curr. Protoc. Cell Biol.* 47, 10.16.1-10.16.16 (2010).

95. Paszek, M. J., DuFort, C. C., Rossier, O., Bainer, R., Mouw, J. K., Godula, K., Hudak, J. E., Lakins, J. N., Wijekoon, A. C., Cassereau, L., Rubashkin, M. G., Magbanua, M. J., Thorn, K. S., Davidson, M. W., Rugo, H. S., Park, J. W., Hammer, D. A., Giannone, G., Bertozzi, C. R., & Weaver, V. M. The cancer glycocalyx mechanically primes integrin-mediated growth and survival. *Nature* 511, 319–325 (2014).

96. Wei, S. C., Fattet, L., Tsai, J. H., Guo, Y., Pai, V. H., Majeski, H. E., Chen, A. C., Sah, R. L., Taylor, S. S., Engler, A. J., & Yang, J. Matrix stiffness drives epithelial–mesenchymal transition and tumour metastasis through a TWIST1–G3BP2 mechanotransduction pathway. *Nat. Cell Biol.* 17, (2015).

97. Ondeck, M. G., Kumar, A., Placone, J. K., Plunkett, C. M., Matte, B. F., Wong, K. C., Fattet, L., Yang, J., & Engler, A. J. Dynamically stiffened matrix promotes malignant transformation of mammary epithelial cells via collective mechanical signaling. *Proc. Natl. Acad. Sci. U. S. A.* 116, 3502–3507 (2019).

98. Pathak, A. & Kumar, S. Biophysical regulation of tumor cell invasion: moving beyond matrix stiffness. *Integr. Biol.* 3, 267 (2011).

99. Shimizu, T., Kurozumi, K., Ishida, J., Ichikawa, T. & Date, I. Adhesion molecules and the extracellular matrix as drug targets for glioma. *Brain Tumor Pathol.* 33, 97–106 (2016).

100. Engler, A. J., Rehfeldt, F., Sen, S. & Discher, D. E. Microtissue Elasticity: Measurements by Atomic Force Microscopy and Its Influence on Cell Differentiation. *Methods in Cell Biology* vol. 83 521–545 (2007).

101. Giussani, M., Landoni, E., Merlino, G., Turdo, F., Veneroni, S., Paolini, B., Cappelletti, V., Miceli, R., Orlandi, R., Triulzi, T., & Tagliabue, E. Extracellular matrix proteins as diagnostic markers of breast carcinoma. *J. Cell. Physiol.* 233, 6280–6290 (2018).

102. Yu, Q., Xue, Y., Liu, J., Xi, Z., Li, Z., & Liu, Y. Fibronectin promotes the malignancy of glioma stem-like cells via modulation of cell adhesion, differentiation, proliferation and chemoresistance. *Front. Mol. Neurosci.* 11, (2018).

103. Caffo, M., Germanò, A., Caruso, G., Meli, F., Galatioto, S., Sciacca, M. P., & Tomasello, F. An immunohistochemical study of extracellular matrix proteins laminin, fibronectin and type IV collagen in paediatric glioblastoma multiforme. *Acta Neurochir. (Wien).* 146, 1113–1118 (2004).

104. Chintala, S. K., Sawaya, R., Gokaslan, Z. L., Fuller, G. & Rao, J. S. Immimohistochemical localization of extracellular matrix proteins in human glioma, both in vivo and in vitro. *Cancer Lett.* 101, 107–114 (1996).

105. Binnig, G., Quate, C. F. & Gerber, C. Atomic force microscope. *Phys. Rev. Lett.* 56, 930–933 (1986).

106. Seidner, G., Alvarez, M. G., Yeh, J. I., O'Driscoll, K. R., Klepper, J., Stump, T. S., Wang, D., Spinner, N. B., Birnbaum, M. J., & De Vivo, D. C. GLUT-1 deficiency syndrome caused by haploinsufficiency of the blood-brain barrier hexose carrier. *Nat. Genet.* 18, 188–91 (1998).

107. Krebs, M. G., Hou, J. M., Ward, T. H., Blackhall, F. H. & Dive, C. Circulating tumour cells: Their utility in cancer management and predicting outcomes. *Therapeutic Advances in Medical Oncology* vol. 2 351–365 (2010).

108. Miller, M. C., Doyle, G. V & Terstappen, L. W. M. M. Significance of Circulating Tumor Cells Detected by the CellSearch System in Patients with Metastatic Breast Colorectal and Prostate Cancer. *J. Oncol.* 2010, (2010).

109. Plaks, V., Koopman, C. D. & Werb, Z. Circulating tumor cells. *Science* vol. 341 1186–1188 (2013).

110. Oulhen, M., Pailler, E., Faugeroux, V. & Farace, F. Filter-adapted fluorescent in situ hybridization (FA-FISH) for filtration-enriched circulating tumor cells. in *Methods in Molecular Biology* vol. 1634 133–141 (Humana Press Inc., 2017).

111. Pailler, E., Auger, N., Lindsay, C. R., Vielh, P., Islas-Morris-Hernandez, A., Borget, I., Ngo-Camus, M., Planchard, D., Soria, J. C., Besse, B., & Farace, F. High level of chromosomal instability in circulating tumor cells of ROS1-rearranged non-small-cell lung cancer. *Ann. Oncol.* 26, 1408–1415 (2015).

112. Marchesi, V. Lung cancer: ALK status of NSCLC reflected in CTCs. *Nature reviews. Clinical oncology* vol. 10 366 (2013).

113. Agarwal, A., Balic, M., El-Ashry, D., & Cote, R. J. (2018). Circulating Tumor Cells: Strategies for Capture, Analyses, and Propagation. Cancer journal (Sudbury, Mass.), 24(2), 70–77.

114. Dean, L. Blood and the cells it contains. (2005).

115. Halfter, W., Candiello, J., Hu, H., Zhang, P., Schreiber, E., & Balasubramani, M. Protein composition and biomechanical properties of in vivo-derived basement membranes. *Cell Adh. Migr.* 7, 64–71 (2013).

116. Pathak, A. & Kumar, S. Independent regulation of tumor cell migration by matrix stiffness and confinement. *Proc. Natl. Acad. Sci. U. S. A.* 109, 10334–9 (2012).

117. Harada, T., Swift, J., Irianto, J., Shin, J. W., Spinler, K. R., Athirasala, A., Diegmiller, R., Dingal, P. C., Ivanovska, I. L., & Discher, D. E. Nuclear lamin stiffness is a barrier to 3D migration, but softness can limit survival. *J. Cell Biol.* 204, 669–682 (2014).

118. Versaevel, M., Riaz, M., Grevesse, T. & Gabriele, S. *Cell confinement: putting the squeeze on the nucleus*. *Soft Matter* (2013). doi:10.1039/c3sm00147d.

119. Lammerding, J. & Wolf, K. Nuclear envelope rupture: Actin fibers are putting the squeeze on the nucleus. *J. Cell Biol.* 215, 5 (2016).

120. Humphries, M. J. Cell adhesion assays. *Methods Mol. Biol.* 522, 203–210 (2009).

121. Zhou, D. W. & García, A. J. Measurement Systems for Cell Adhesive Forces. *J. Biomech. Eng.* 137, 0209081 (2015).

122. Marshall, B. T., Long, M., Piper, J. W., Yago, T., McEver, R. P., & Zhu, C. Direct observation of catch bonds involving cell-adhesion molecules. *Nature* 423, 190–193 (2003).

123. Amano, M., Chihara, K., Kimura, K., Fukata, Y., Nakamura, N., Matsuura, Y., & Kaibuchi, K. Formation of actin stress fibers and focal adhesions enhanced by Rho- kinase. *Science (80-.).* 275, 1308–1311 (1997).

124. Reyes, C. D. & García, A. J. A centrifugation cell adhesion assay for high-throughput screening of biomaterial surfaces. *J. Biomed. Mater. Res. - Part A* 67, 328–333 (2003).

125. Friedrichs, J., Legate, K. R., Schubert, R., Bharadwaj, M., Werner, C., Müller, D. J., & Benoit, M. A practical guide to quantify cell adhesion using single-cell force spectroscopy. *Methods* 60, 169–178 (2013).

126. Engler, A. J., Chan, M., Boettiger, D. & Schwarzbauer, J. E. A novel mode of cell detachment from fibrillar fibronectin matrix under shear. *J. Cell Sci.* 122, 1647–53 (2009).

127. Boettiger, D. Quantitative measurements of integrin-mediated adhesion to extracellular matrix. *Methods Enzymol.* 426, 1–25 (2007).

128. García, A. J., Ducheyne, P. & Boettiger, D. Quantification of cell adhesion using a spinning disc device and application to surface-reactive materials. *Biomaterials* 18, 1091–8 (1997).

129. van Kooten, T. G., Schakenraad, J. M., Van der Mei, H. C. & Busscher, H. J. Development and use of a parallel-plate flow chamber for studying cellular adhesion to solid surfaces. *J. Biomed. Mater. Res.* 26, 725–738 (1992).

130. Fuhrmann, A. & Engler, A. J. Acute shear stress direction dictates adherent cell remodeling and verifies shear profile of spinning disk assays. *Phys. Biol.* 12, 016011 (2015).

131. Fuhrmann, A., Li, J., Chien, S., Engler, A. J. & Herrmann, K. Cation Type Specific Cell Remodeling Regulates Attachment Strength. *PLoS One* 9, e102424 (2014).

132. Fuhrmann, A., Banisadr, A., Beri, P., Tlsty, T. D. & Engler, A. J. Metastatic State of Cancer Cells May Be Indicated by Adhesion Strength. *Biophys. J.* 112, 736–745 (2017).

133. Beri, P., Popravko, A., Yeoman, B., Kumar, A., Chen, K., Hodzic, E., Chiang, A., Banisadr, A., Placone, J. K., Carter, H., Fraley, S. I., Katira, P., & Engler, A. J. Cell adhesiveness serves as a biophysical marker for metastatic potential. *Cancer Res.* 80, 901–911 (2020).

134. Tan, C.-S., Gilligan, D. & Pacey, S. *TREATMENT APPROACHES FOR PATIENTS WITH NON-SMALL CELL LUNG CANCER THAT HAVE ACQUIRED RESISTANCE TO EGFR INHIBITORS*.

135. Ayeni, D., Politi, K. & Goldberg, S. B. Emerging agents and new mutations in EGFR-mutant lung cancer. *Clin. Cancer Res.* 21, 3818–3820 (2015).

136. Carnemolla, B., Castellani, P., Ponassi, M., Borsi, L., Urbini, S., Nicolo, G., Dorcaratto, A., Viale, G., Winter, G., Neri, D., & Zardi, L. Identification of a glioblastoma-associated Tenascin-C isoform by a high affinity recombinant antibody. *Am. J. Pathol.* 154, 1345–1352 (1999).

137. Pinho, S. S. & Reis, C. A. Glycosylation in cancer: Mechanisms and clinical implications. *Nature Reviews Cancer* vol. 15 540–555 (2015).

138. Behrem, S., Žarkovic, K., Eškinja, N. & Jonjic, N. *Distribution Pattern of Tenascin-C in*

Glioblastoma: Correlation with Angiogenesis and Tumor Cell Proliferation. *PATHOLOGY ONCOLOGY RESEARCH* vol. 11 (2005).

139. Wade, A., Robinson, A. E., Engler, J. R., Petritsch, C., James, C. D., & Phillips, J. J. Proteoglycans and their roles in brain cancer. *FEBS Journal* vol. 280 2399–2417 (2013).

140. Lorger, M. Tumor Microenvironment in the Brain. *Cancers (Basel).* 4, 218–243 (2012).

141. Xia, S., Lal, B., Tung, B., Wang, S., Goodwin, C. R., & Laterra, J. Tumor microenvironment tenascin-C promotes glioblastoma invasion and negatively regulates tumor proliferation. *Neuro. Oncol.* 18, 507–517 (2016).

142. Miroshnikova, Y. A., Mouw, J. K., Barnes, J. M., Pickup, M. W., Lakins, J. N., Kim, Y., Lobo, K., Persson, A. I., Reis, G. F., McKnight, T. R., Holland, E. C., Phillips, J. J., & Weaver, V. M.Tissue mechanics promote IDH1-dependent HIF1α-tenascin C feedback to regulate glioblastoma aggression. *Nat. Cell Biol.* 18, 1336–1345 (2016).

143. Miroshnikova, Y. A., Mouw, J. K., Barnes, J. M., Pickup, M. W., Lakins, J. N., Kim, Y., Lobo, K., Persson, A. I., Reis, G. F., McKnight, T. R., Holland, E. C., Phillips, J. J., & Weaver, V. M. A tension-mediated glycocalyx–integrin feedback loop promotes mesenchymal-like glioblastoma. *Nat. Cell Biol.* 20, 1203–1214 (2018).

144. Paul, C. D., Hung, W.-C., Wirtz, D. & Konstantopoulos, K. Engineered Models of Confined Cell Migration. *Annu. Rev. Biomed. Eng.* 18, 159–180 (2016).

145. Stroka, K. M., Jiang, H., Chen, S. H., Tong, Z., Wirtz, D., Sun, S. X., & Konstantopoulos, K.Water permeation drives tumor cell migration in confined microenvironments. *Cell* 157, 611–623 (2014).

146. Ridley, A. J., Schwartz, M. A., Burridge, K., Firtel, R. A., Ginsberg, M. H., Borisy, G., Parsons, J. T., & Horwitz, A. R. Cell migration: integrating signals from front to back. *Science* 302, 1704–1709 (2003).

147. Bijian, K., Lougheed, C., Su, J., Xu, B., Yu, H., Wu, J. H., Riccio, K., & Alaoui-Jamali, M. A. Targeting focal adhesion turnover in invasive breast cancer cells by the purine derivative reversine. *Br. J. Cancer* 109, 2810–2818 (2013).

148. Indra, I., Undyala, V., Kandow, C., Thirumurthi, U., Dembo, M., & Beningo, K. A. An in vitro correlation of mechanical forces and metastatic capacity. *Phys. Biol.* 8, 015015 (2011).

149. Gallant, N. D. & García, A. J. Model of integrin-mediated cell adhesion strengthening. *J. Biomech.* 40, 1301–1309 (2007).

150. Yates, C. M., McGettrick, H. M., Nash, G. B. & Rainger, G. E. Adhesion of Tumor Cells to

Matrices and Endothelium. in 57–75 (Humana Press, New York, NY, 2014). doi:10.1007/978-1-4614-8244-4_5.

151. Palmer, C. P., Mycielska, M. E., Burcu, H., Osman, K., Collins, T., Beckerman, R., Perrett, R., Johnson, H., Aydar, E., & Djamgoz, M. B. Single cell adhesion measuring apparatus (SCAMA): application to cancer cell lines of different metastatic potential and voltage-gated Na+ channel expression. *Eur. Biophys. J.* 37, 359–368 (2008).

152. Reticker-Flynn, N. E., Malta, D. F., Winslow, M. M., Lamar, J. M., Xu, M. J., Underhill, G. H., Hynes, R. O., Jacks, T. E., & Bhatia, S. N. A combinatorial extracellular matrix platform identifies cell-extracellular matrix interactions that correlate with metastasis. *Nat. Commun.* 3, 1122 (2012).

153. Fischer, E. G., Riewald, M., Huang, H. Y., Miyagi, Y., Kubota, Y., Mueller, B. M., & Ruf, W. Tumor cell adhesion and migration supported by interaction of a receptor-protease complex with its inhibitor. *J. Clin. Invest.* 104, 1213–21 (1999).

154. Gupta, P. B., Fillmore, C. M., Jiang, G., Shapira, S. D., Tao, K., Kuperwasser, C., & Lander, E. S. Stochastic state transitions give rise to phenotypic equilibrium in populations of cancer cells. *Cell* 146, 633–644 (2011).

155. Seltzer, M. H., Rosato, F. E. & Fletcher, M. J. Serum and tissue calcium in human breast carcinoma. *Cancer Res.* 30, 615–6 (1970).

156. Seltzer, M., Rosato, F. & Fletcher, M. Serum and tissue magnesium levels in human breast carcinoma. *J. Surg. Res.* 159–162 (1970).

157. Nasulewicz, A., Wietrzyk, J., Wolf, F. I., Dzimira, S., Madej, J., Maier, J. A., Rayssiguier, Y., Mazur, A., & Opolski, A. Magnesium deficiency inhibits primary tumor growth but favors metastasis in mice. *Biochim. Biophys. Acta - Mol. Basis Dis.* 1739, 26–32 (2004).

158. Dai, Q., Motley, S. S., Smith, J. A., Jr, Concepcion, R., Barocas, D., Byerly, S., & Fowke, J. H. Blood Magnesium, and the Interaction with Calcium, on the Risk of High-Grade Prostate Cancer. *PLoS One* 6, e18237 (2011).

159. Mould, A. P., Akiyama, S. K. & Humphries, M. J. Regulation of integrin α5β1-fibronectin interactions by divalent cations. Evidence for distinct classes of binding sites for Mn2+, Mg2+,and Ca2+. *J. Biol. Chem.* 270, 26270–26277 (1995).

160. Geiger, B., Spatz, J. P. & Bershadsky, A. D. Environmental sensing through focal adhesions. *Nature Reviews Molecular Cell Biology* vol. 10 21–33 (2009).

161. Parsons, J. T., Horwitz, A. R. & Schwartz, M. A. Cell adhesion: Integrating cytoskeletal dynamics and cellular tension. *Nature Reviews Molecular Cell Biology* vol. 11 633–643

(2010).

162. Kraning-Rush, C. M., Califano, J. P. & Reinhart-King, C. A. Cellular Traction Stresses Increase with Increasing Metastatic Potential. *PLoS One* 7, e32572 (2012).

163. Heppner, G. H. & Wolman, S. R. MCF-10AT: A Model for Human Breast Cancer Development. *Breast J.* 5, 122–129 (1999).

164. Dawson, P. J., Wolman, S. R., Tait, L., Heppner, G. H. & Miller, F. R. MCF10AT: a model for the evolution of cancer from proliferative breast disease. *Am. J. Pathol.* 148, 313–9 (1996).

165. van 't Veer, L. J., Dai, H., van de Vijver, M. J., He, Y. D., Hart, A. A., Mao, M., Peterse, H. L., van der Kooy, K., Marton, M. J., Witteveen, A. T., Schreiber, G. J., Kerkhoven, R. M., Roberts, C., Linsley, P. S., Bernards, R., & Friend, S. H. Gene expression profiling predicts clinical outcome of breast cancer. *Nature* 415, 530–536 (2002).

166. Paik, S., Shak, S., Tang, G., Kim, C., Baker, J., Cronin, M., Baehner, F. L., Walker, M. G., Watson, D., Park, T., Hiller, W., Fisher, E. R., Wickerham, D. L., Bryant, J., & Wolmark, N.A Multigene Assay to Predict Recurrence of Tamoxifen-Treated, Node-Negative Breast Cancer. *N. Engl. J. Med.* 351, 2817–2826 (2004).

167. Subramaniam, D. S. & Isaacs, C. Utilizing Prognostic and Predictive Factors in Breast Cancer. *Curr. Treat. Options Oncol.* 6, 147–159 (2005).

168. Fraley, S. I., Feng, Y., Krishnamurthy, R., Kim, D. H., Celedon, A., Longmore, G. D., & Wirtz, D. A distinctive role for focal adhesion proteins in three-dimensional cell motility. *Nat. Cell Biol.* 12, 598–604 (2010).

169. Mao, Y. & Schwarzbauer, J. E. Stimulatory effects of a three-dimensional microenvironment on cell-mediated fibronectin fibrillogenesis. *J. Cell Sci.* 118, 4427–4436 (2005).

Huth, J., Buchholz, M., Kraus, J. M., Mølhave, K., Gradinaru, C., v Wichert, G., Gress, T. M., Neumann, H., & Kestler, H. A. TimeLapseAnalyzer: Multi-target analysis for live-cell imaging and time-lapse microscopy. *Comput. Methods Programs Biomed.* 104, 227–234 (2011).

171. Siegel, R. L., Miller, K. D. & Jemal, A. Cancer statistics, 2017. *CA. Cancer J. Clin.* 67, 7–30 (2017).

172. Furnari, F. B., Fenton, T., Bachoo, R. M., Mukasa, A., Stommel, J. M., Stegh, A., Hahn, W. C., Ligon, K. L., Louis, D. N., Brennan, C., Chin, L., DePinho, R. A., & Cavenee, W. K. Malignant astrocytic glioma: genetics, biology, and paths to treatment. *Genes Dev.* 21, 2683–710 (2007).

173. Jennifer M. Propp, N. E. S. and C. K. T. A. D. CBTRUS Statistical Report: Primary Brain and Central Nervous System Tumors Diagnosed in the United States in 2007–2011. *Neuro Oncol* 16, 1–57 (2014).

174. Dunn, G. P., Rinne, M. L., Wykosky, J., Genovese, G., Quayle, S. N., Dunn, I. F., Agarwalla, P. K., Chheda, M. G., Campos, B., Wang, A., Brennan, C., Ligon, K. L., Furnari, F., Cavenee, W. K., Depinho, R. A., Chin, L., & Hahn, W. C. Emerging insights into the molecular and cellular basis of glioblastoma. 756–784 (2012) doi:10.1101/gad.187922.112.and.

175. Paw, I., Carpenter, R. C., Watabe, K., Debinski, W. & Lo, H.-W. Mechanisms regulating glioma invasion. *Cancer Lett.* 362, 1–7 (2015).

176. Stupp, R., Mason, W. P., van den Bent, M. J., Weller, M., Fisher, B., Taphoorn, M. J., Belanger, K., Brandes, A. A., Marosi, C., Bogdahn, U., Curschmann, J., Janzer, R. C., Ludwin, S. K., Gorlia, T., Allgeier, A., Lacombe, D., Cairncross, J. G., Eisenhauer, E., Mirimanoff, R. O. Radiotherapy plus Concomitant and Adjuvant Temozolomide for Glioblastoma. *N. Engl. J. Med.* 352, 987–996 (2005).

177. Kleihues, P., Louis, D. N., Scheithauer, B. W., Rorke, L. B., Reifenberger, G., Burger, P. C., & Cavenee, W. K. The WHO classification of tumors of the nervous system. *J. Neuropathol. Exp. Neurol.* 61, 215–225 (2002).

178. Nishikawa, R., Furnari, F. B., Lin, H., Arap, W., Berger, M. S., Cavenee, W. K., & Su Huang, H. J. Loss of P16INK4 expression is frequent in high grade gliomas. *Cancer Res.* 55, 1941–5 (1995).

179. Holland, E. C., Hively, W. P., DePinho, R. A. & Varmus, H. E. A constitutively active epidermal growth factor receptor cooperates with disruption of G1 cell-cycle arrest pathways to induce glioma-like lesions in mice. *Genes Dev.* 12, 3675–85 (1998).

180. Verhaak, R. G., Hoadley, K. A., Purdom, E., Wang, V., Qi, Y., Wilkerson, M. D., Miller, C. R., Ding, L., Golub, T., Mesirov, J. P., Alexe, G., Lawrence, M., O'Kelly, M., Tamayo, P., Weir, B. A., Gabriel, S., Winckler, W., Gupta, S., Jakkula, L., Feiler, H. S. Hodgson, J.G., James, C.D., Sarkaria, J.N., Brennan, C., Kahn, A., Spellman, P.T., Wilson, R.K., Speed, T.P., Gray, J.W., Meyerson, M., Getz, G., Perou, C.M., Hayes, D.N. Integrated Genomic Analysis Identifies Clinically Relevant Subtypes of Glioblastoma Characterized by Abnormalities in PDGFRA, IDH1, EGFR, and NF1. *Cancer Cell* 17, 98–110 (2010).

181. Brennan, C. W., Verhaak, R. G., McKenna, A., Campos, B., Noushmehr, H., Salama, S. R., Zheng, S., Chakravarty, D., Sanborn, J. Z., Berman, S. H., Beroukhim, R., Bernard, B., Wu, C. J., Genovese, G., Shmulevich, I., Barnholtz-Sloan, J., Zou, L., Vegesna, R., Shukla, S. A., Ciriello, G., Yung, W.K., Zhang, W., Sougnez, C., Mikkelsen, T., Aldape. K., Bigner. D.D., Van Meir, E.G., Prados, M., Sloan, A., Black, K.L., Eschbacher, J., Finocchiaro, G., Friedman, W., Andrews, D.W., Guha, A., Iacocca, M., O'Neill, B.P., Foltz, G., Myers, J., Weisenberger, D.J.,

Penny, R., Kucherlapati, R., Perou, C.M., Hayes, D.N., Gibbs, R., Marra, M., Mills, G.B., Lander, E., Spellman, P., Wilson, R., Sander, C., Weinstein, J., Meyerson, M., Gabriel, S., Laird, P.W., Haussler, D., Getz, G., Chin, L. The Somatic Genomic Landscape of Glioblastoma. *Cell* 155, 462–477 (2013).

182. Liu, F., Hon, G. C., Villa, G. R., Turner, K. M., Ikegami, S., Yang, H., Ye, Z., Li, B., Kuan, S., Lee, A. Y., Zanca, C., Wei, B., Lucey, G., Jenkins, D., Zhang, W., Barr, C. L., Furnari, F. B., Cloughesy, T. F., Yong, W. H., Gahman, T. C., Shiau, A.K., Cavenee, W.K., Ren, B., Mischel, P.S. EGFR Mutation Promotes Glioblastoma through Epigenome and Transcription Factor Network Remodeling. *Mol. Cell* 60, 307–318 (2015).

183. Gan, H. K., Kaye, A. H. & Luwor, R. B. The EGFRvIII variant in glioblastoma multiforme. *J. Clin. Neurosci.* 16, 748–754 (2009).

184. Francis, J. M., Zhang, C. Z., Maire, C. L., Jung, J., Manzo, V. E., Adalsteinsson, V. A., Homer, H., Haidar, S., Blumenstiel, B., Pedamallu, C. S., Ligon, A. H., Love, J. C., Meyerson, M., & Ligon, K. L. EGFR variant heterogeneity in glioblastoma resolved through single-nucleus sequencing. *Cancer Discov.* 4, 956–971 (2014).

185. Furnari, F. B., Cloughesy, T. F., Cavenee, W. K. & Mischel, P. S. Heterogeneity of epidermal growth factor receptor signalling networks in glioblastoma. *Nature Reviews Cancer* vol. 15 302–310 (2015).

186. Huang, H. S., Nagane, M., Klingbeil, C. K., Lin, H., Nishikawa, R., Ji, X. D., Huang, C. M., Gill, G. N., Wiley, H. S., & Cavenee, W. K. The enhanced tumorigenic activity of a mutant epidermal growth factor receptor common in human cancers is mediated by threshold levels of constitutive tyrosine phosphorylation and unattenuated signaling. *J. Biol. Chem.* 272, 2927–2935 (1997).

187. Narita, Y., Nagane, M., Mishima, K., Huang, H. J., Furnari, F. B., & Cavenee, W. K. (2002). Mutant epidermal growth factor receptor signaling down-regulates p27 through activation of the phosphatidylinositol 3-kinase/Akt pathway in glioblastomas. Cancer research, 62(22), 6764–6769.

188. Nagane, M., Lin, H., Cavenee, W. K. & Huang, H. J. S. Aberrant receptor signaling in human malignant gliomas: Mechanisms and therapeutic implications. *Cancer Lett.* 162, S17–S21 (2001).

189. Bachoo, R. M., Maher, E. A., Ligon, K. L., Sharpless, N. E., Chan, S. S., You, M. J., Tang, Y., DeFrances, J., Stover, E., Weissleder, R., Rowitch, D. H., Louis, D. N., & DePinho, R. A. Epidermal growth factor receptor and Ink4a/ArfConvergent mechanisms governing terminal differentiation and transformation along the neural stem cell to astrocyte axis. *Cancer Cell* 1, 269–277 (2002).

190. Hesselager, G. & Holland, E. C. Using Mice to Decipher the Molecular Genetics of Brain Tumors. *Neurosurgery* 53, 685–695 (2003).

191. Nishikawa, R., Sugiyama, T., Narita, Y., Furnari, F., Cavenee, W. K., & Matsutani, M. Immunohistochemical analysis of the mutant epidermal growth factor, ΔEGFR, in glioblastoma. *Brain Tumor Pathol.* 21, 53–56 (2004).

192. Zanca, C., Villa, G. R., Benitez, J. A., Thorne, A. H., Koga, T., D'Antonio, M., Ikegami, S., Ma, J., Boyer, A. D., Banisadr, A., Jameson, N. M., Parisian, A. D., Eliseeva, O. V., Barnabe, G. F., Liu, F., Wu, S., Yang, H., Wykosky, J., Frazer, K. A., Verkhusha, V. V., Isaguliants, M.G., Weiss, W.A., Gahman, T.C., Shiau, A.K., Chen, C.C., Mischel, P.S., Cavenee, W.K., Furnari, F.B. Glioblastoma cellular cross-talk converges on NF-κB to attenuate EGFR inhibitor sensitivity. *Genes Dev.* 31, (2017).

193. Liu, Z., Han, L., Dong, Y., Tan, Y., Li, Y., Zhao, M., Xie, H., Ju, H., Wang, H., Zhao, Y., Zheng, Q., Wang, Q., Su, J., Fang, C., Fu, S., Jiang, T., Liu, J., Li, X., Kang, C., & Ren, H. EGFRvIII/integrin Beta3 interaction in hypoxic and vitronectinenriching microenvironment promote GBM progression and metastasis. *Oncotarget* 7, 4680–4694 (2016).

194. Honegger, A. M., Dull, T. J., Felder, S., Van Obberghen, E., Bellot, F., Szapary, D., Schmidt, A., Ullrich, A., & Schlessinger, J. Point mutation at the ATP binding site of EGF receptor abolishes protein-tyrosine kinase activity and alters cellular routing. *Cell* 51, 199–209 (1987).

195. Schmidt, M. H. H., Furnari, F. B., Cavenee, W. K. & Bögler, O. Epidermal growth factor receptor signaling intensity determines intracellular protein interactions, ubiquitination, and internalization. *Proc. Natl. Acad. Sci. U. S. A.* 100, 6505–10 (2003).

196. Huang, P. H., Xu, A. M. & White, F. M. Oncogenic EGFR signaling networks in glioma. *Sci. Signal.* 2, re6 (2009).

197. Guo, G., Gong, K., Wohlfeld, B., Hatanpaa, K. J., Zhao, D., & Habib, A. A. Ligand-independent EGFR signaling. *Cancer Research* vol. 75 3436–3441 (2015).

198. Gan, H. K., Cvrljevic, A. N. & Johns, T. G. The epidermal growth factor receptor variant III (EGFRvIII): where wild things are altered. *FEBS J.* 280, 5350–5370 (2013).

199. Ning, Y., Zeineldin, R., Liu, Y., Rosenberg, M., Stack, M. S., & Hudson, L. G. Down-regulation of integrin α2 surface expression by mutant epidermal growth factor receptor (EGFRvIII) induces aberrant cell spreading and focal adhesion formation. *Cancer Res.* 65, 9280–9286 (2005).

200. Yu, X., Miyamoto, S. & Mekada, E. Integrin alpha 2 beta 1-dependent EGF receptor activation at cell-cell contact sites. *J. Cell Sci.* 2139–2147 (2000).

201. Wu, Y. & Zhou, B. P. TNF-α/NFκ-B/Snail pathway in cancer cell migration and invasion. *British Journal of Cancer* vol. 102 639–644 (2010).

202. Dirkse, A., Golebiewska, A., Buder, T., Nazarov, P. V., Muller, A., Poovathingal, S., Brons, N., Leite, S., Sauvageot, N., Sarkisjan, D., Seyfrid, M., Fritah, S., Stieber, D., Michelucci, A., Hertel, F., Herold-Mende, C., Azuaje, F., Skupin, A., Bjerkvig, R., Deutsch, A., Voss-Böhme, A., Niclou, S.P. Stem cell-associated heterogeneity in Glioblastoma results from intrinsic tumor plasticity shaped by the microenvironment. *Nat. Commun.* 10, 1–16 (2019).

203. Alieva, M., Leidgens, V., Riemenschneider, M. J., Klein, C. A., Hau, P., & van Rheenen, J.Intravital imaging of glioma border morphology reveals distinctive cellular dynamics and contribution to tumor cell invasion. *Sci. Rep.* 9, 1–11 (2019).

204. Wykosky, J., Hu, J., Gomez, G. G., Taylor, T., Villa, G. R., Pizzo, D., VandenBerg, S. R., Thorne, A. H., Chen, C. C., Mischel, P. S., Gonias, S. L., Cavenee, W. K., & Furnari, F. B. A urokinase receptor-bim signaling axis emerges during EGFR inhibitor resistance in mutant EGFR glioblastoma. *Cancer Res.* 75, 394–404 (2015).